

Supplementary Data

Streptogramin A derivatives as mitochondrial translation inhibitors to suppress glioblastoma stem cells growth

Denise Sighel^{a,1,*}, Giulia Battistini^{b,1}, Emanuele Filiberto Rosatti^{a,1}, Jacopo Vigna^{b,1}, Matteo Pavan^c, Romina Belli^d, Daniele Peroni^d, Federica Alessandrini^a, Sara Longhi^a, Michael Pancher^e, Joanna Rorbach^f, Stefano Moro^c, Alessandro Quattrone^{a,2}, Ines Mancini^{b,2,**}

^a *Laboratory of Translational Genomics, Department of Cellular, Computational and Integrative Biology (CIBIO), University of Trento, via Sommarive 9, 38123, Povo, Trento, Italy*

^b *Laboratory of Bioorganic Chemistry, Department of Physics, University of Trento, via Sommarive 14, 38123, Povo, Trento, Italy*

^c *Molecular Modeling Section (MMS), Department of Pharmaceutical and Pharmacological Sciences, University of Padova, via F. Marzolo 5, 35131 Padova, Italy*

^d *Mass Spectrometry and Proteomics Core Facility, Department of Cellular, Computational and Integrative Biology (CIBIO), University of Trento, via Sommarive 9, 38123, Povo, Trento, Italy*

^e *High Throughput Screening (HTS) and Validation core facility, Department of Cellular, Computational and Integrative Biology (CIBIO), University of Trento, via Sommarive 9, 38123, Povo, Trento, Italy*

^f *Department of Medical Biochemistry and Biophysics, Division of Molecular Metabolism, Biomedicum, Solnavägen 9, 171 65 Solna, Stockholm, Sweden*

* Corresponding Author

** Corresponding Author

Email addresses: denise.sighel@unitn.it (D. Sighel); ines.mancini@unitn.it (I. Mancini)

¹ These authors contributed equally

² Co-last authors

Contents:	Page(s):
Fig. S1. The molecular structures of each of the four possible diastereomers generated by the Diels-Alder reactions between dalfopristin (1) or virginiamycin M1 (2) and maleic anhydride or maleimide as dienophiles.	S3
Fig. S2. Per-residue interaction energy decomposition performed on the docking-predicted binding mode for C10/C13 derivatives.	S4
Fig. S3. Per-residue interaction energy decomposition performed on the docking-predicted binding mode for C16 derivatives.	S5
Fig. S4. Per-residue interaction energy decomposition performed on the docking-predicted binding mode for C26 derivatives.	S6
Fig. S5. Western blot analysis for the evaluation of mitochondrial translation inhibition of C10/C13 derivatives.	S7
Fig. S6. Western blot analysis for the evaluation of mitochondrial translation inhibition of C16 hydroxyl derivatives.	S7
Fig. S7. Western blot analysis for the evaluation of mitochondrial translation inhibition of 16 <i>S</i> fluoro derivatives.	S8
Fig. S8. Western blot analysis for the evaluation of mitochondrial translation inhibition of 16 <i>R</i> NHMe derivatives.	S8
Fig. S9. Western blot analysis for the evaluation of mitochondrial translation inhibition of 6 and 7 derivatives.	S8
Fig. S10. UHPLC-MS spectra of compound 2 .	S9
Fig. S11. UHPLC-MS Extracted ion chromatograms of compound 2 .	S10
Fig. S12. Calibration curve for compound 2 .	S10
Table S1. Retention time of compounds in UHPLC analysis.	S11
Fig. S13-S80. ¹ H-NMR, ¹³ C-NMR and HRMS spectra and HPLC chromatograms of tested compounds.	S12-S57

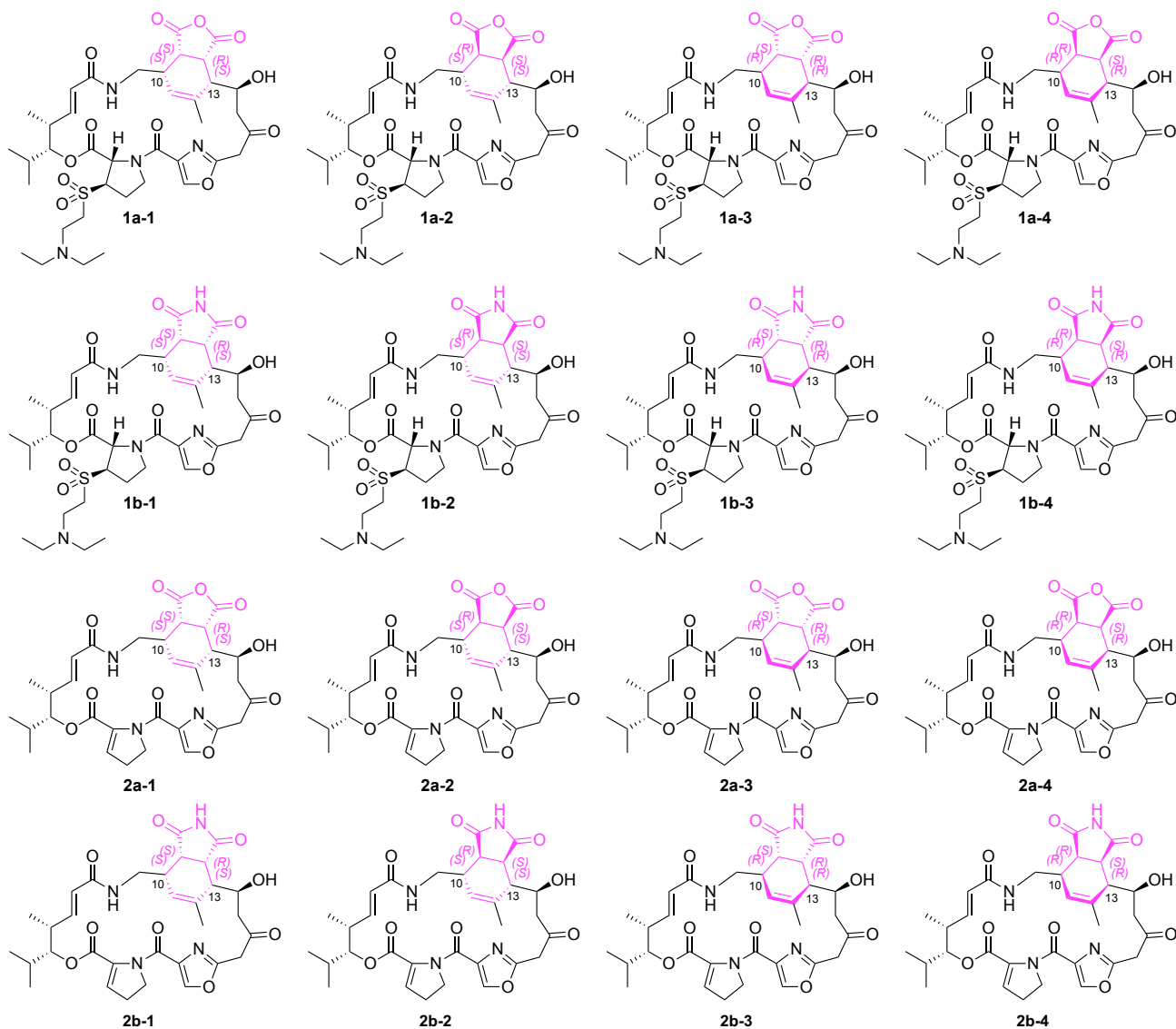


Fig. S1. The molecular structures of each of the four possible diastereomers generated by the Diels-Alder reactions between dalfopristin (**1**) or virginiamycin M1 (**2**) and maleic anhydride or maleimide as dienophiles. The stereochemistry of each possible diastereomer obtainable from the reaction is highlighted.

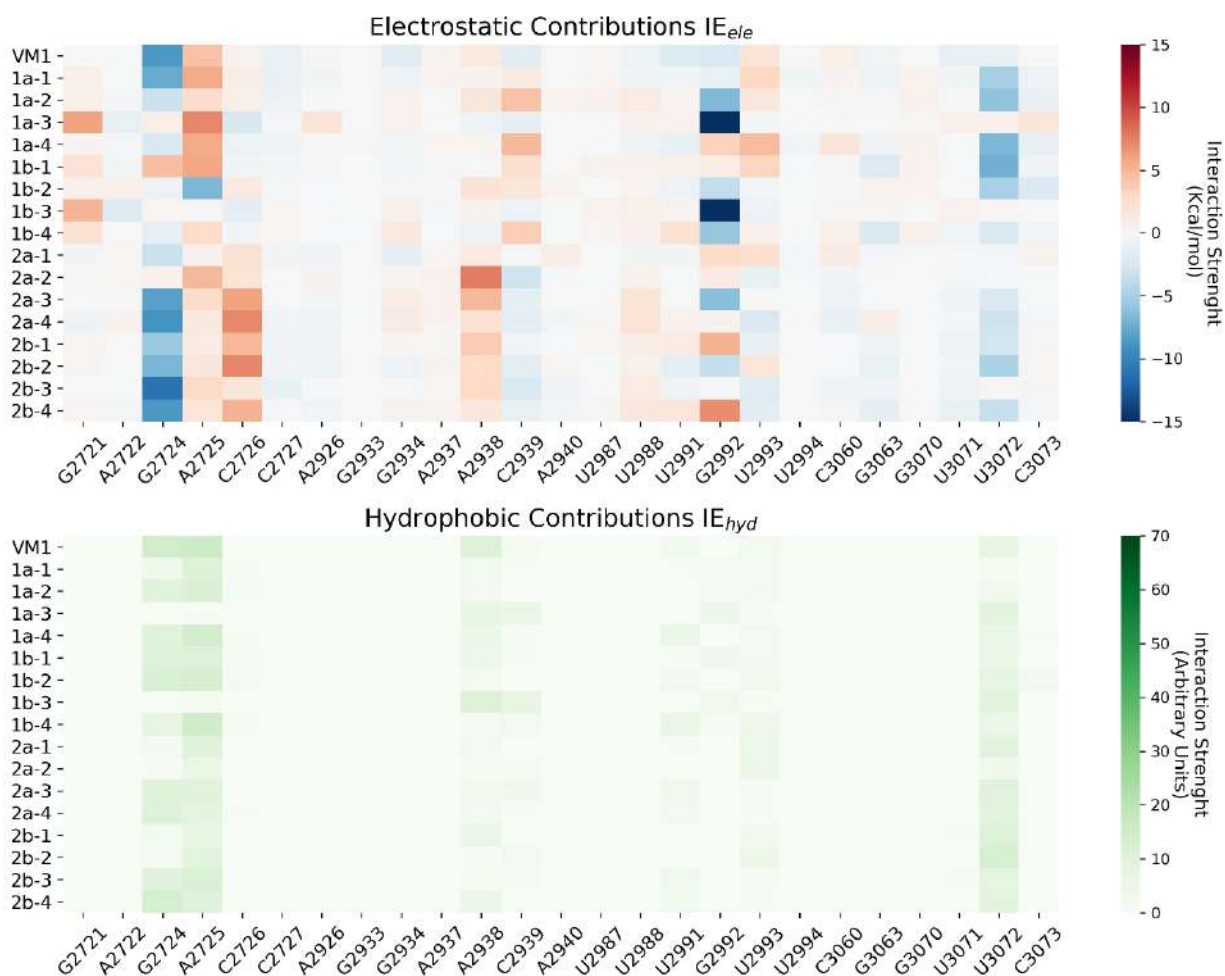


Fig. S2. Per-residue interaction energy decomposition performed on the docking-predicted binding mode for C10/C13 derivatives. VM1 (**2**) binding mode from structure 6I9R is also reported for reference. In detail, the upper panel reports a per-residue decomposition of electrostatic interaction energy: values (in Kcal/mol) are plotted according to the colour scale reported on the right, ranging from red (positive value, repulsive interaction) to black (negative value, attractive interaction). The lower panel, instead, reports a per-residue decomposition of hydrophobic interactions: values (in arbitrary/adimensional units) are plotted according to the color scale reported on the right, ranging from white (zero, absence of interaction) to dark teal (indicating a good hydrophobic interaction).

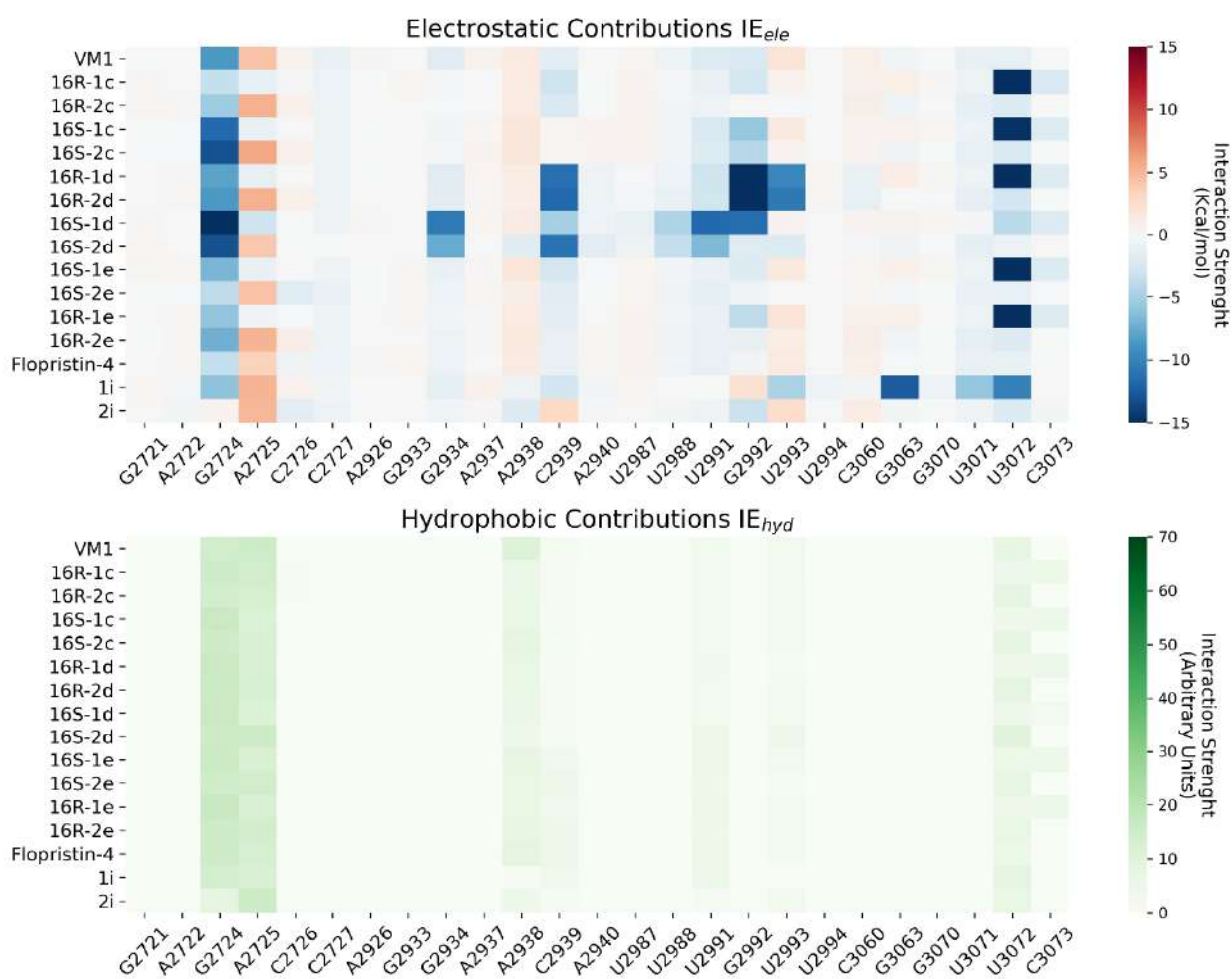


Fig. S3. Per-residue interaction energy decomposition performed on the docking-predicted binding mode for C16 derivatives. VM1 (**2**) binding mode from structure 6I9R is also reported for reference. In detail, the upper panel reports a per-residue decomposition of electrostatic interaction energy: values (in Kcal/mol) are plotted according to the colour scale reported on the right, ranging from red (positive value, repulsive interaction) to black (negative value, attractive interaction). The lower panel, instead, reports a per-residue decomposition of hydrophobic interactions: values (in arbitrary/adimensional units) are plotted according to the color scale reported on the right, ranging from white (zero, absence of interaction) to dark teal (indicating a good hydrophobic interaction).

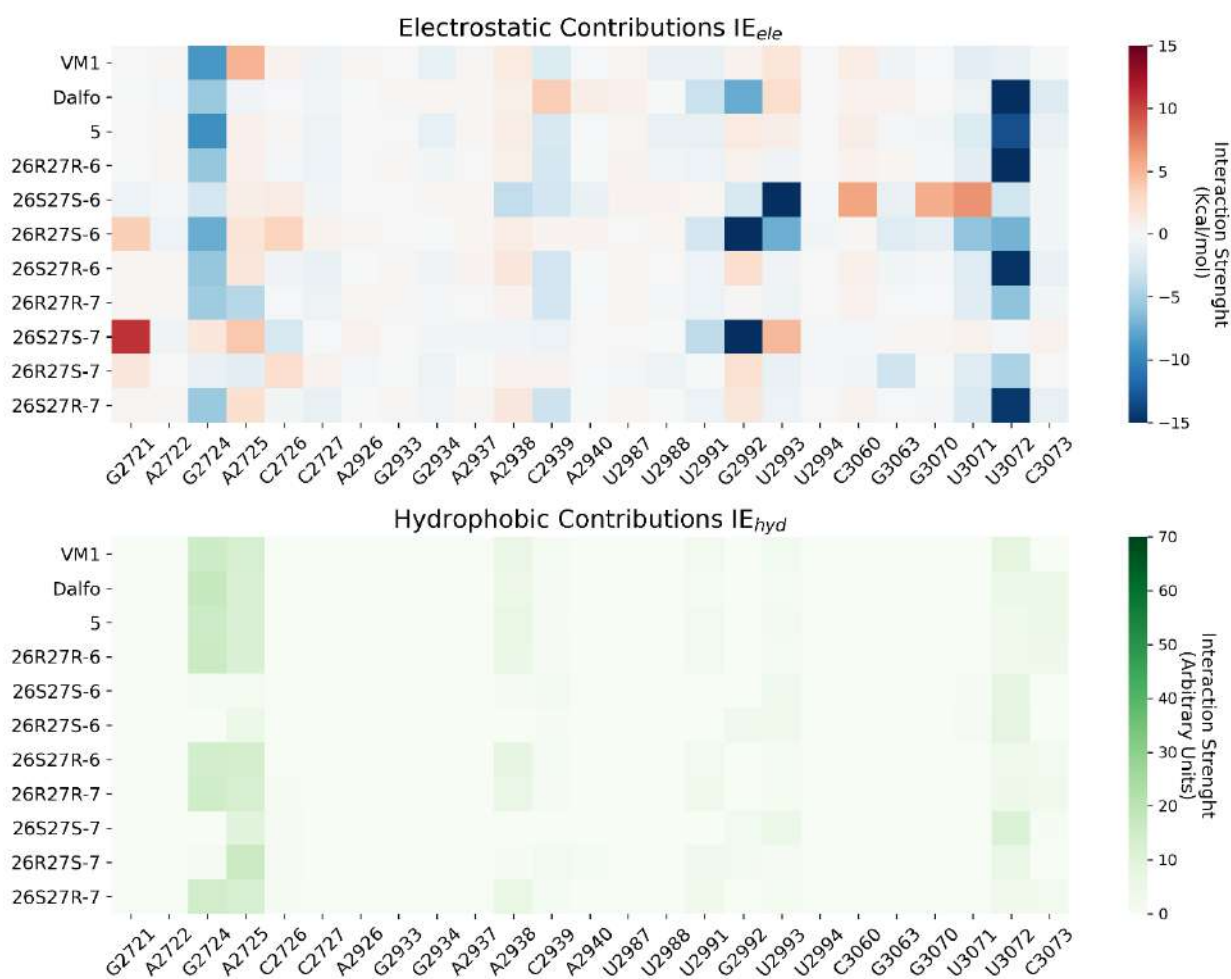


Fig. S4. Per-residue interaction energy decomposition performed on the docking-predicted binding mode for C26 derivatives. VM1 (**2**) binding mode from structure 6I9R is also reported for reference. In detail, the upper panel reports a per-residue decomposition of electrostatic interaction energy: values (in Kcal/mol) are plotted according to the colour scale reported on the right, ranging from red (positive value, repulsive interaction) to black (negative value, attractive interaction). The lower panel, instead, reports a per-residue decomposition of hydrophobic interactions: values (in arbitrary/adimensional units) are plotted according to the color scale reported on the right, ranging from white (zero, absence of interaction) to dark teal (indicating a good hydrophobic interaction).

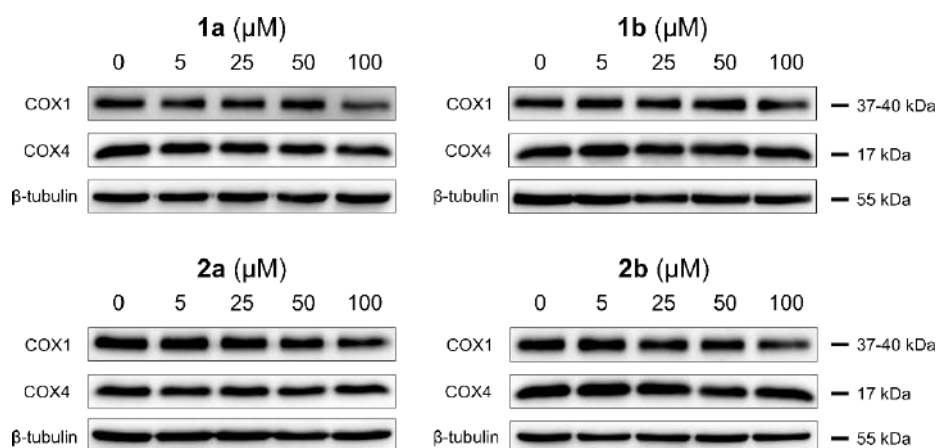


Fig. S5. Western blot analysis for the evaluation of mitochondrial translation inhibition of C10/C13 derivatives. C10/C13 derivatives do not inhibit mitochondrial translation. Immunoblotting on COMI cells after 48 hours of treatment with increasing concentrations of **1a**, **1b**, **2a**, and **2c**, alone (*left column*) or in combination with Q (**3**) (*right column*). Effects on COX1, COX4 and beta tubulin proteins are shown. One representative result, n=3 biological replicates.

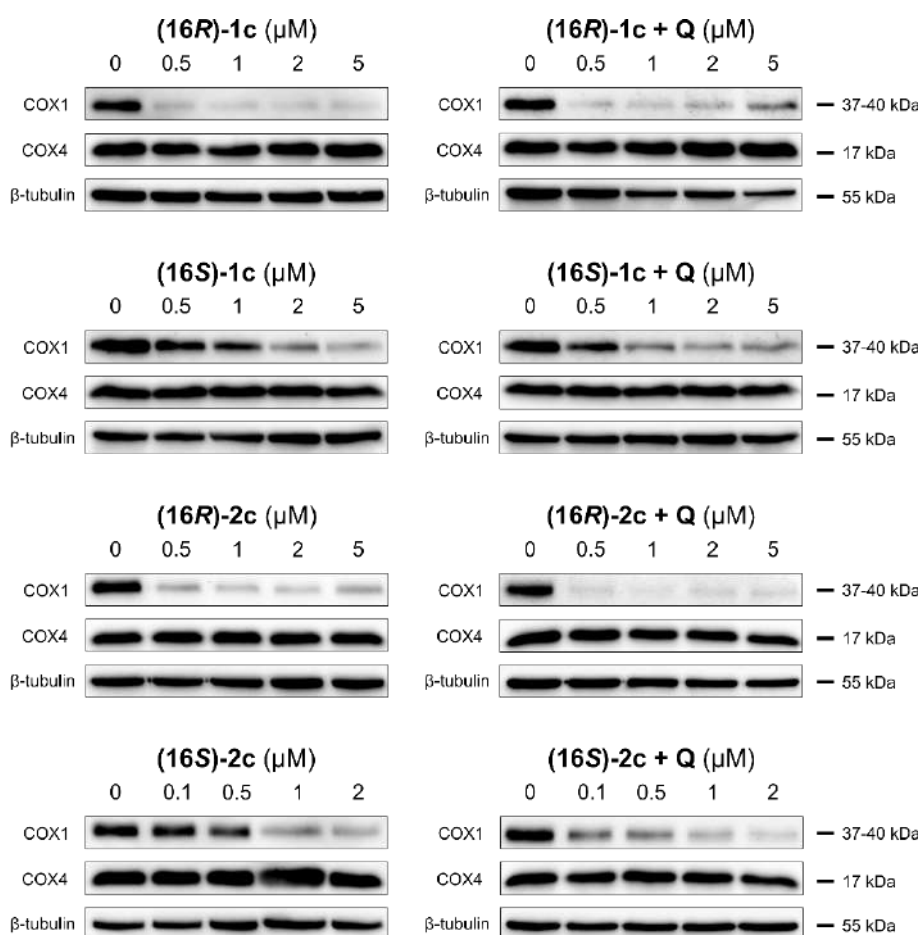


Fig. S6. Western blot analysis for the evaluation of mitochondrial translation inhibition of C16 hydroxyl derivatives. C16 hydroxyl derivatives inhibit mitochondrial translation. Immunoblotting on COMI cells after 48 hours of treatment with increasing concentrations of **(16R)-1c**, **(16S)-1c**, **(16R)-2c**, and **(16S)-2c**, alone (*left column*) or in combination with Q (**3**) (*right column*). Effects on COX1, COX4 and beta tubulin proteins are shown. One representative result, n=3 biological replicates.

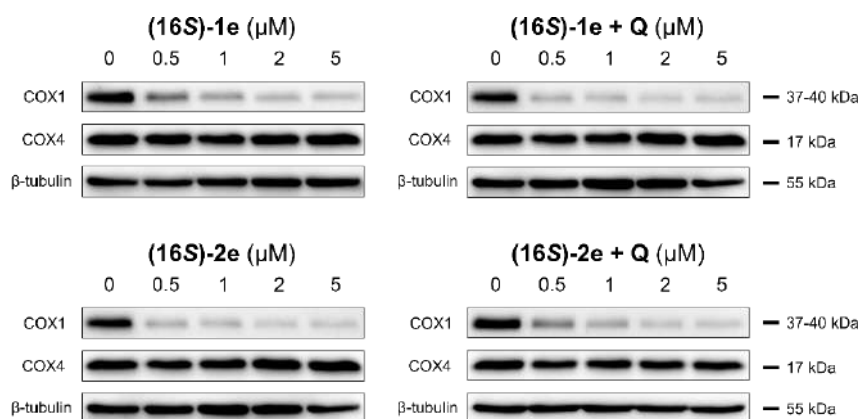


Fig. S7. Western blot analysis for the evaluation of mitochondrial translation inhibition of (16*S*) fluoro derivatives. (16*S*) fluoro derivatives inhibit mitochondrial translation. Immunoblotting on COMI cells after 48 hours of treatment with increasing concentrations of (16*S*)-1e, and (16*S*)-2e, alone (*left column*) or in combination with Q (3) (*right column*). Effects on COX1, COX4 and beta-tubulin proteins are shown. One representative result, n=3 biological replicates.

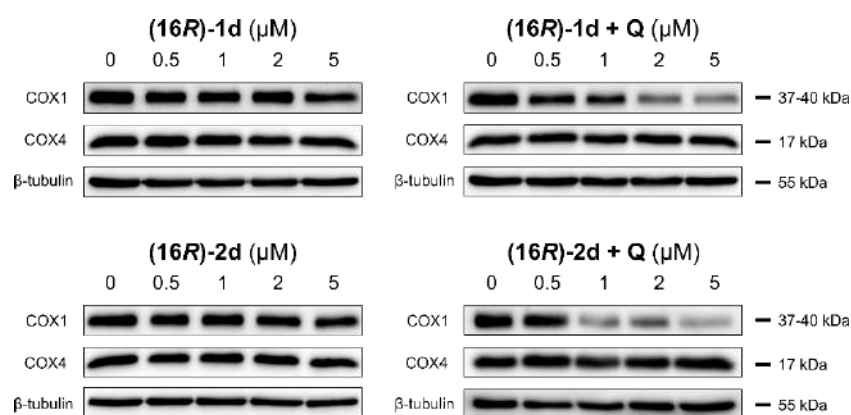


Fig. S8. Western blot analysis for the evaluation of mitochondrial translation inhibition of (16*R*) NHMe derivatives. (16*R*) NHMe derivatives do not inhibit mitochondrial translation. Immunoblotting on COMI cells after 48 hours of treatment with increasing concentrations of (16*R*)-1d, and (16*R*)-2d, alone (*left column*) or in combination with Q (3) (*right column*). Effects on COX1, COX4 and beta-tubulin proteins are shown. One representative result, n=3 biological replicates.

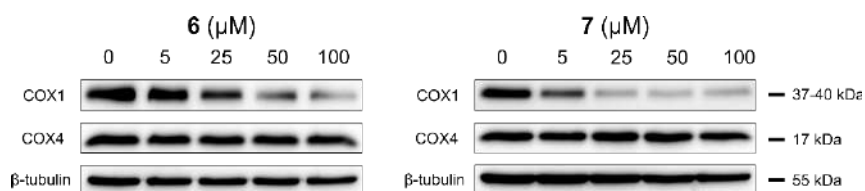


Fig. S9. Western blot analysis for the evaluation of mitochondrial translation inhibition of 6 and 7 derivatives. Compounds 6 and 7 inhibit mitochondrial translation only at high concentrations. Immunoblotting on COMI cells after 48 hours of treatment with increasing concentrations of 6 and 7. Effects on COX1, COX4 and beta tubulin proteins are shown. One representative result, n=3 biological replicates.

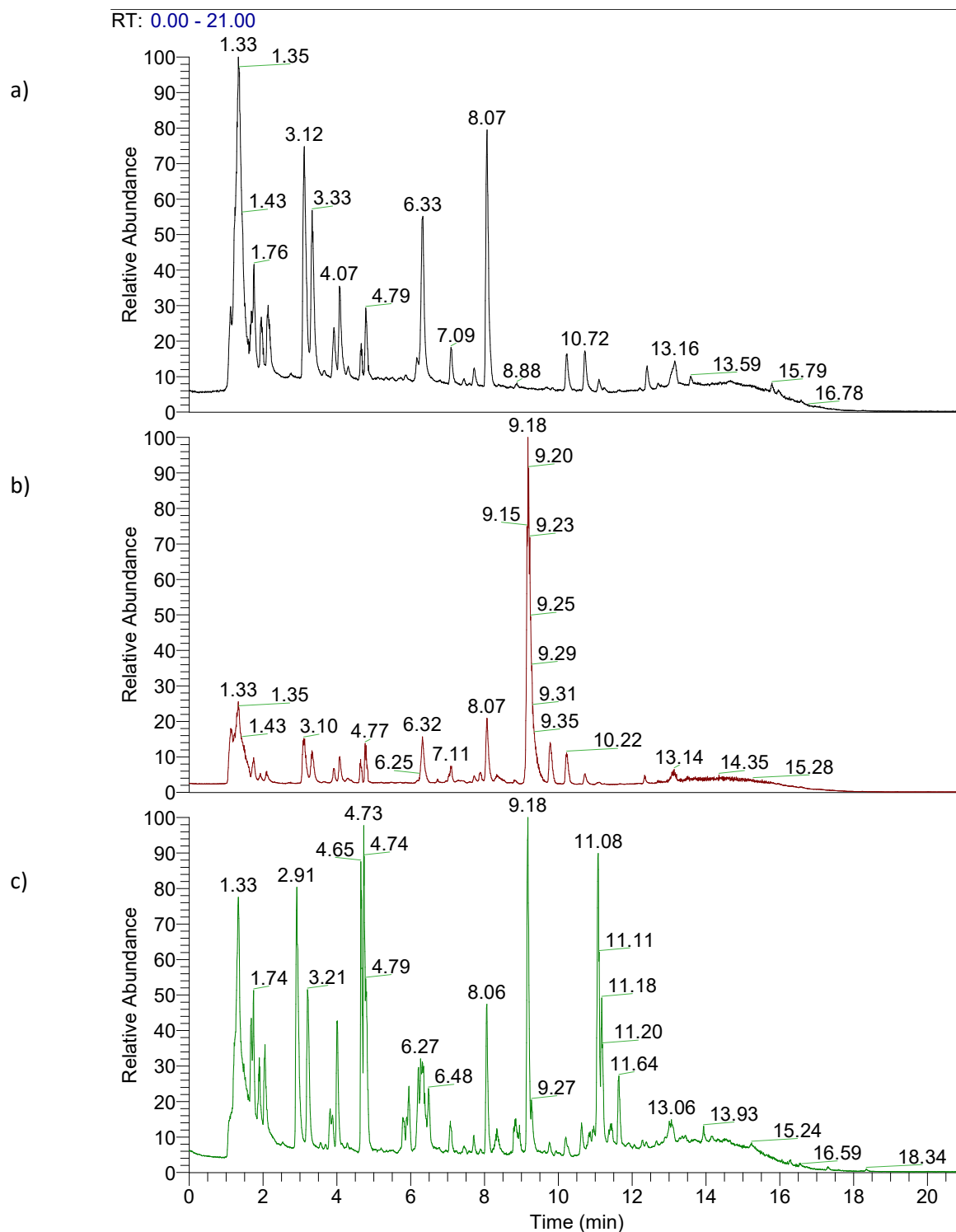


Fig. S10. UHPLC chromatograms of a) drug-free sample (blank); b) standard sample used for calibration curve of VM1 (2) (50 ng/mL); c) sample treated with VM1 (2). UHPLC conditions: Hypersil Gold C18 column (ThermoFisher, 100 x 2.1 mm, particle size: 1.9 μ m); linear gradient from 5 to 100% B (B: acetonitrile 0.1% of formic acid; A: water + 0.1% formic acid) over 15 min, followed by 4 min at 100%; flow 0.2 mL/min; MS spray voltage 3500 V; full scan at 120.000 FWHM (200 m/z); scan range 100-1000 m/z.

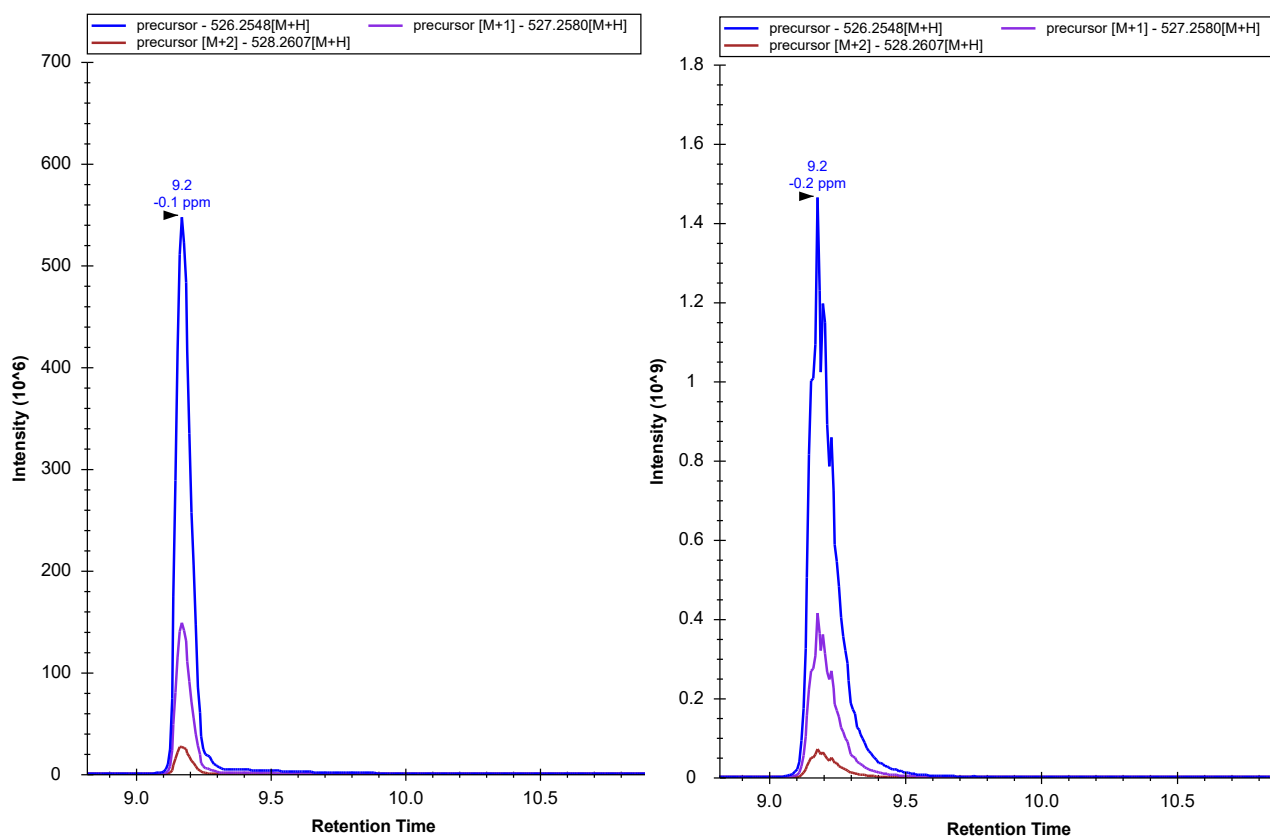


Fig. S11. Extracted ion chromatograms of the $[M+H]^+$ adducts (Skyline software) of a representative standard sample of VM1 (**2**) conc. 50 ng/mL (on the left) and sample treated with VM1 (**2**) (on the right). The peak area of the precursor ions were extracted from chromatograms for both standards and treated samples to build the standard curves of each compound and to compute concentration values of the compound in samples, respectively.

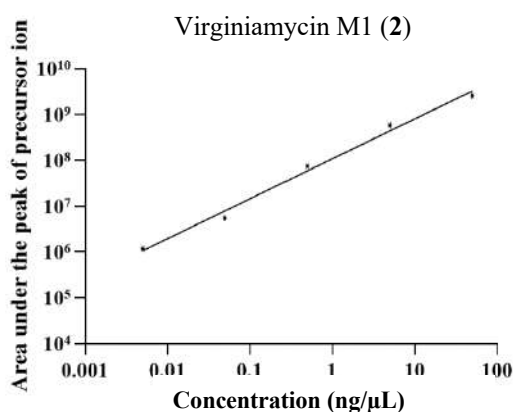


Fig. S12. Calibration curve for VM1 (**2**); $R^2 = 0.9917$. Five serial drug dilutions, from 0.005 to 50 ng/ μ L, were prepared in non-treated metabolite extracts resuspended in 5% acetonitrile/0.1% formic acid aqueous solution starting from a 10 mM stock of VM1 (**2**). 20 μ L of each dilution plus a blank samples were loaded into the LC autosampler. After the analysis, the log-transformed value of the total area of precursor ions of each standard sample was plotted in function of the concentration to construct the standard curve. The error on concentrations was calculated as the physical error deriving from the weighting of the compound plus the error from pipetting. For each serial dilution performed, the error was propagated using the variance formula.

Table S1

UHPLC-MS retention time (min) returned by Skyline software for extracted peak of each compound.

	RT		RT
D (1)	6.9	VM1 (2)	9.2
1a	6.6	2a	8.6
(16R)-1c	6.6	(16R)-2c	8.3
(16R)-1e	7.3	(16R)-2e	9.3
5	7.0		
6	6.2		

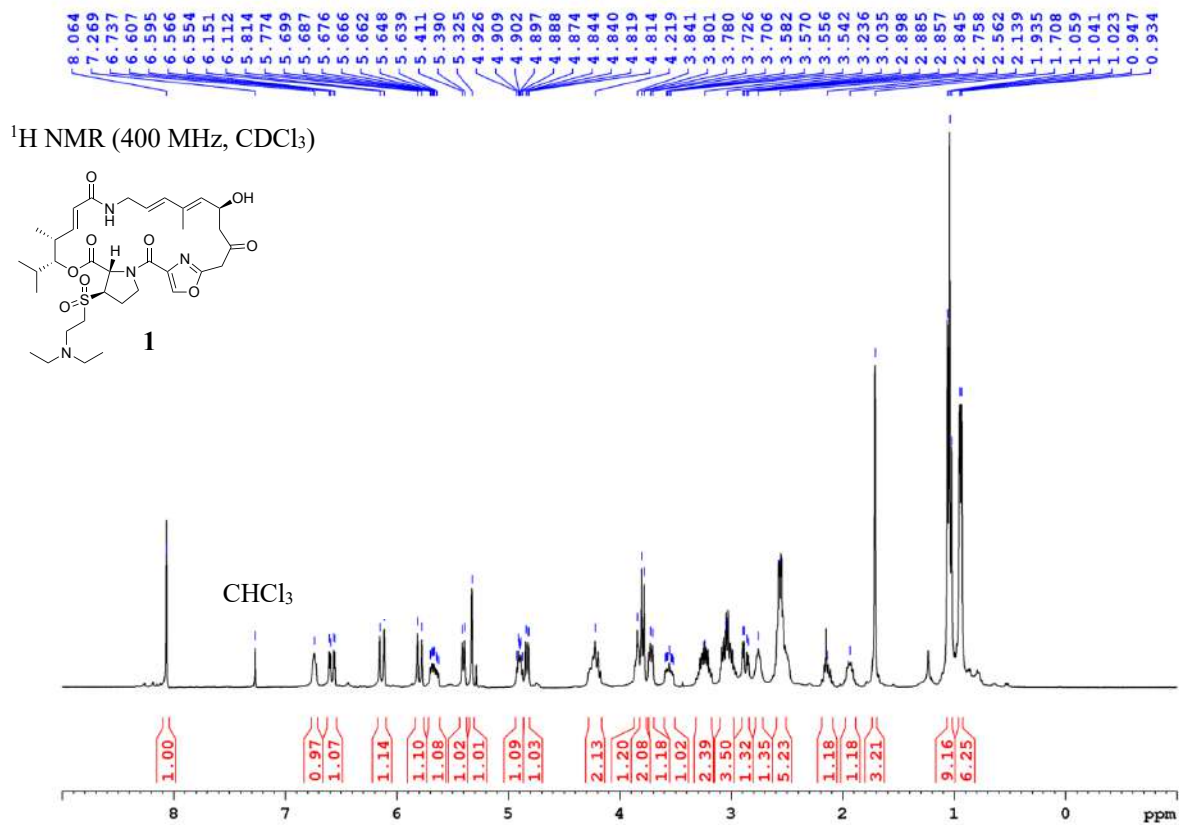


Fig. S13. ¹H NMR and ¹³C NMR spectra of compound **1**.

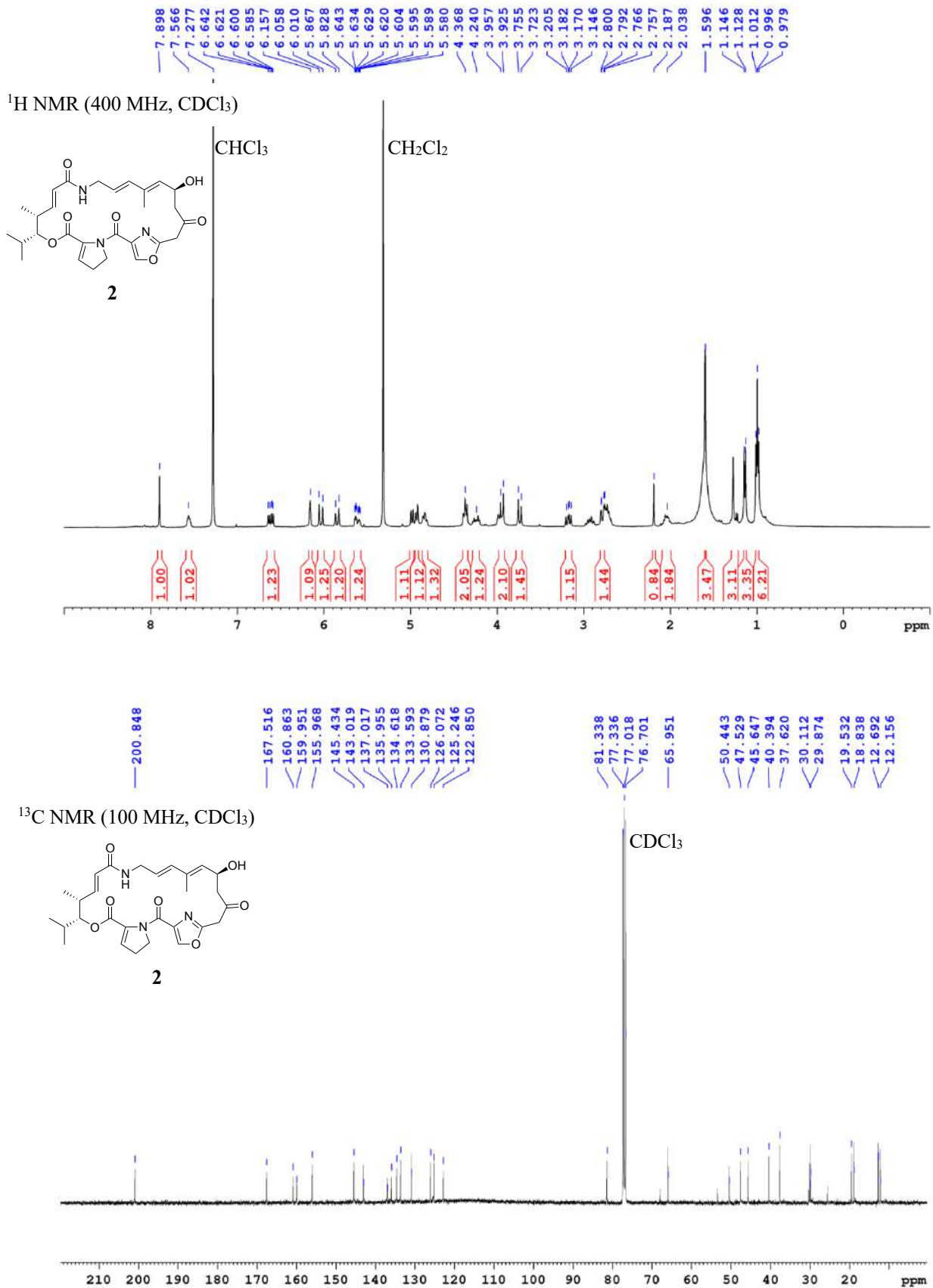


Fig. S14. ¹H NMR and ¹³C NMR spectra of compound **2**.

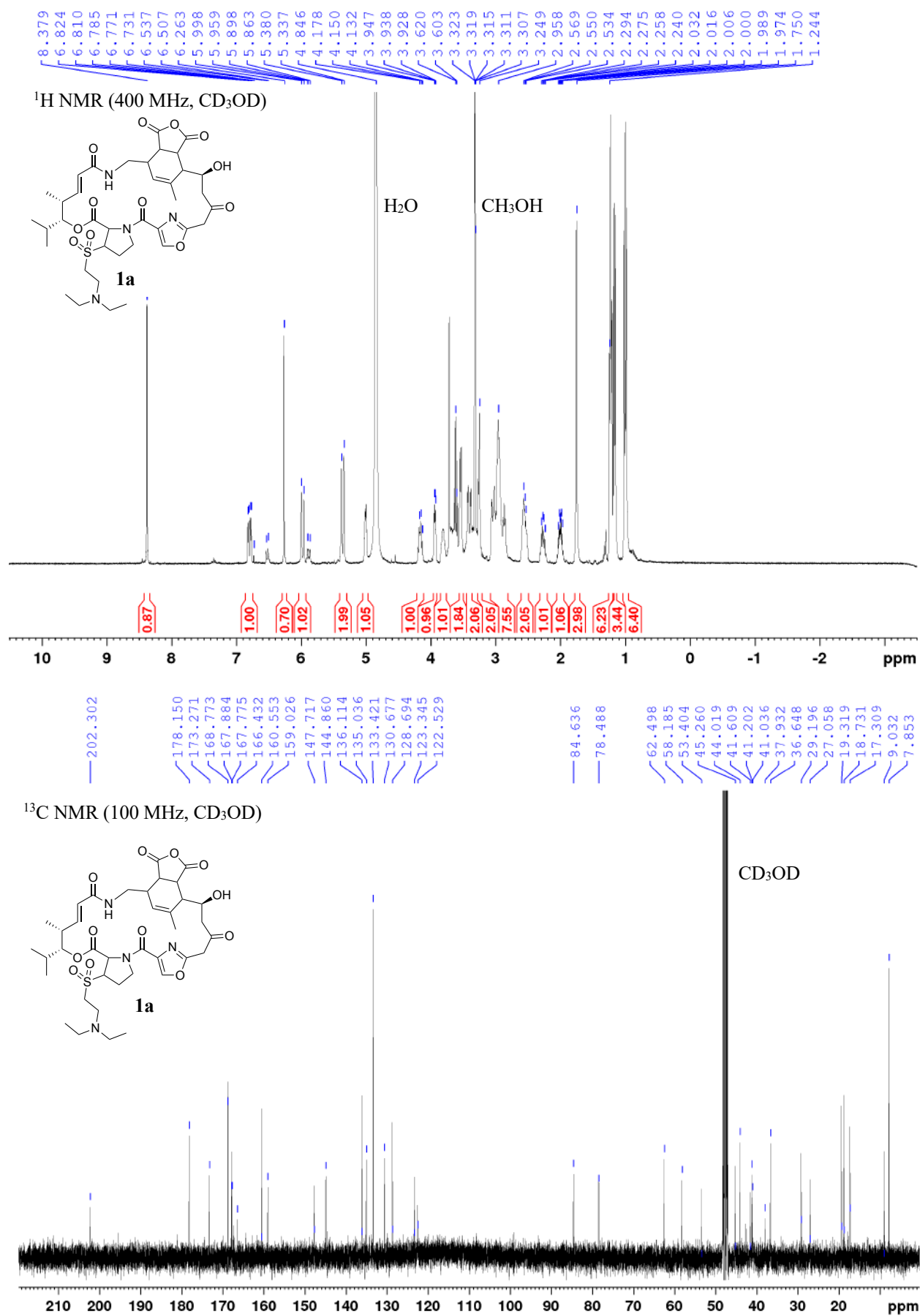


Fig. S15. ¹H NMR and ¹³C NMR spectra of compound **1a**.

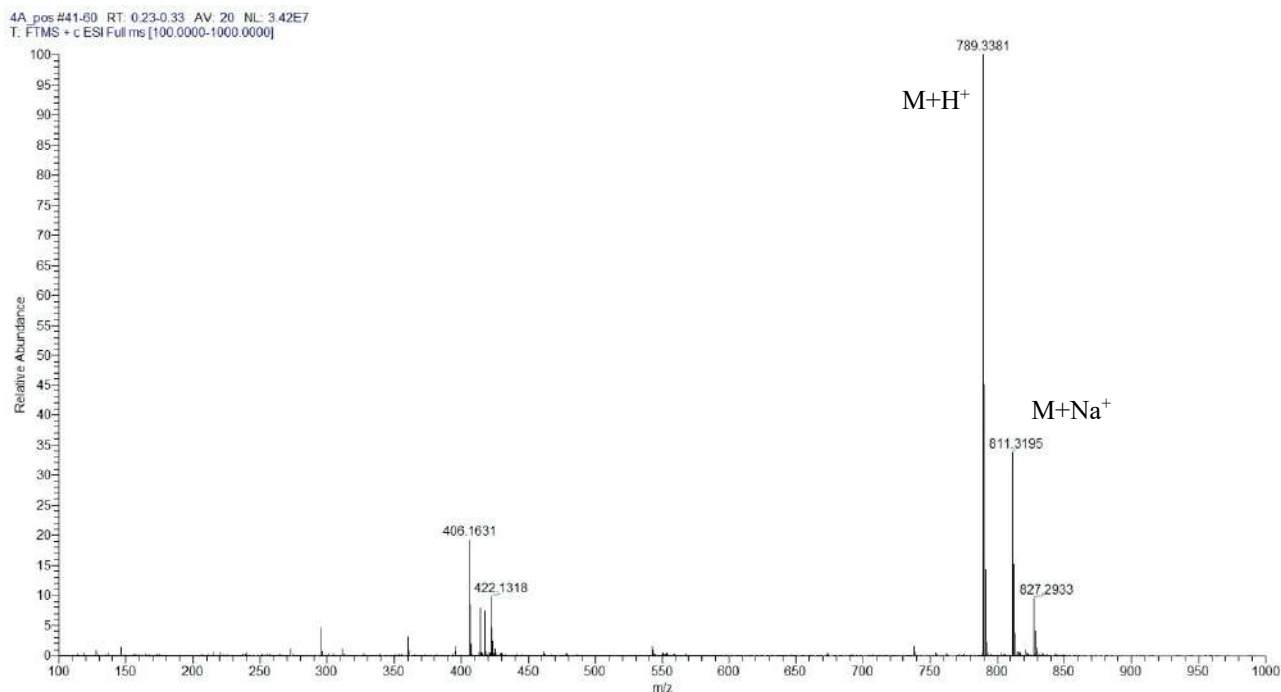


Fig. S16. High resolution ESI(+)-MS spectrum of compound **1a**.

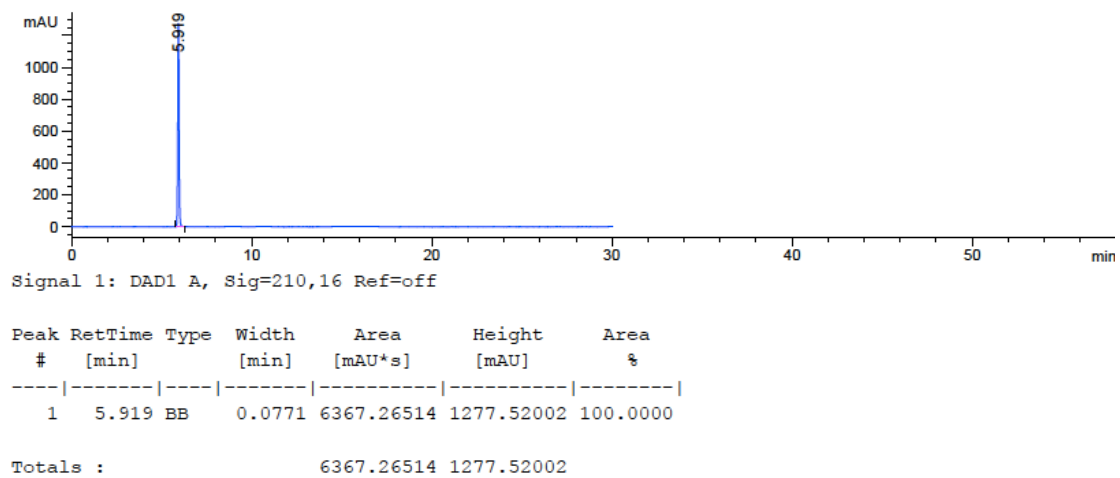


Fig. S17. HPLC chromatogram of compound **1a** (RP18 column, isocratic water/acetonitrile 30:70 + 1% trifluoroacetic acid).

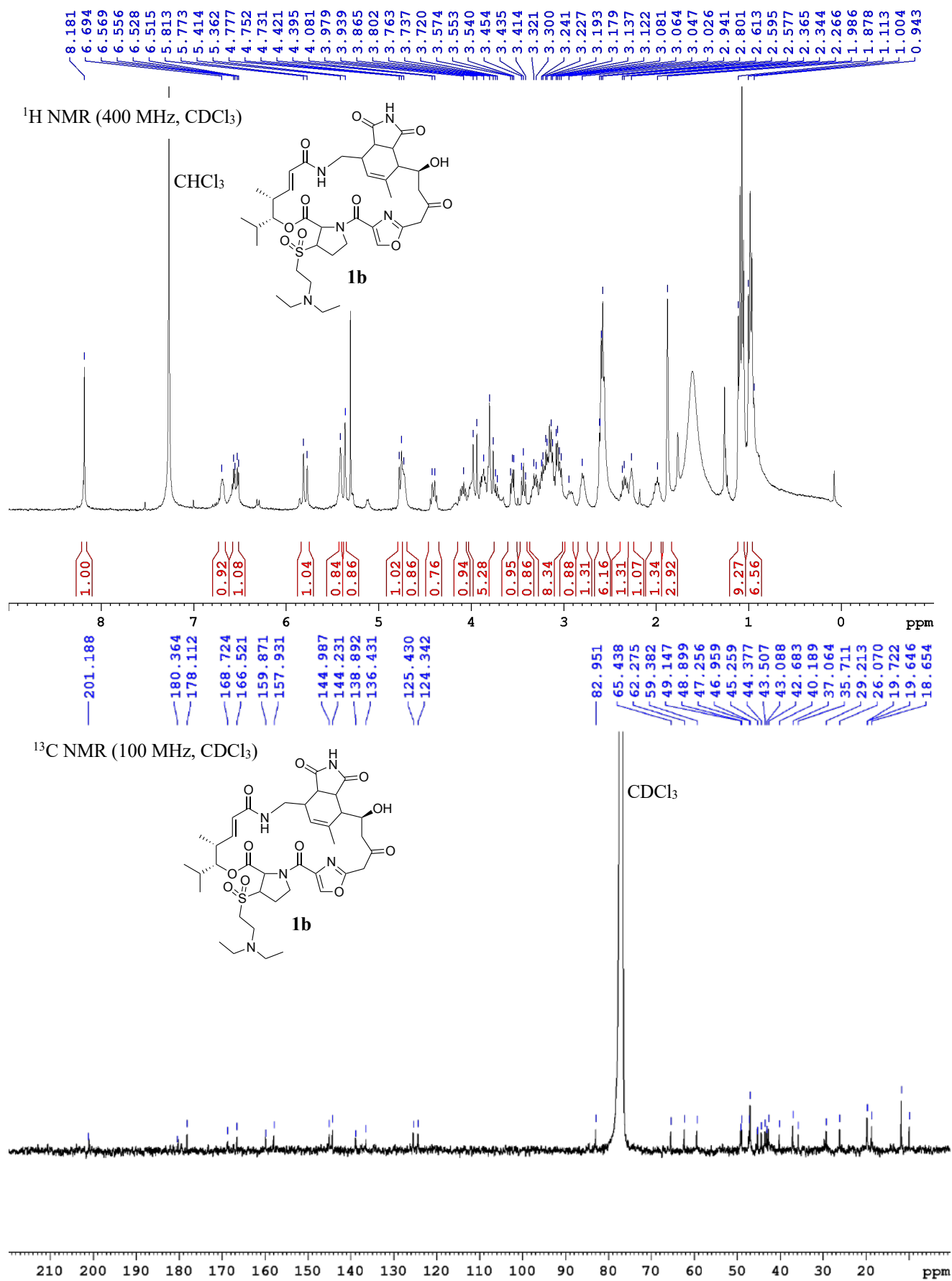


Fig. S18. ¹H NMR and ¹³C NMR spectra of compound **1b**.

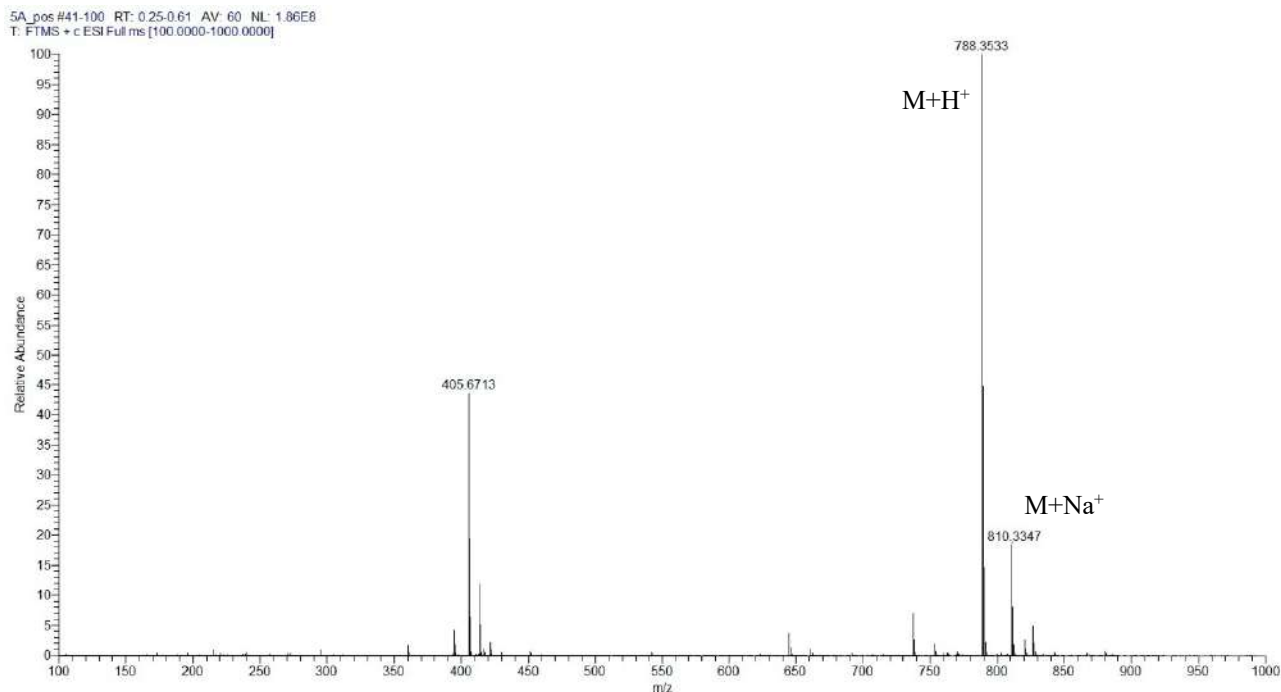


Fig. S19. High resolution ESI(+)-MS spectrum of compound **1b**.

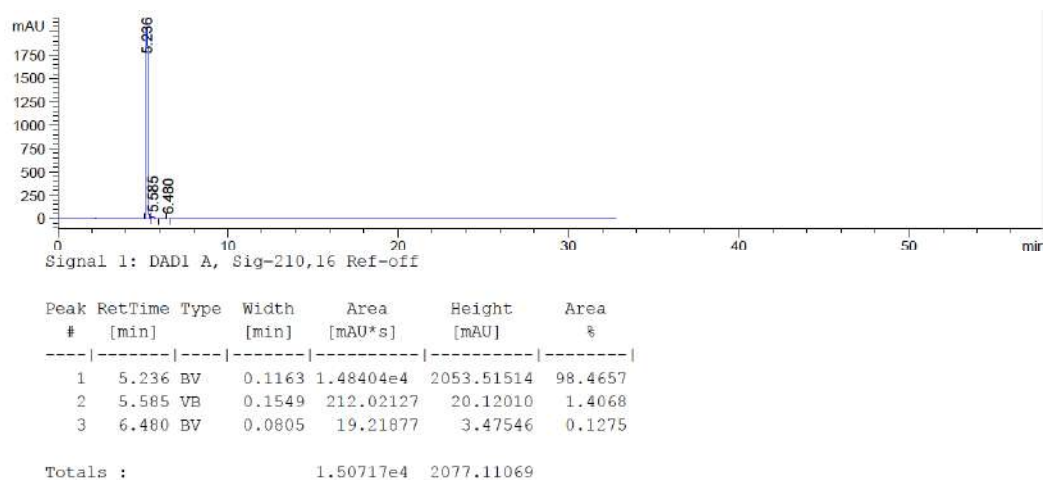


Fig. S20. HPLC chromatogram of compound **1b** (RP18 column, isocratic water/acetonitrile 30:70 + 1% trifluoroacetic acid).

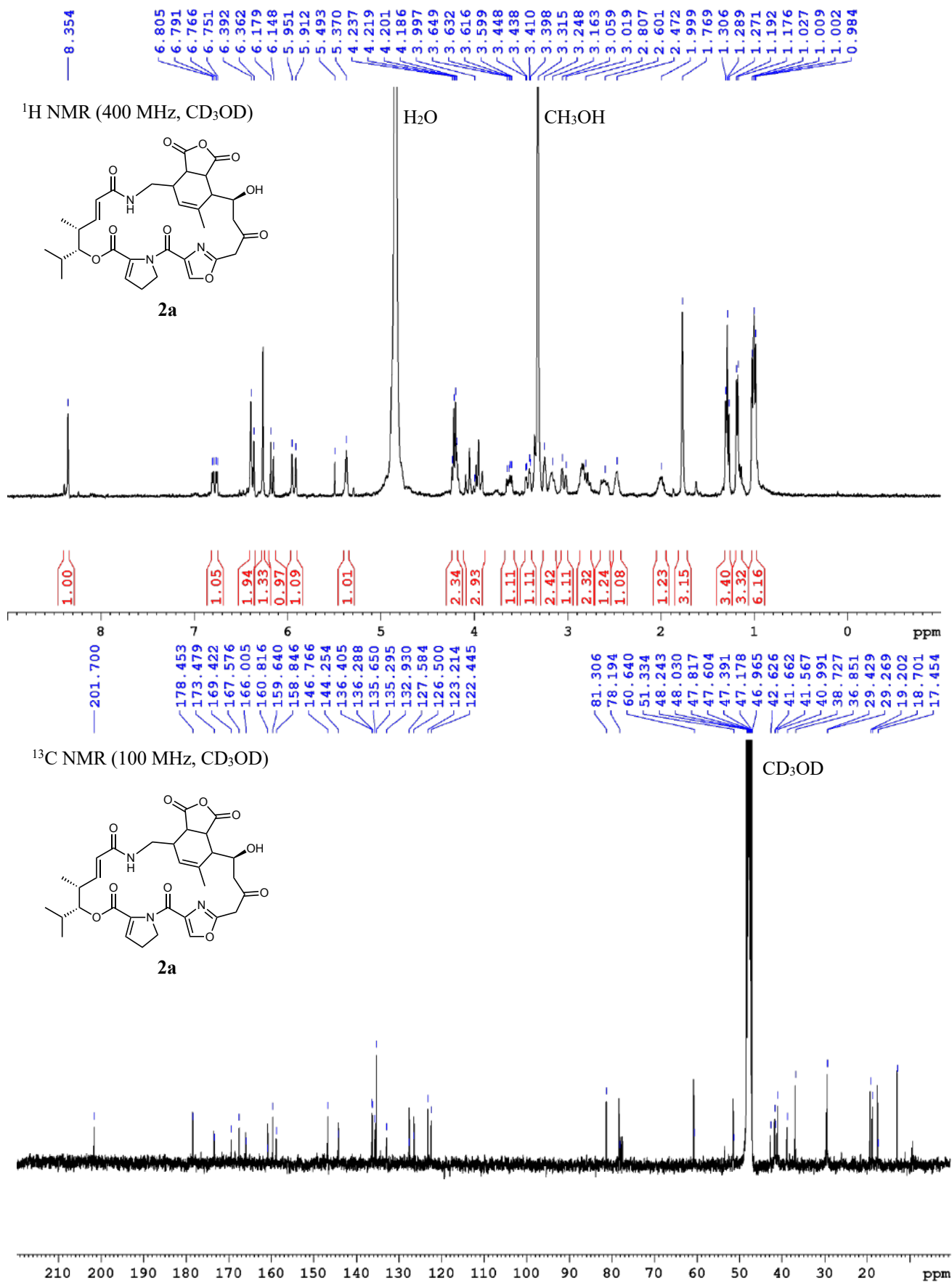


Fig. S21. ¹H NMR and ¹³C NMR spectra of compound **2a**.

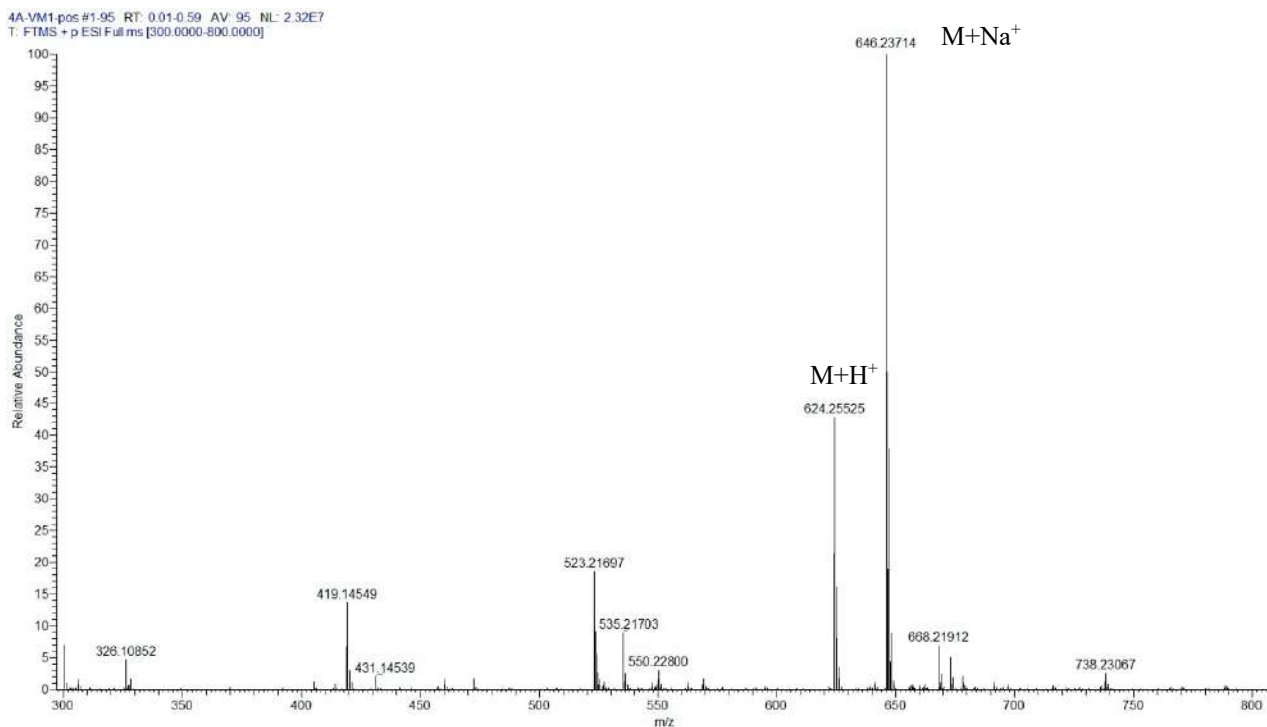


Fig. S22. High resolution ESI(+)-MS spectrum of compound **2a**.

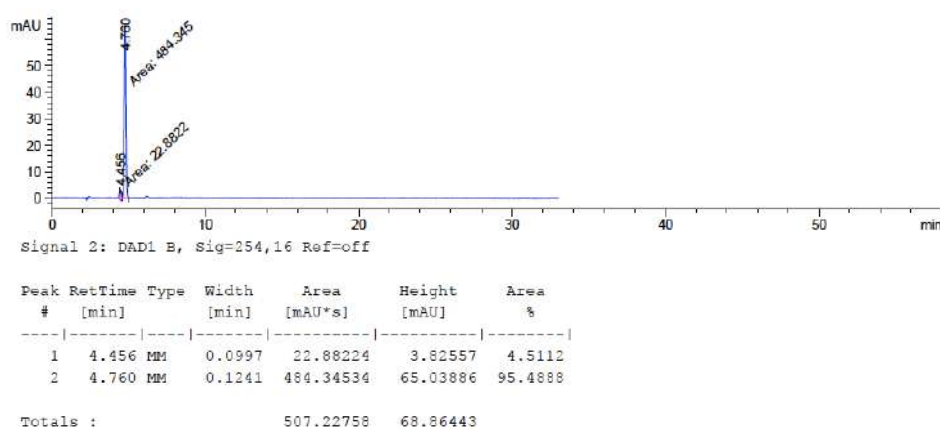


Fig. S23. HPLC chromatogram of compound **2a** (RP18 column, gradient water/acetonitrile 30:70 to 80:20).

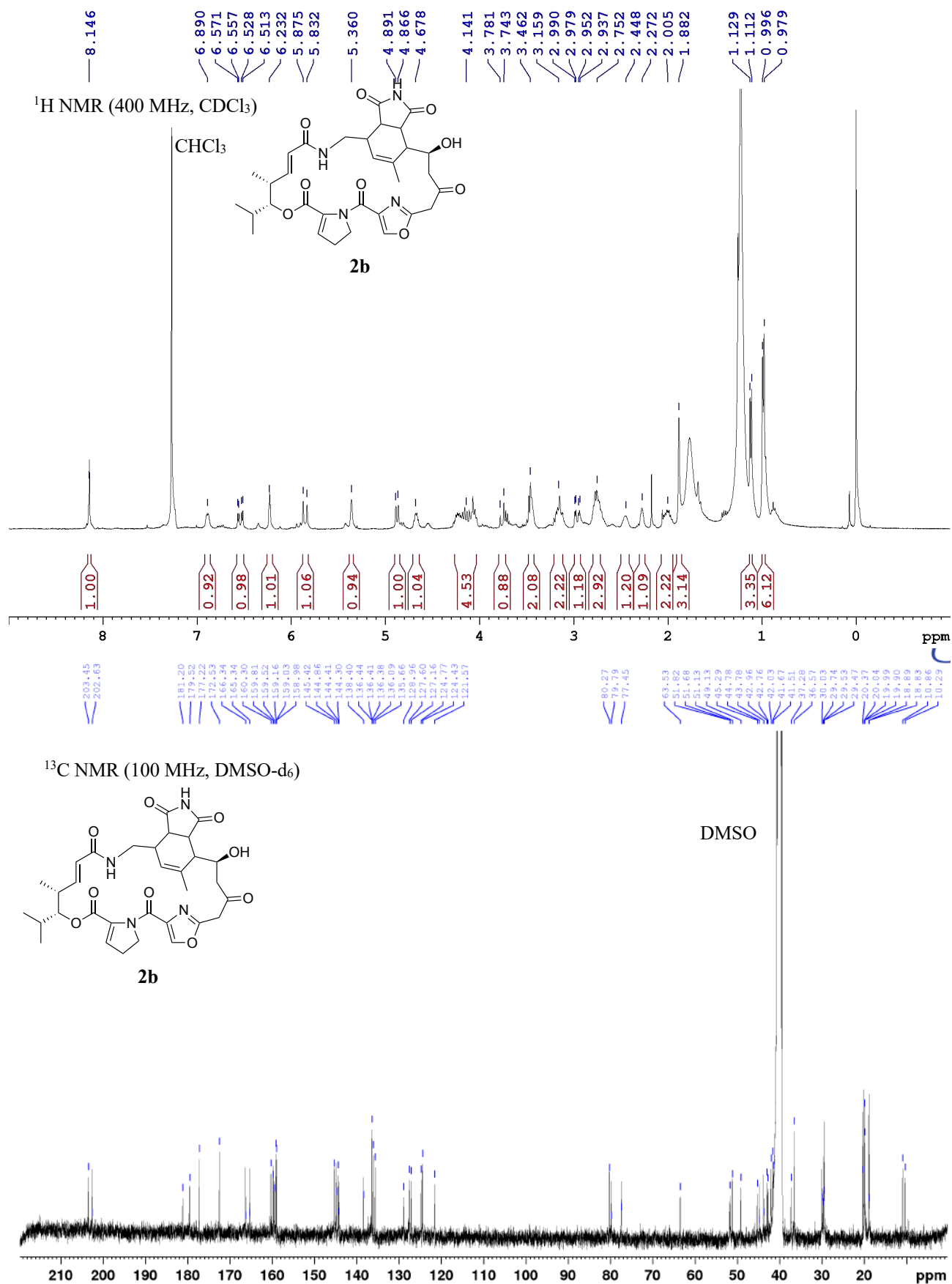


Fig. S24. ¹H NMR and ¹³C NMR spectra of compound **2b**.

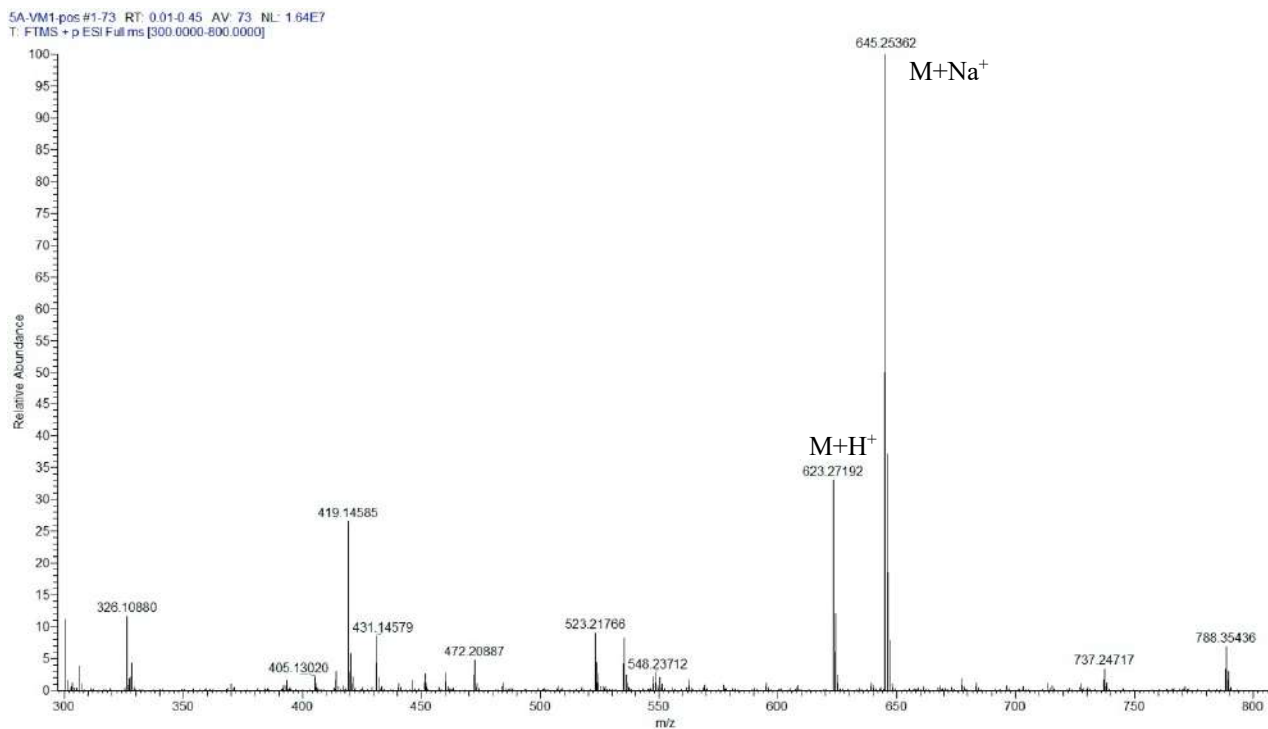


Fig. S25. High resolution ESI(+)-MS spectrum of compound **2b**.

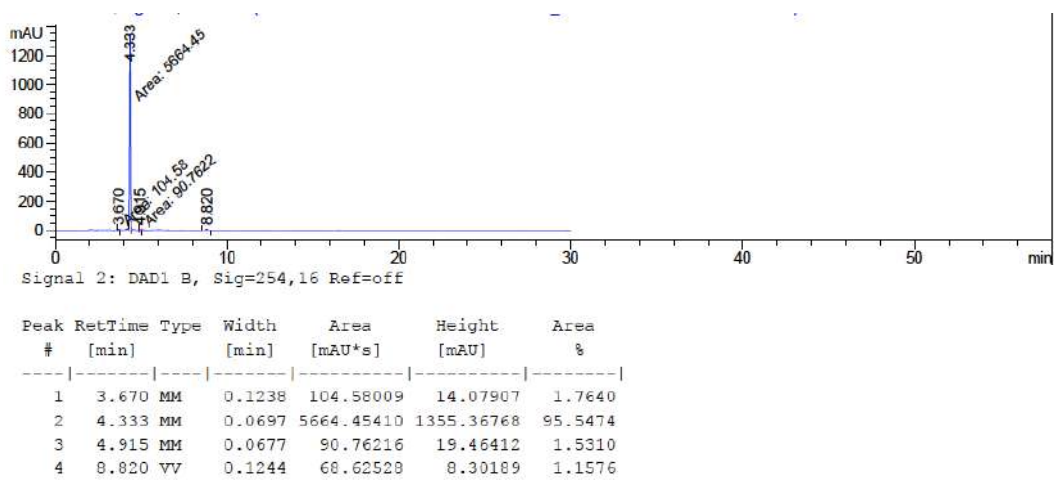


Fig. S26. HPLC chromatogram of compound **2b** (RP18, gradient water/acetonitrile 30:70 to 80:20).

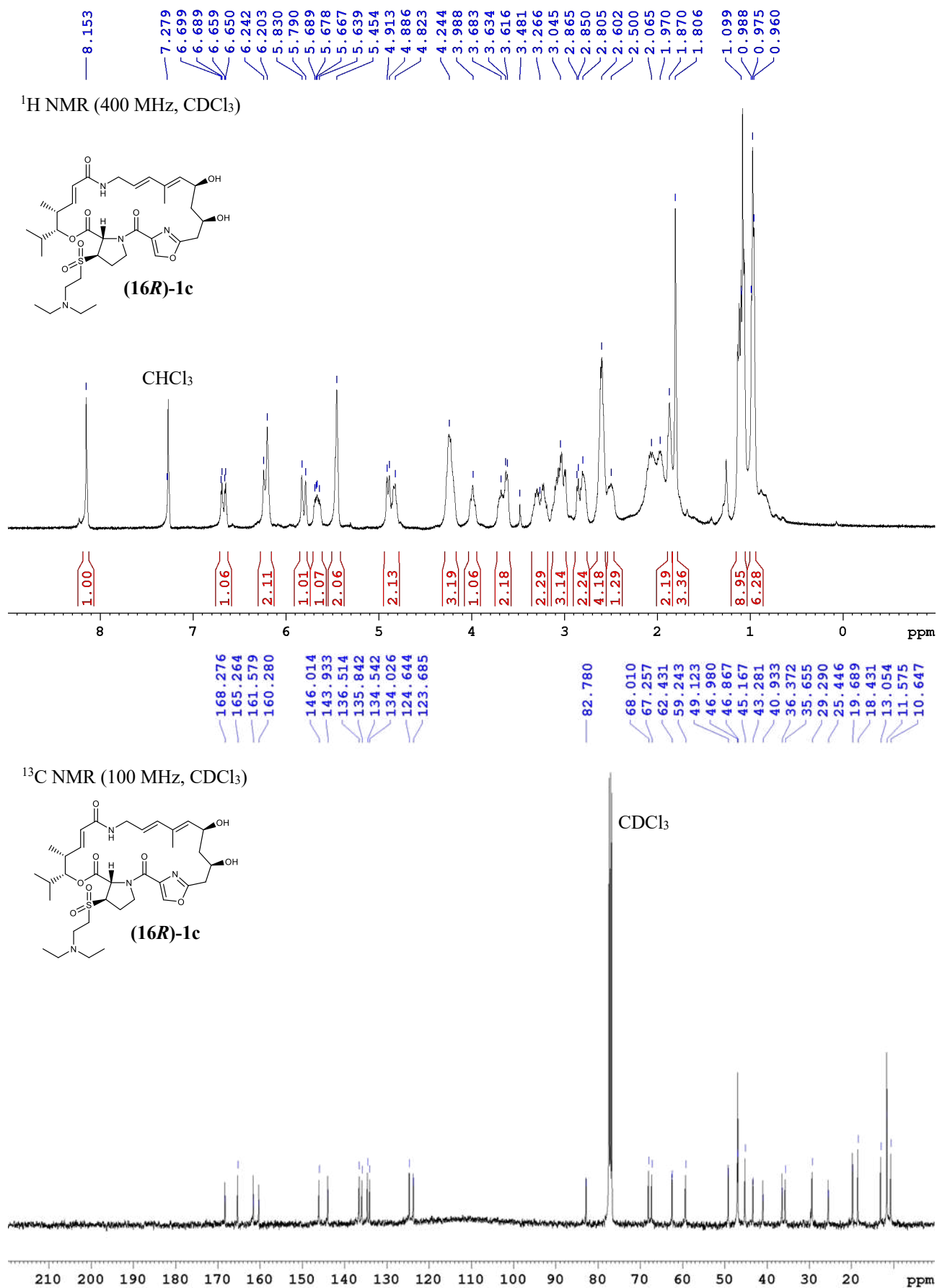


Fig. S27. ¹H NMR and ¹³C NMR spectra of compound (16*R*)-1c.

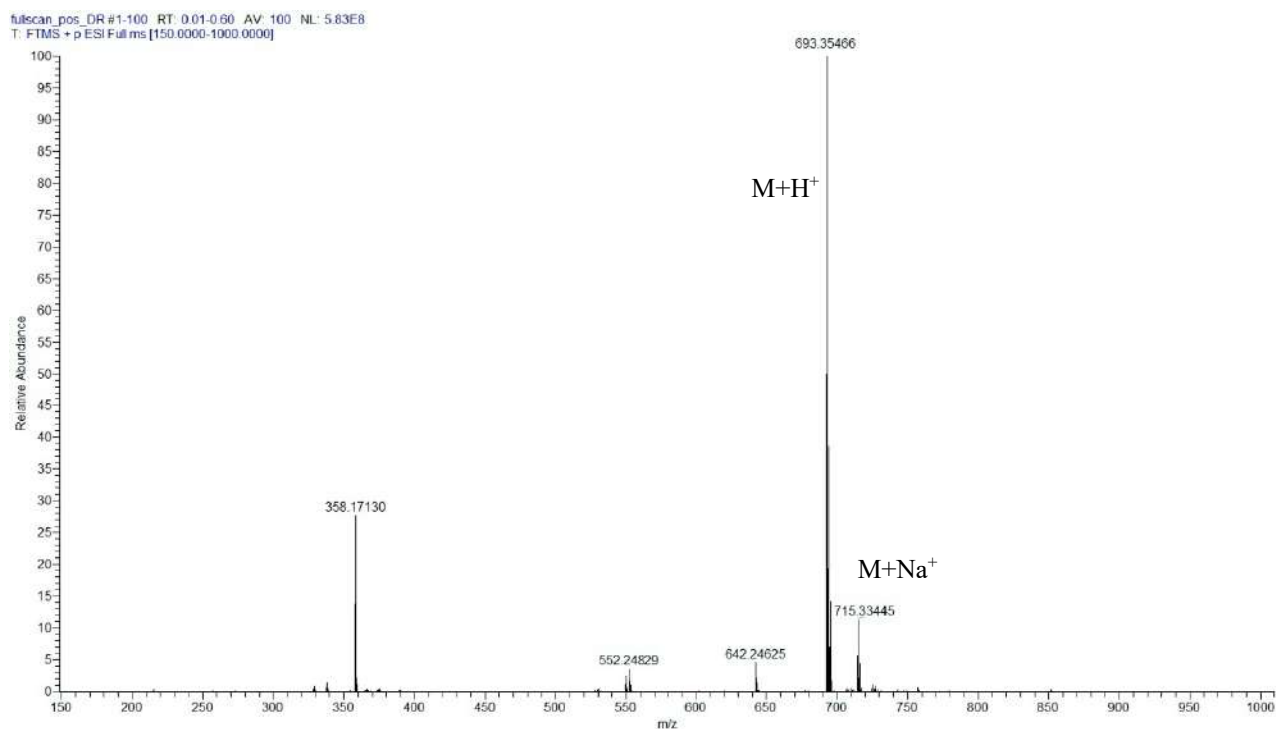


Fig. S28. High resolution ESI(+)-MS spectrum of compound **(16R)-1c**.

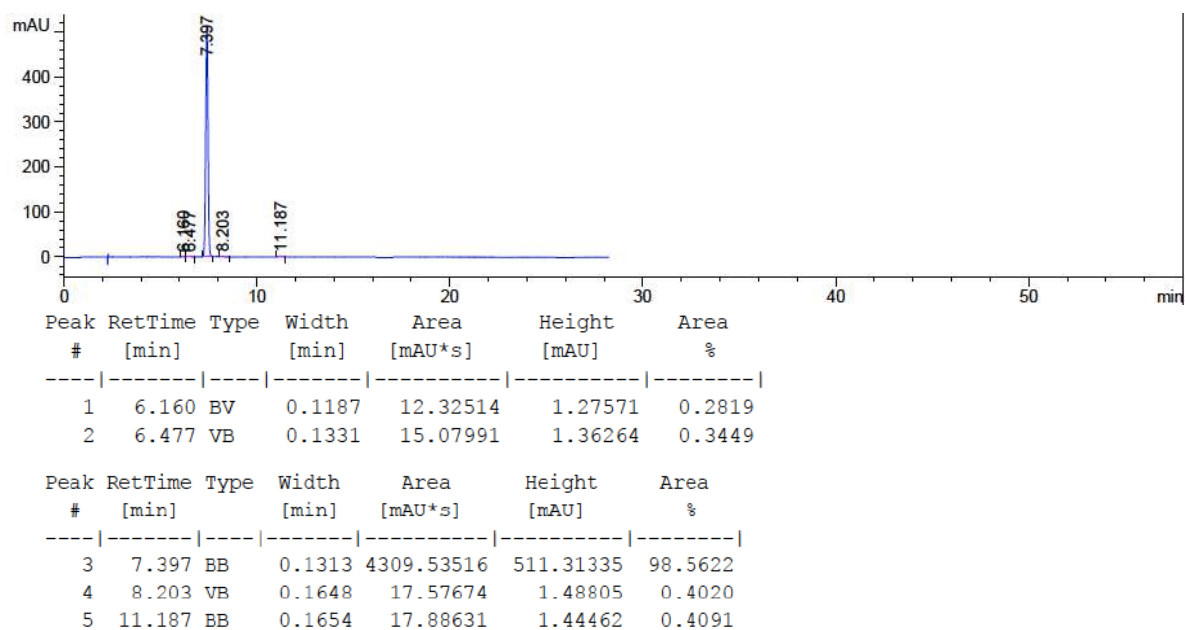


Fig. S29. HPLC chromatogram of compound **(16R)-1c** (RP18, isocratic water/acetonitrile 30:70 + 1% trifluoroacetic acid).

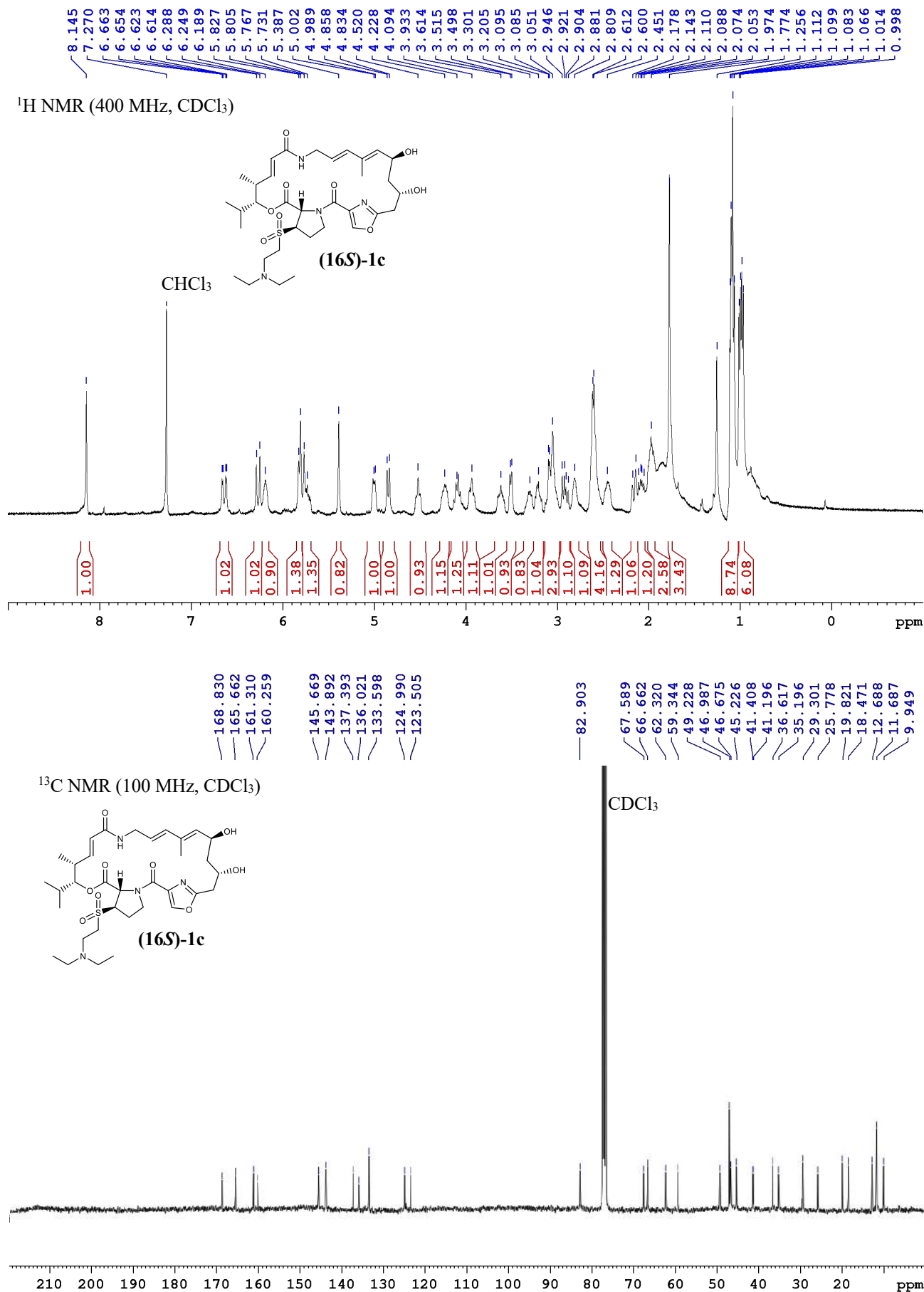


Fig. S30. ¹H NMR and ¹³C NMR spectra of compound (16*S*)-1c.

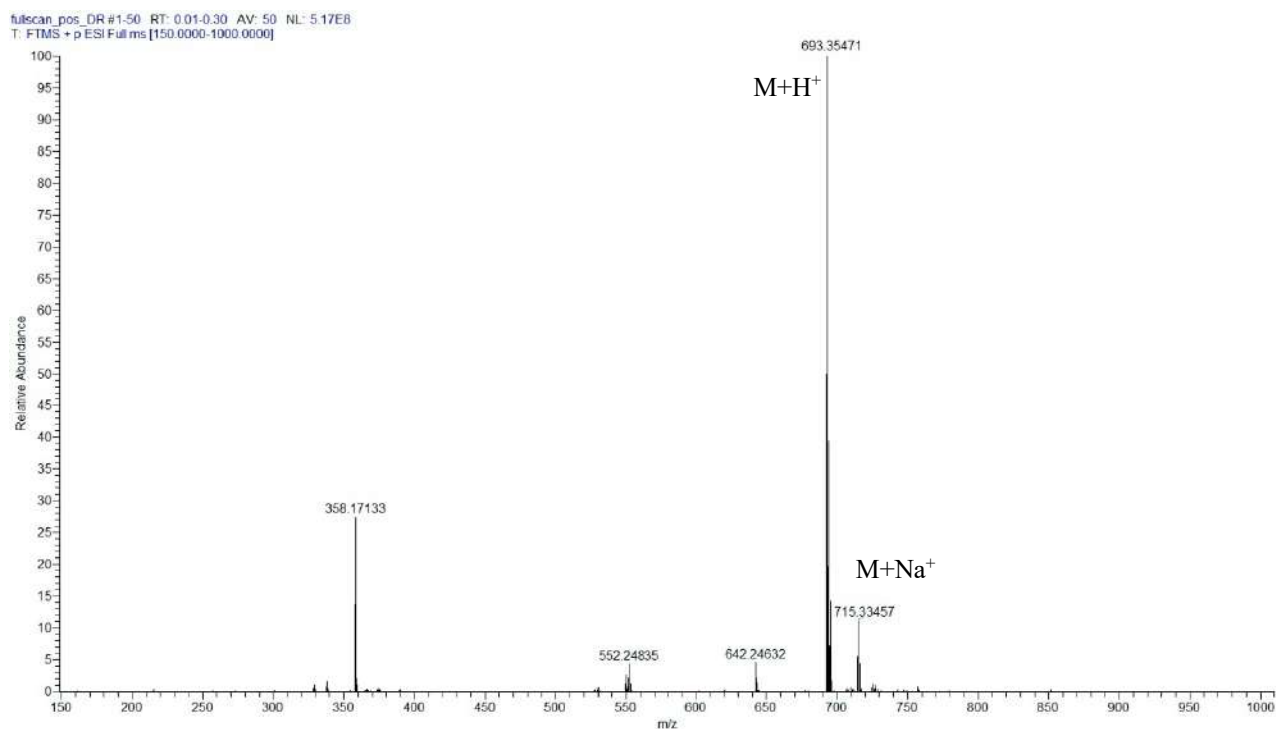


Fig. S31. High resolution ESI(+)-MS spectrum of compound **(16S)-1c**.

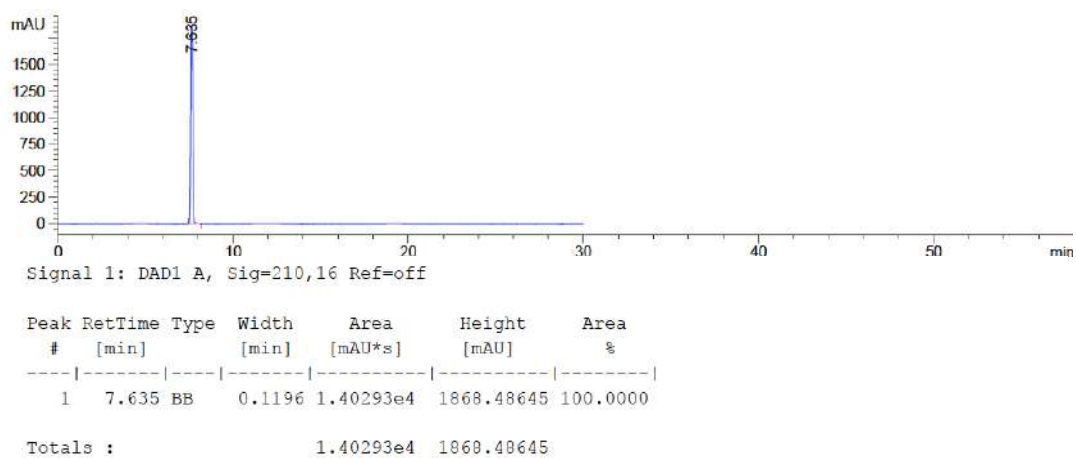


Fig. S32. HPLC chromatogram of compound **(16S)-1c** (RP18, isocratic water/acetonitrile 30:70 + 1% trifluoroacetic acid).

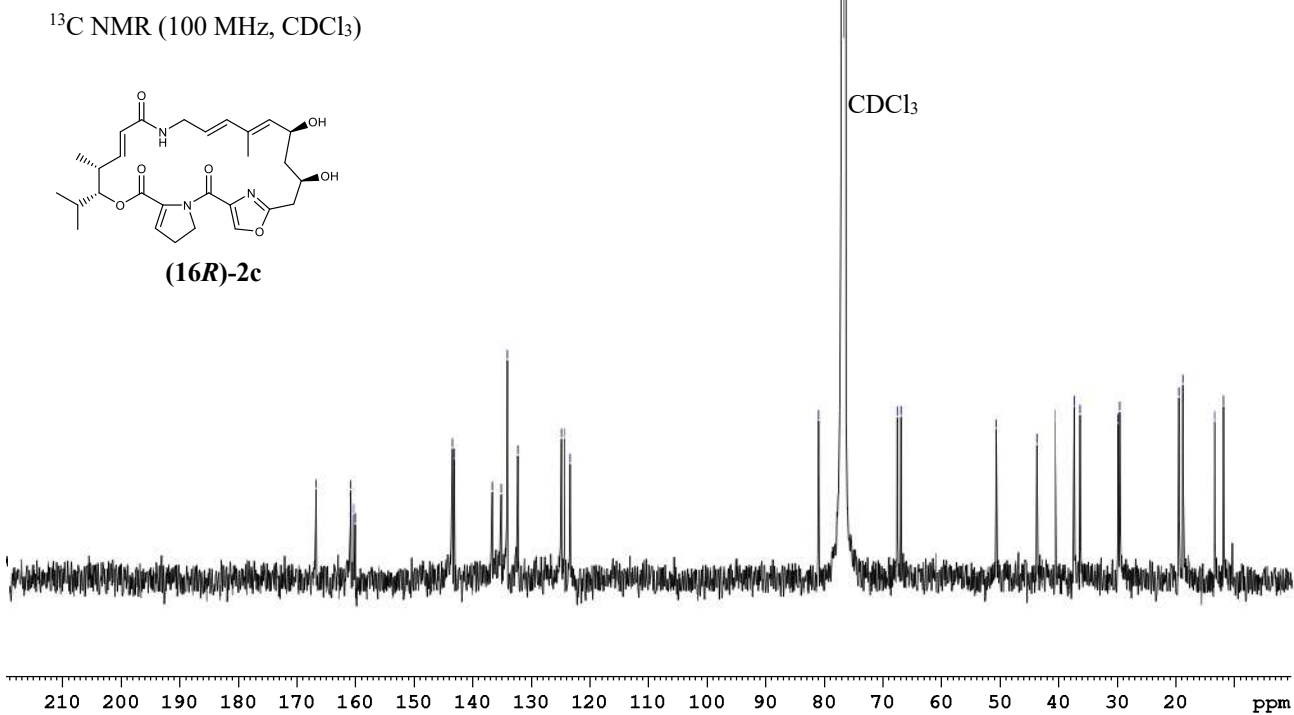
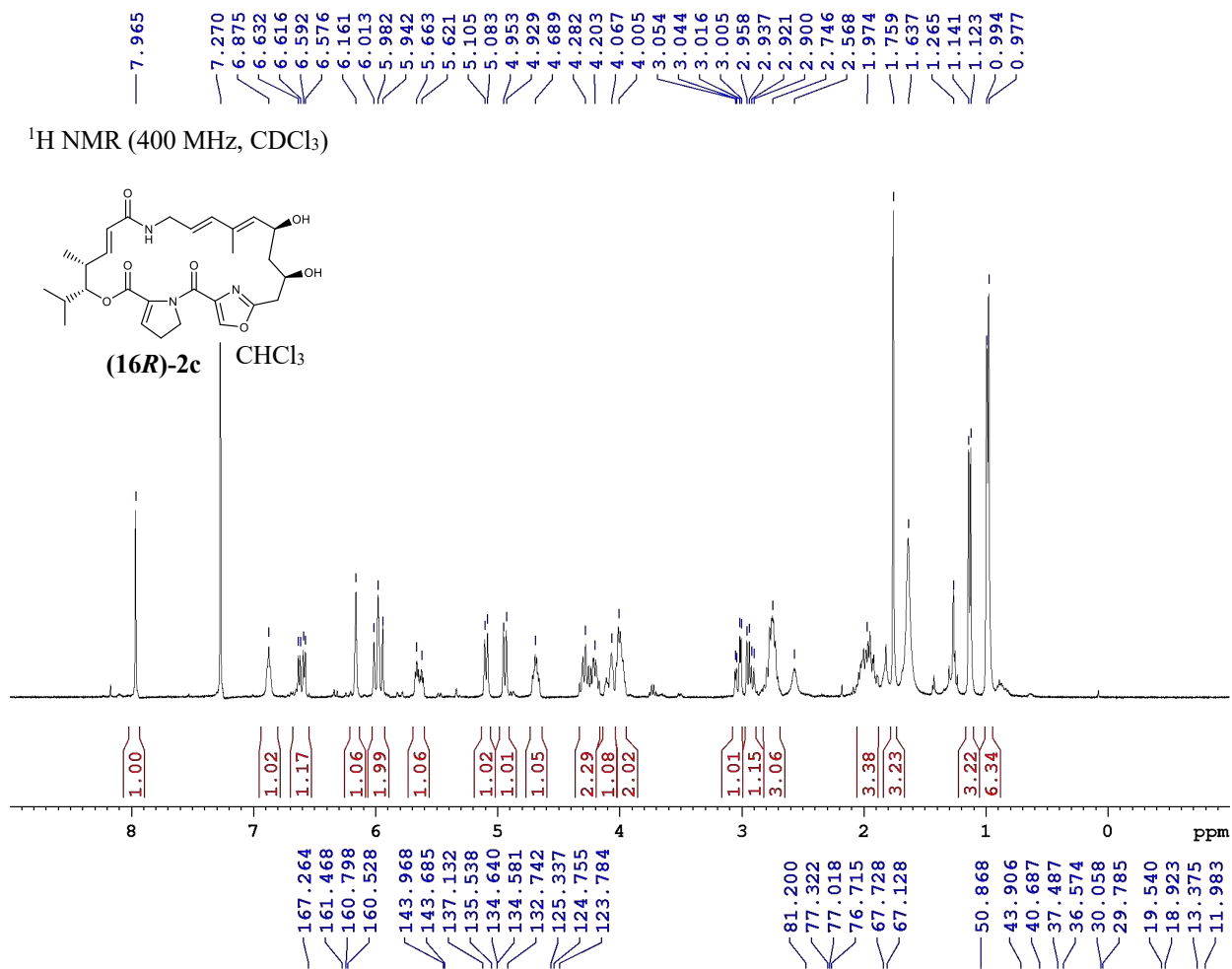


Fig. S33. ¹H NMR and ¹³C NMR spectra of compound (16R)-2c.

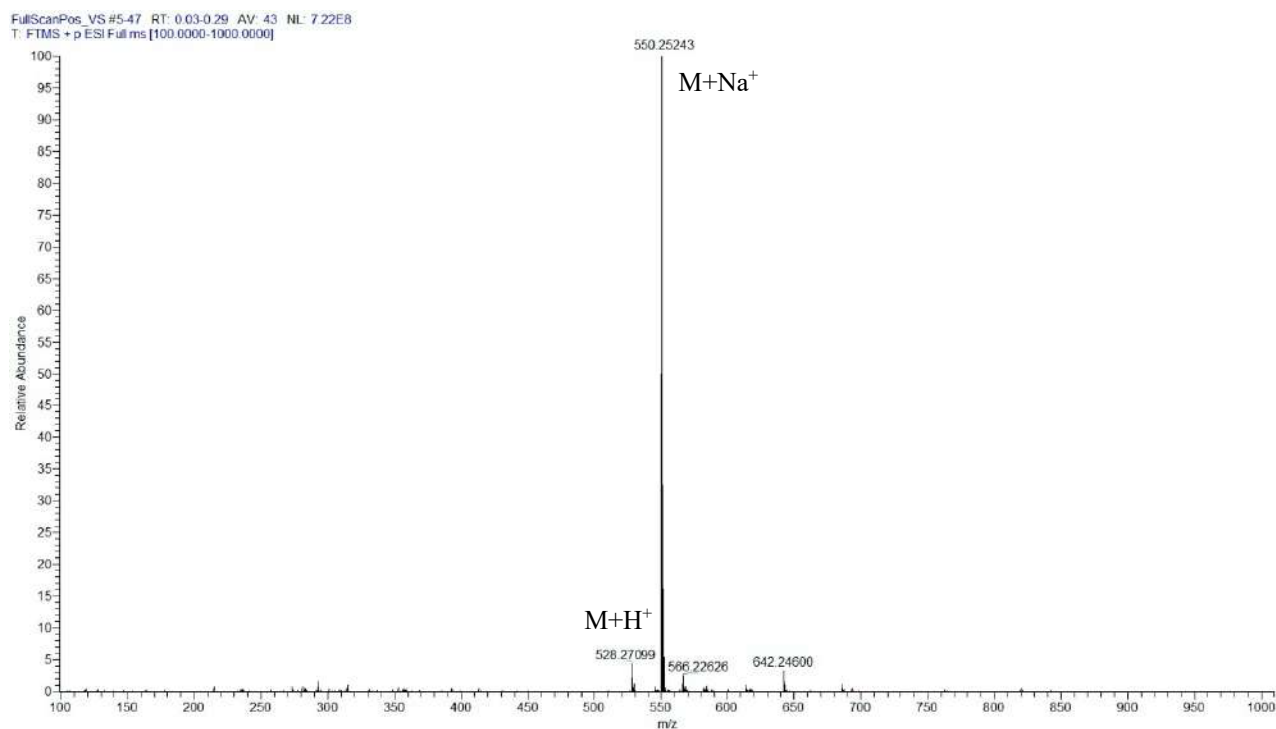
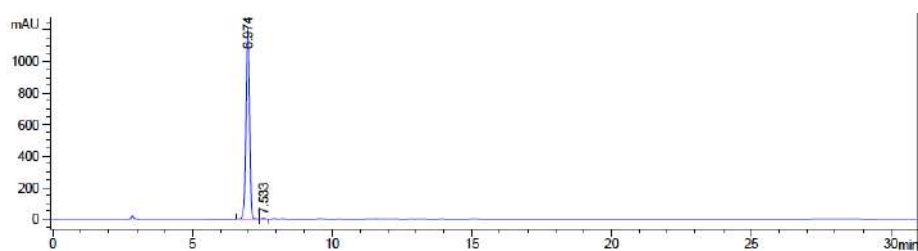


Fig. S34. High resolution ESI(+)-MS spectrum of compound **(16R)-2c**.



Signal 2: DAD1 B, Sig=254,16 Ref=off

Peak #	RetTime [min]	Type	Width [min]	Area [mAU*s]	Height [mAU]	Area %
1	6.974	BV	0.1502	1.11277e4	1222.59326	99.5675
2	7.533	VV	0.1482	48.33984	5.41012	0.4325

Totals : 1.11760e4 1228.00338

Fig. S35. HPLC chromatogram of compound **(16R)-2c** (RP18, gradient water/acetonitrile 30:70 to 80:20).

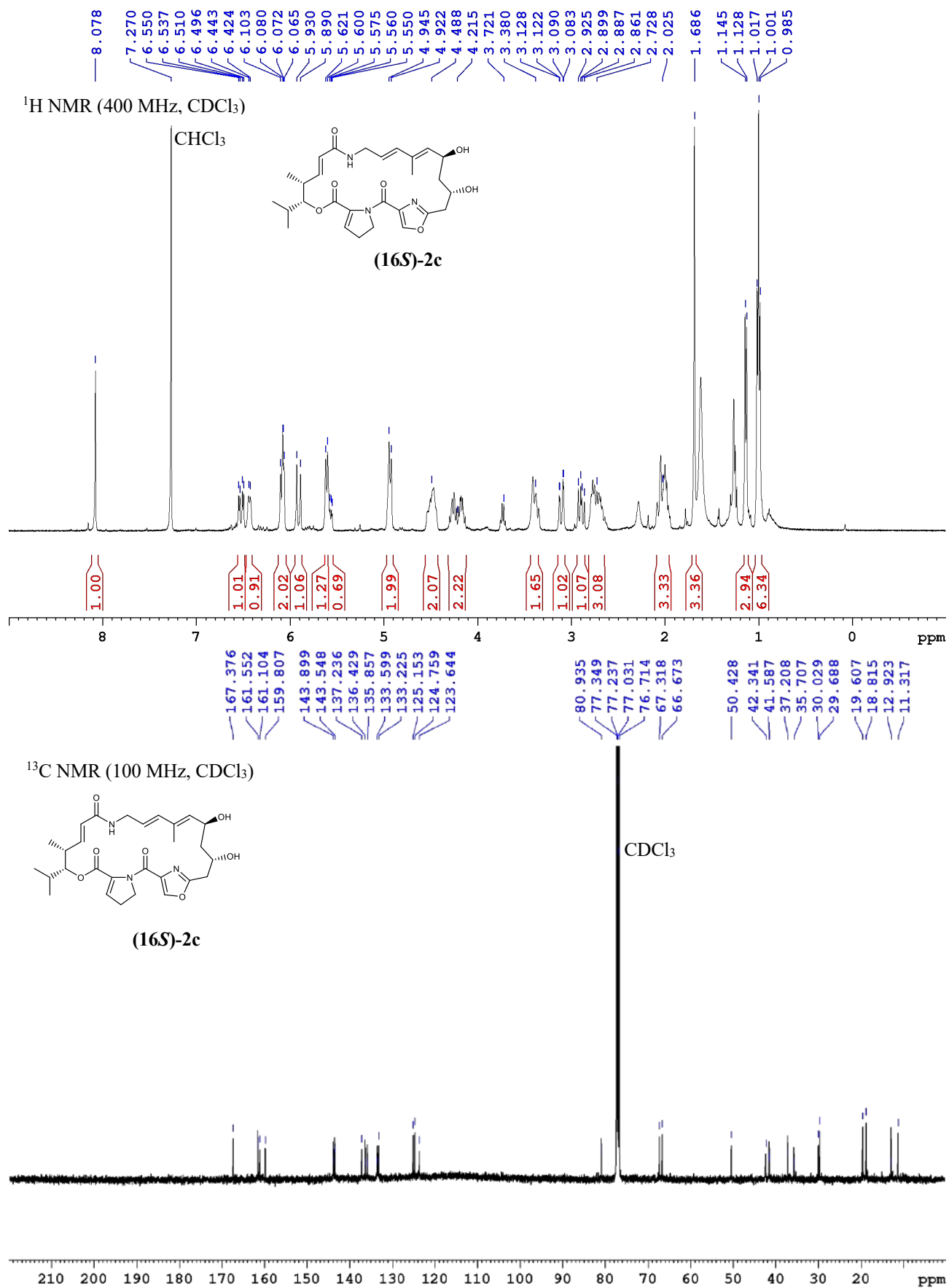


Fig. S36. ¹H NMR and ¹³C NMR spectra of compound (16S)-2c.

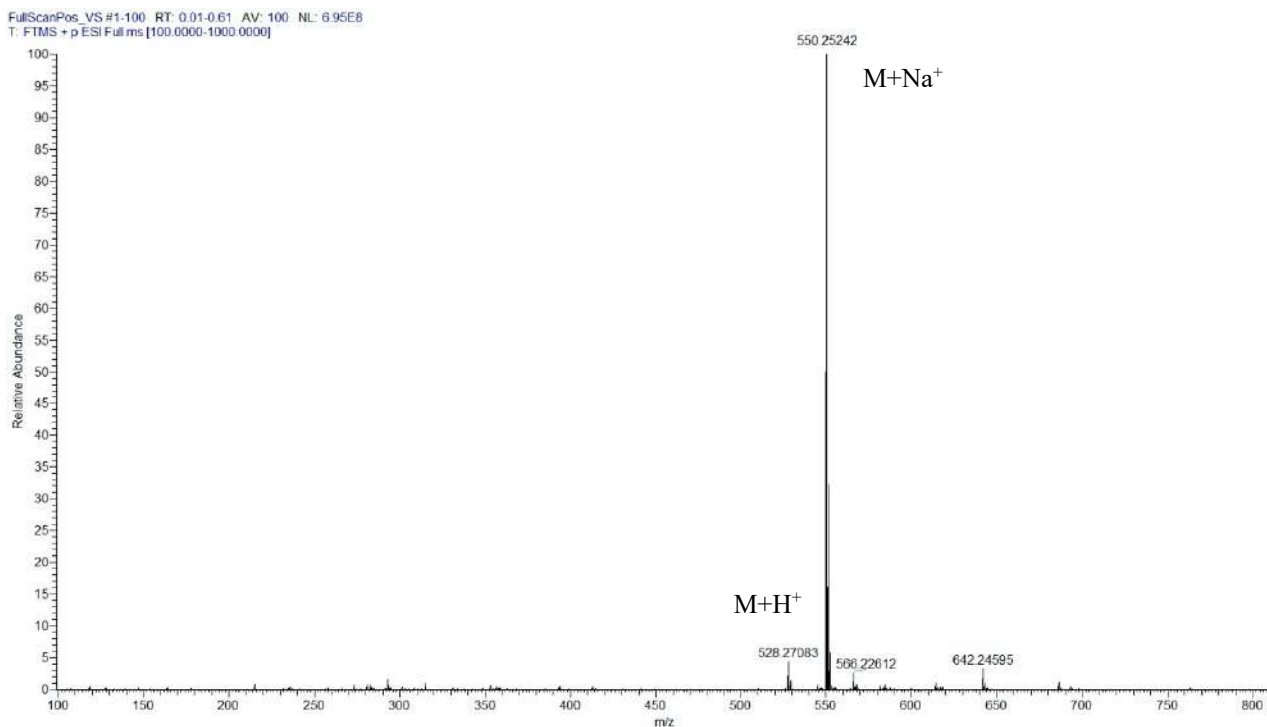


Fig. S37. High resolution ESI(+) MS spectrum of compound (16S)-2c.

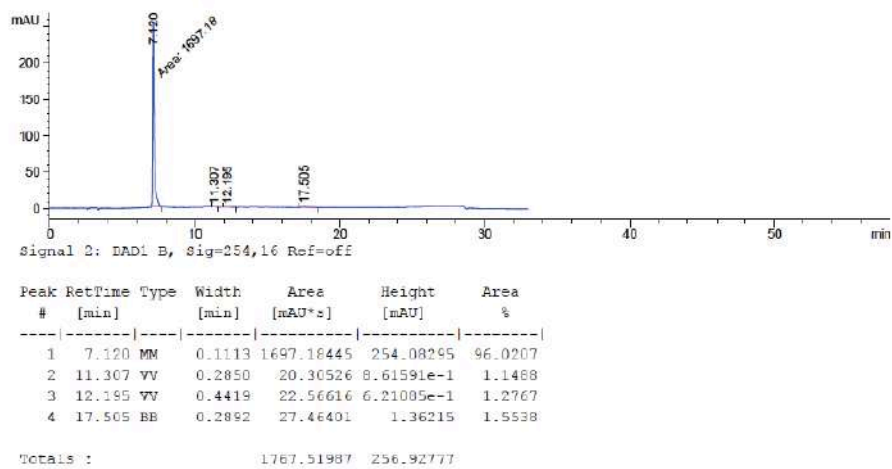


Fig. S38. HPLC chromatogram of compound (16S)-2c (RP18, gradient water/acetonitrile 30:70 to 80:20).

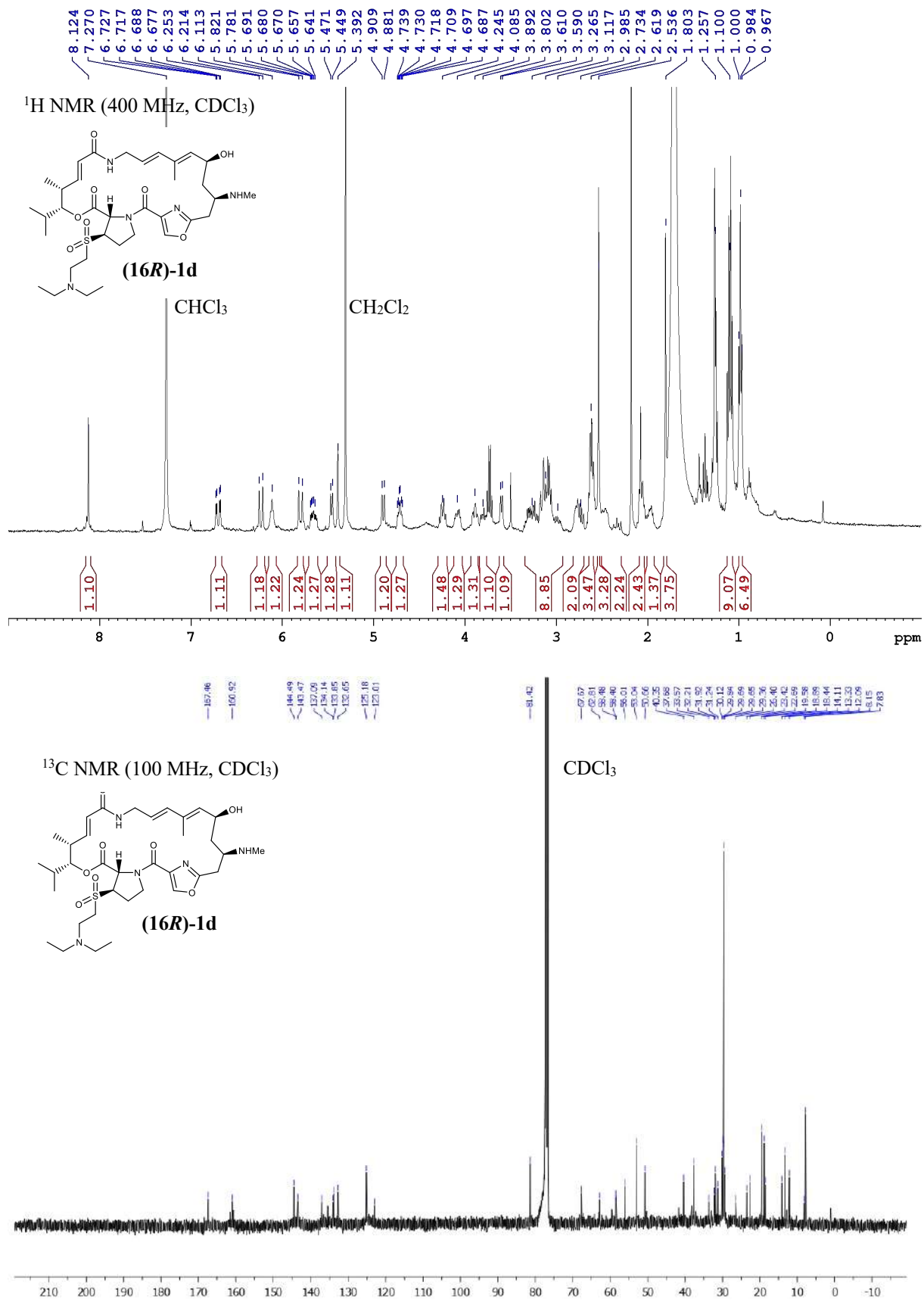


Fig. S39. ¹H NMR and ¹³C NMR spectra of compound (16R)-1d.

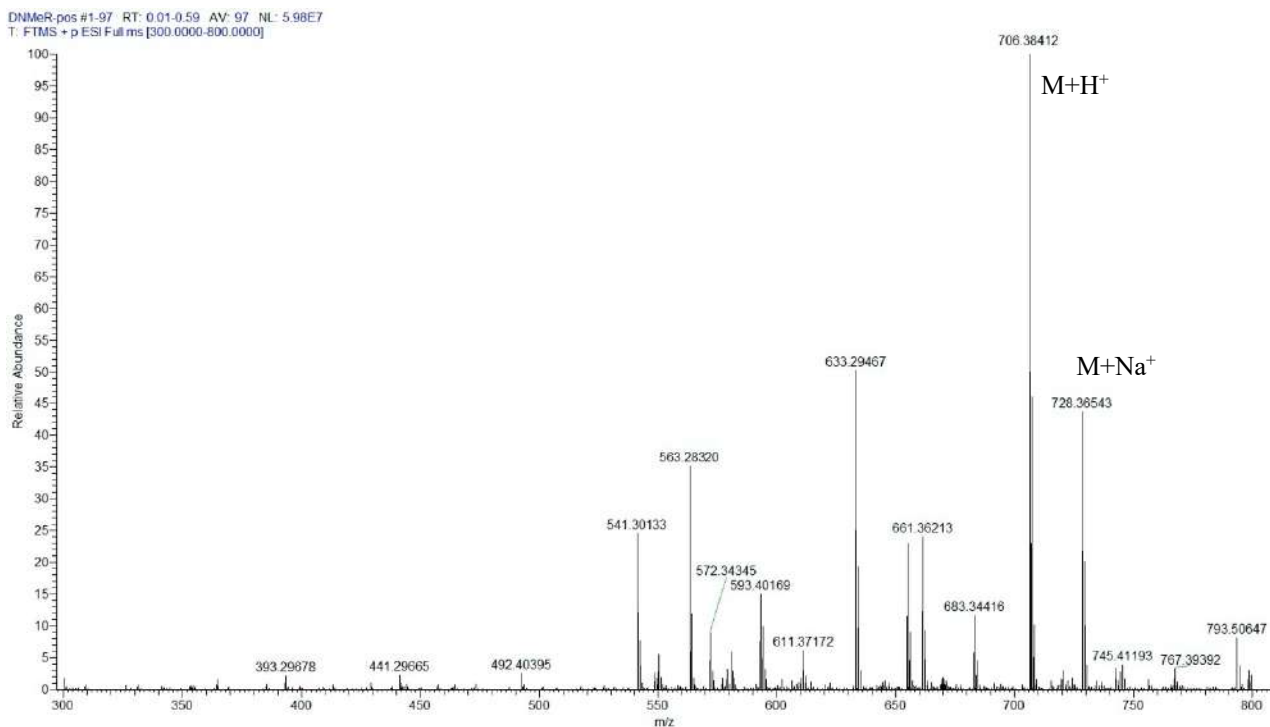


Fig. S40. High resolution ESI(+)-MS spectrum of compound **(16R)-1d**.

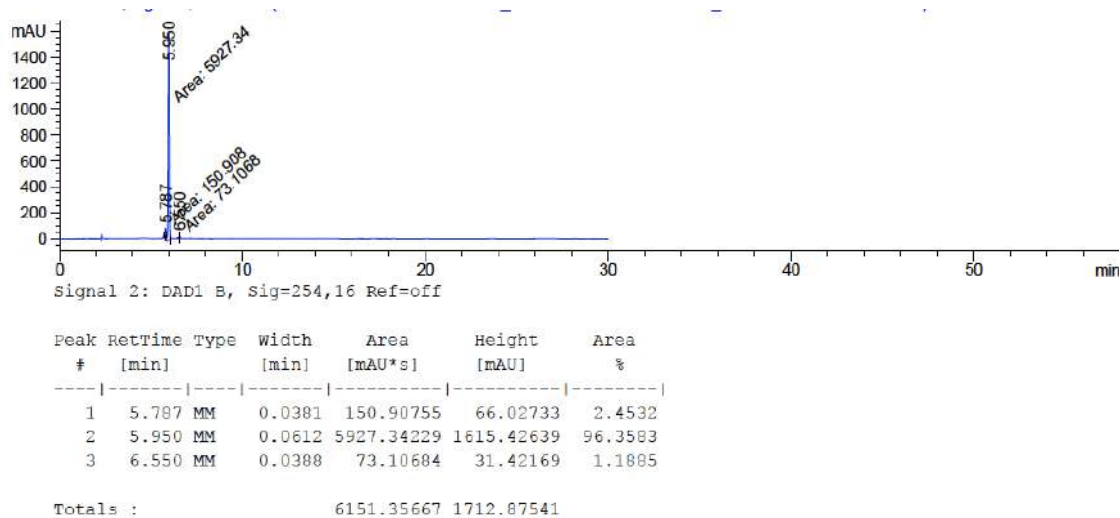


Fig. S41. HPLC chromatogram of compound **(16R)-1d** (RP18, isocratic water/acetonitrile 30:70 + 1% trifluoroacetic acid).

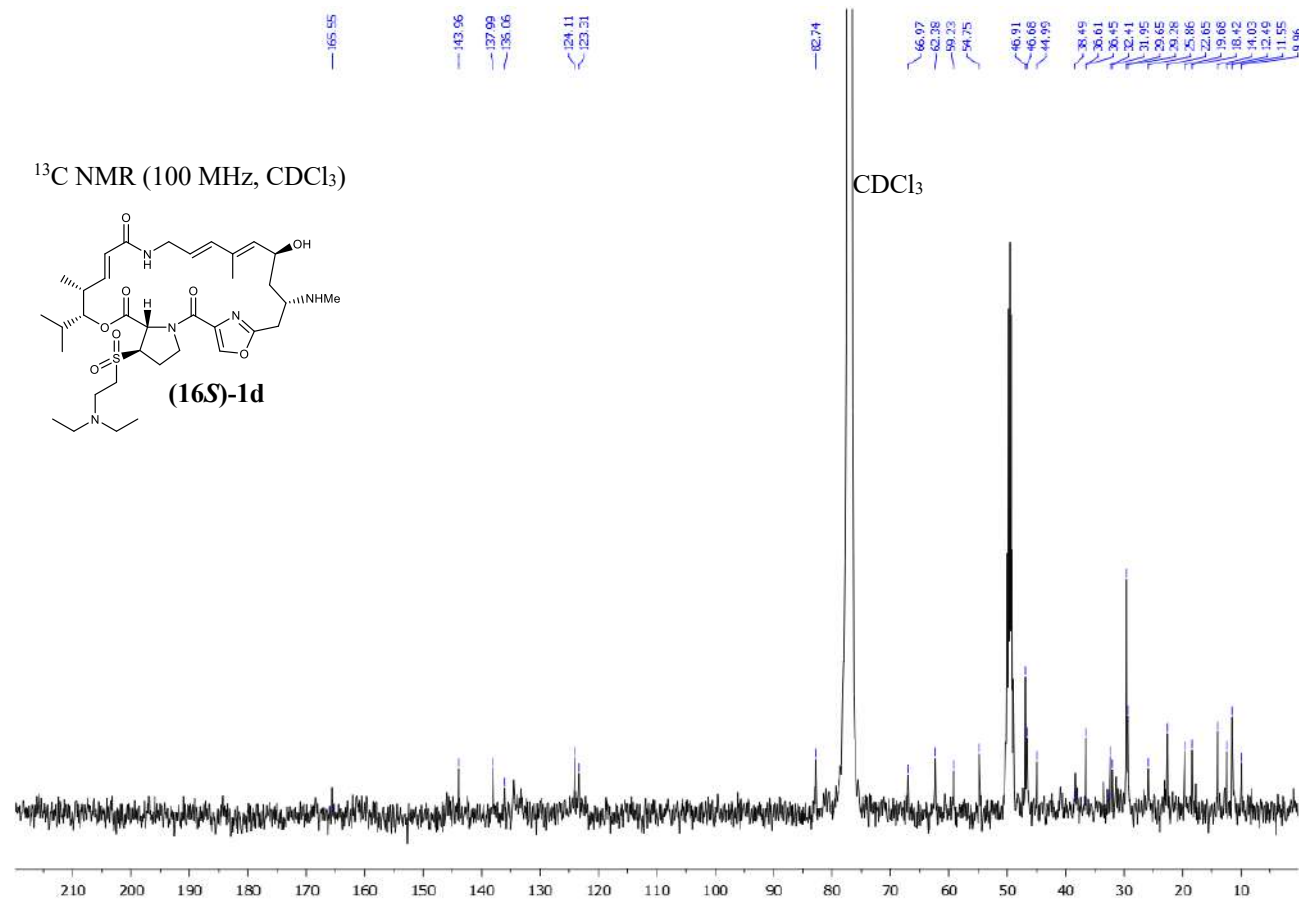
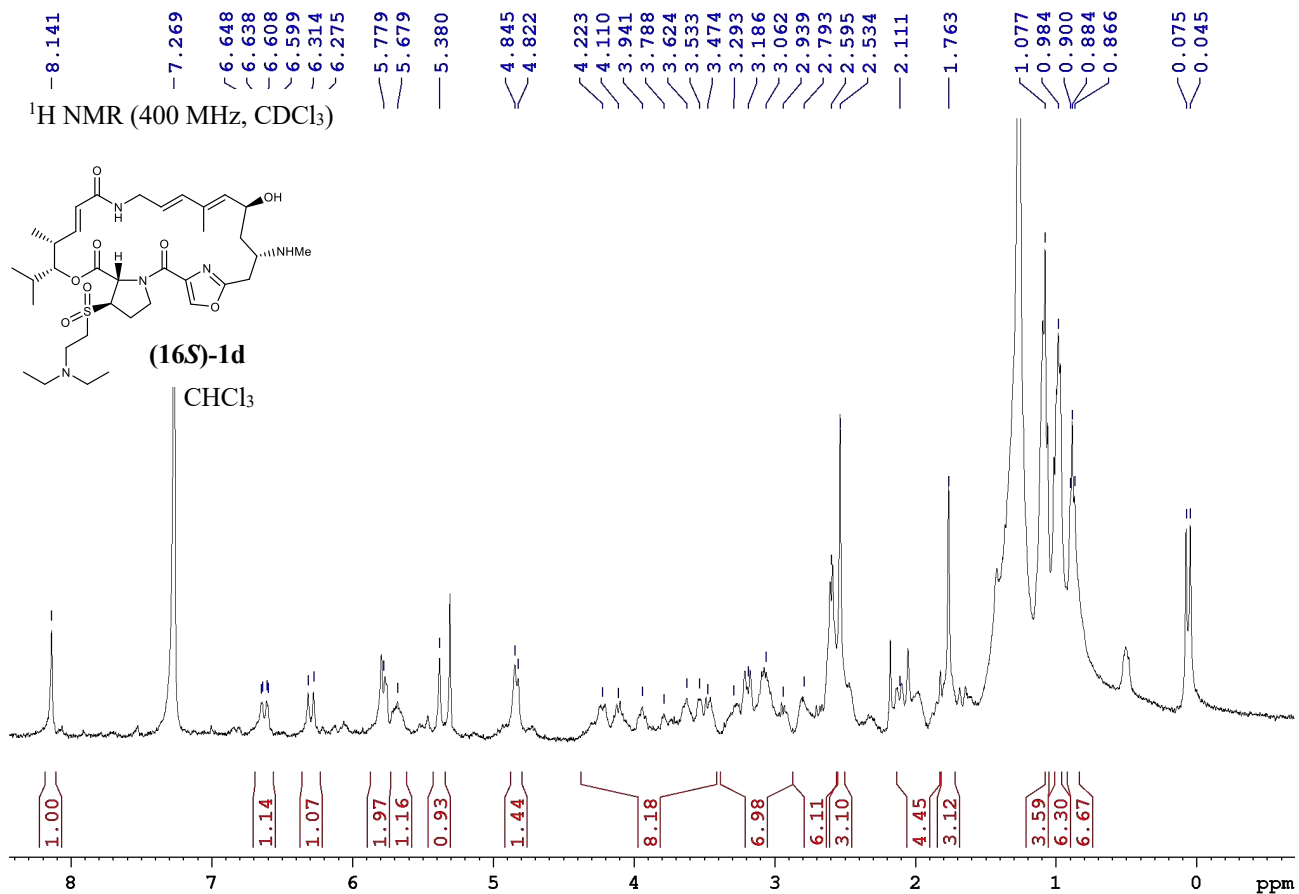


Fig. S42. ¹H NMR and ¹³C NMR spectra of compound (16*S*)-1d.

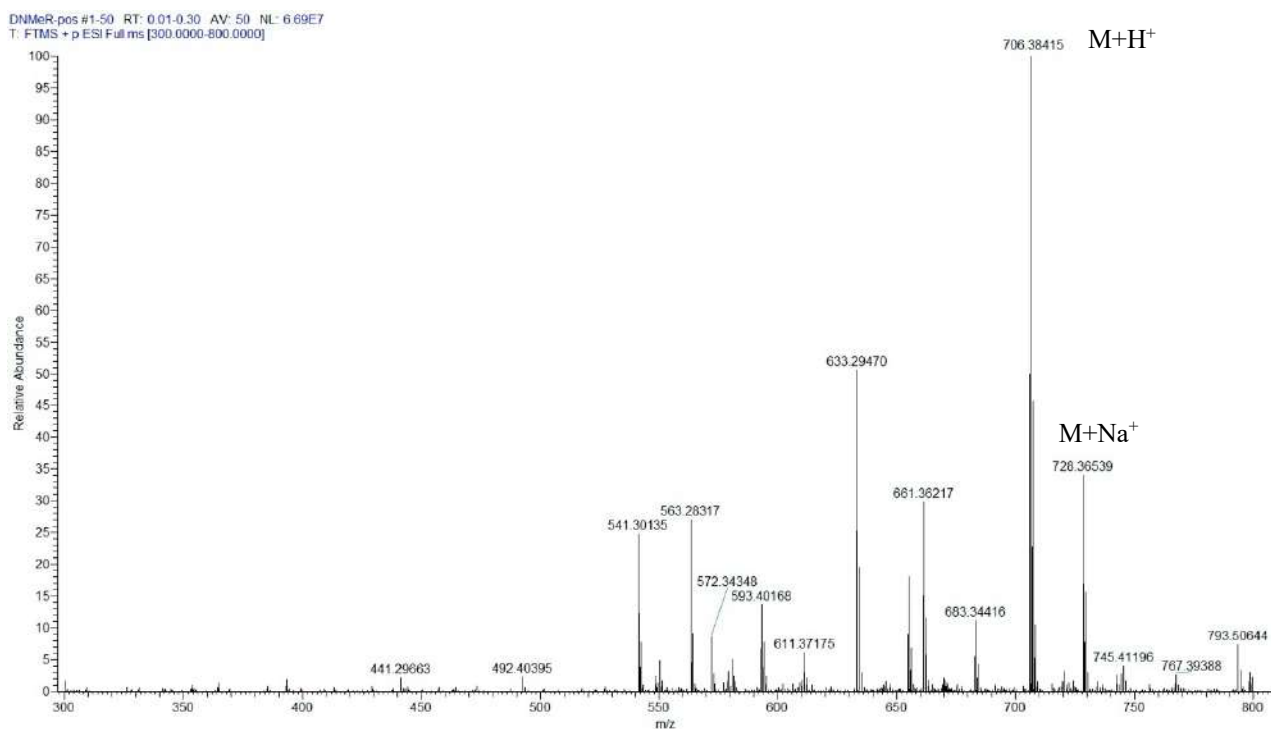


Fig. S43. High resolution ESI(+)-MS spectrum of compound **(16S)-1d**.

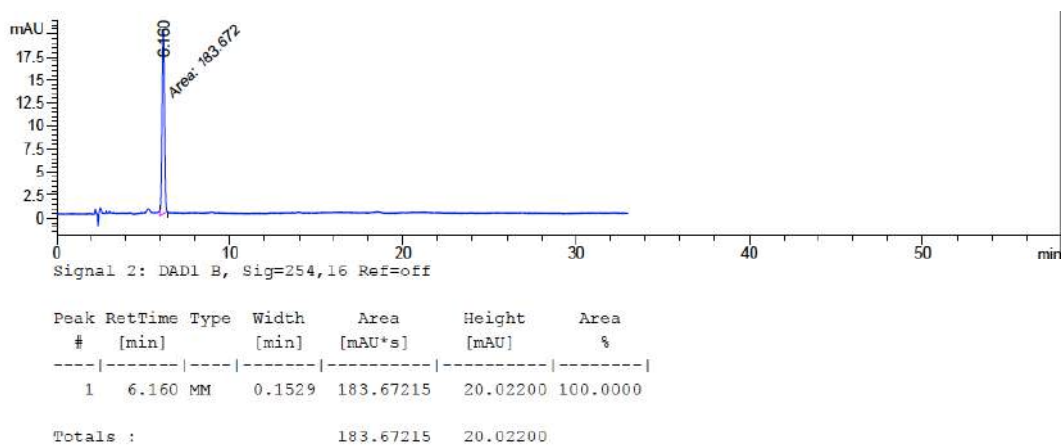


Fig. S44. HPLC chromatogram of compound **(16S)-1d** (RP18, isocratic water/acetonitrile 30:70 + 1% trifluoroacetic acid).

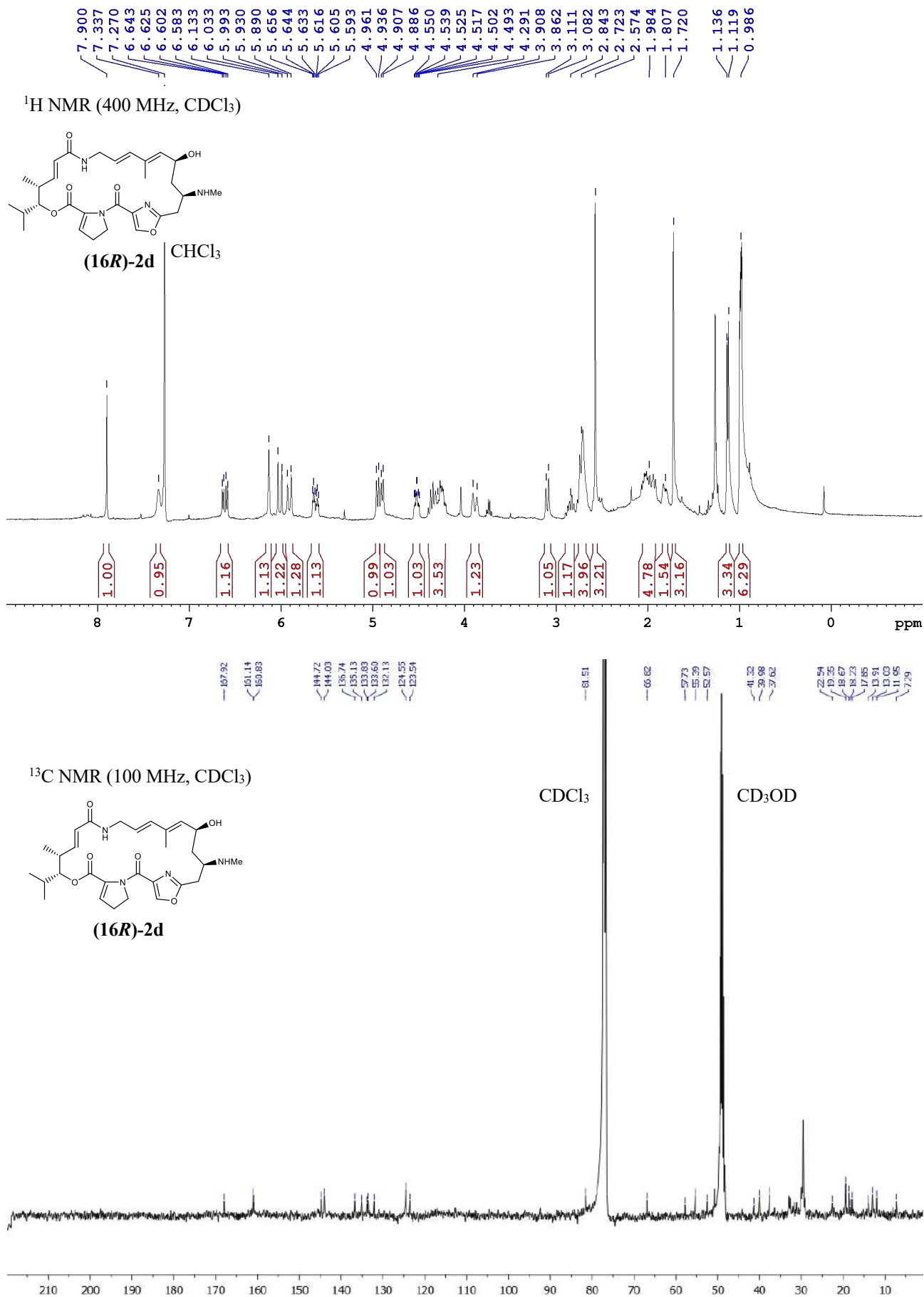


Fig. S45. ¹H NMR and ¹³C NMR spectra of compound **(16R)-2d**.

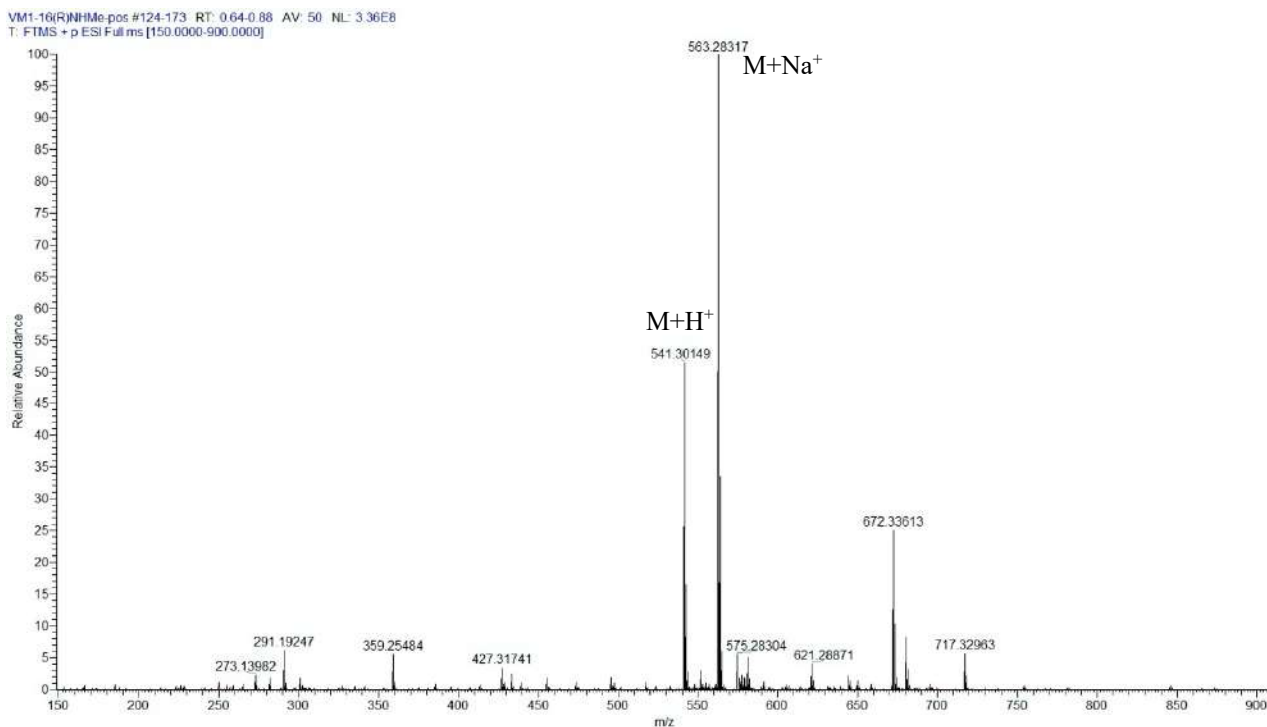


Fig. S46. High resolution ESI(+) MS spectrum of compound (16R)-2d.

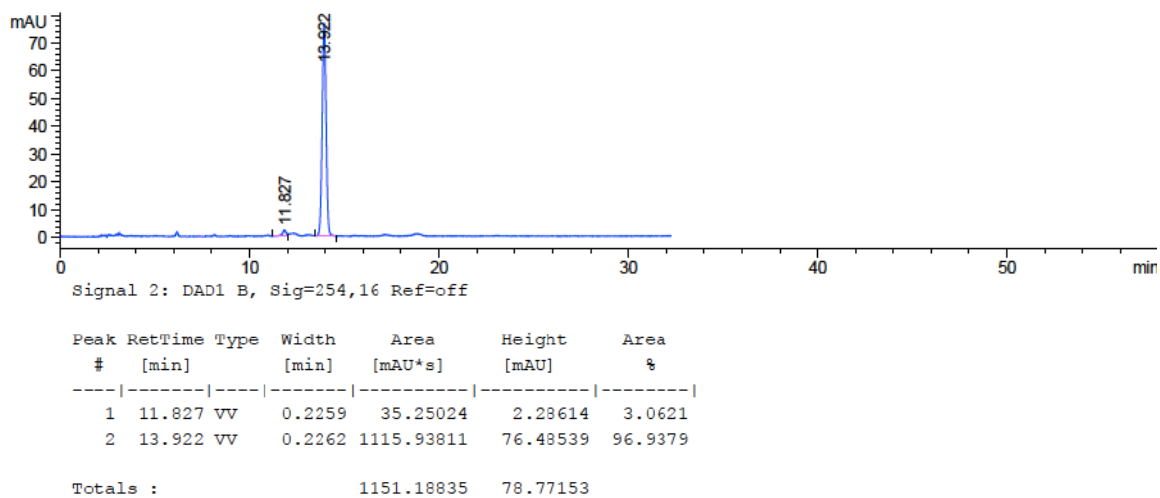


Fig. S47. HPLC chromatogram of compound (16R)-2d (RP18, isocratic water/acetonitrile 30:70 + 1% trifluoroacetic acid).

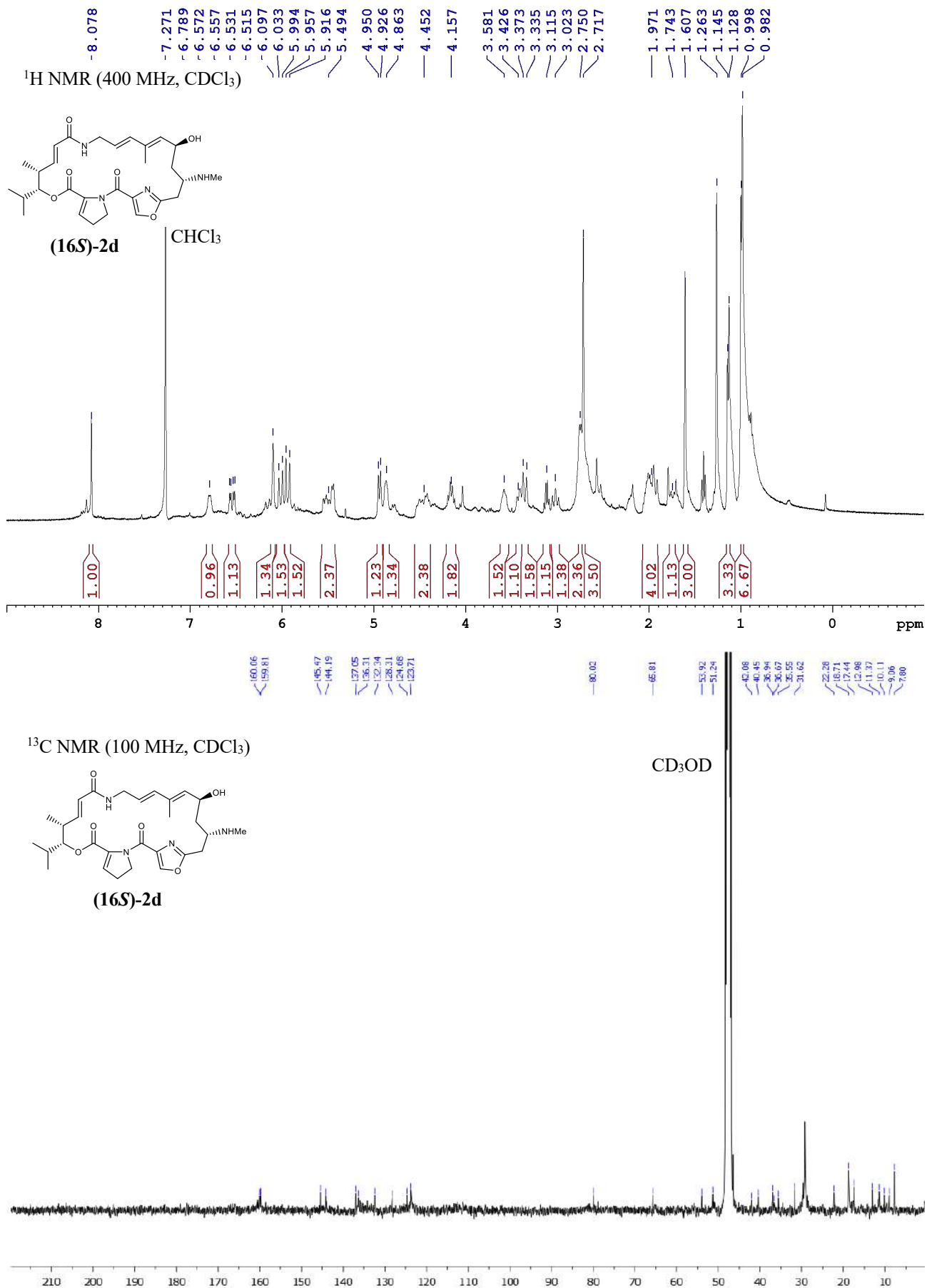


Fig. S48. ¹H NMR and ¹³C NMR spectra of compound (16*S*)-2d.

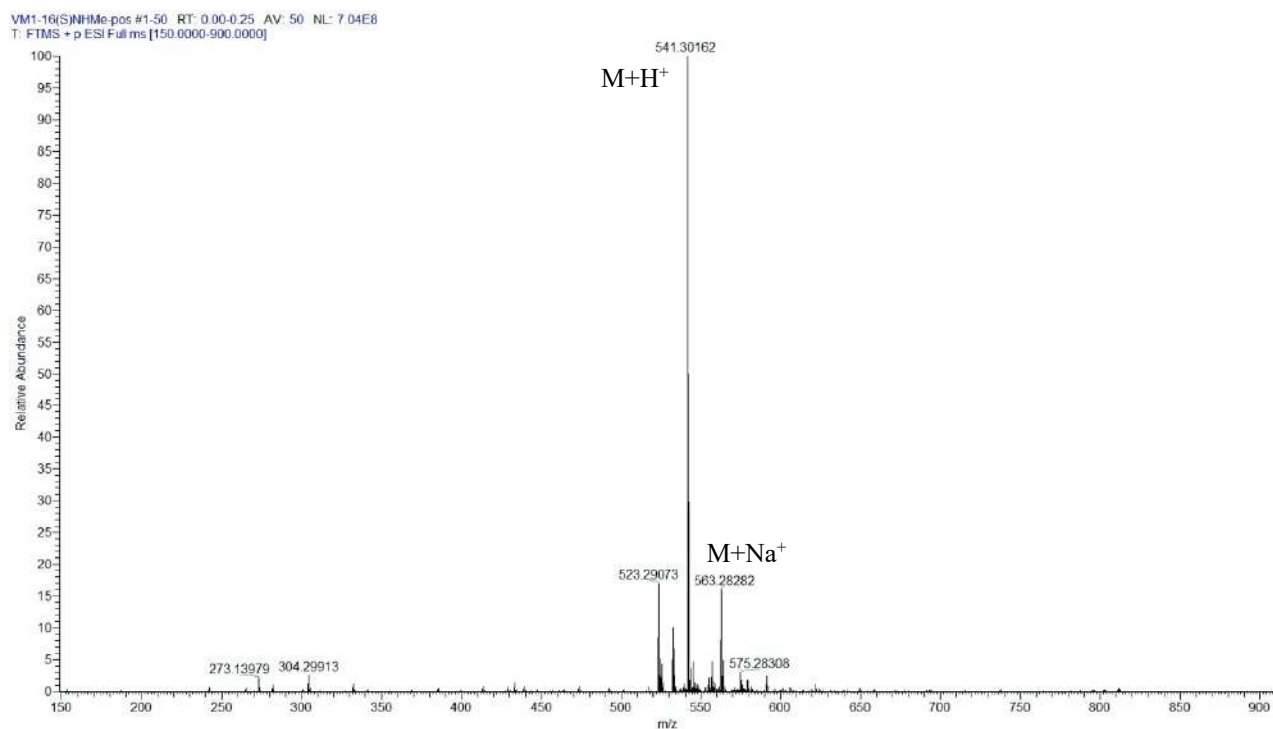
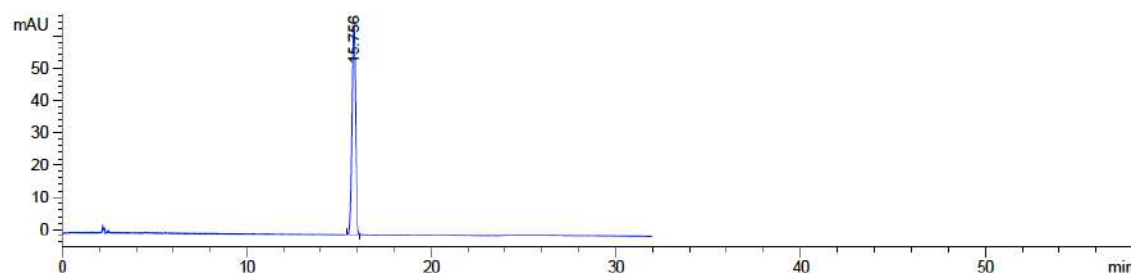


Fig. S49. High resolution ESI(+) MS spectrum of compound **(16S)-2d**.



Signal 1: DAD1 A, Sig=210,16 Ref=off

Peak #	RetTime [min]	Type	Width [min]	Area [mAU*s]	Height [mAU]	Area %
1	15.756	BB	0.2148	899.62329	64.46941	100.0000
Totals :				899.62329	64.46941	

Fig. S50. HPLC chromatogram of compound **(16S)-2d** (RP18, isocratic water/acetonitrile 30:70 + 1% trifluoroacetic acid).

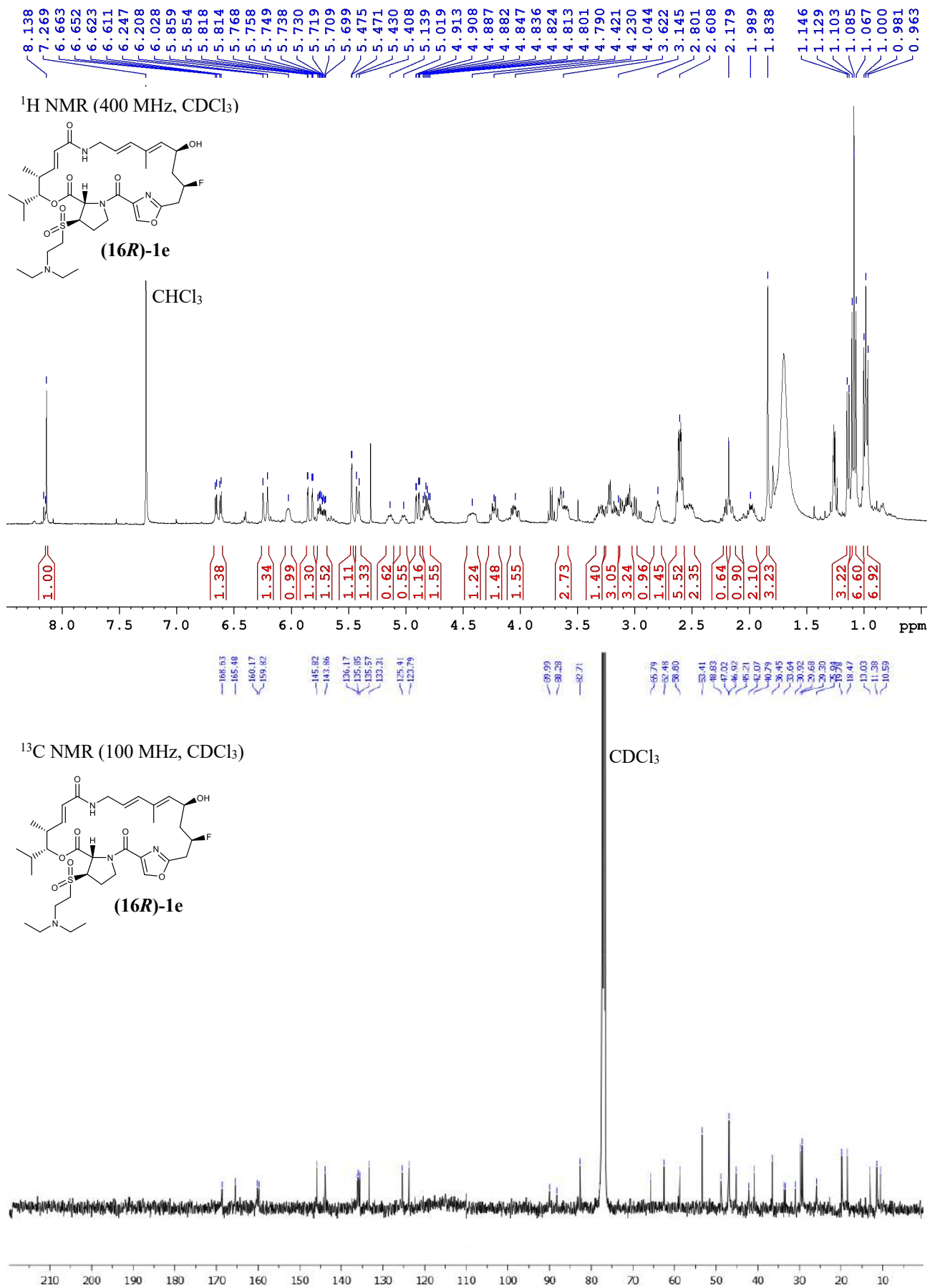


Fig. S51. ¹H NMR and ¹³C NMR spectra of compound (16R)-1e.

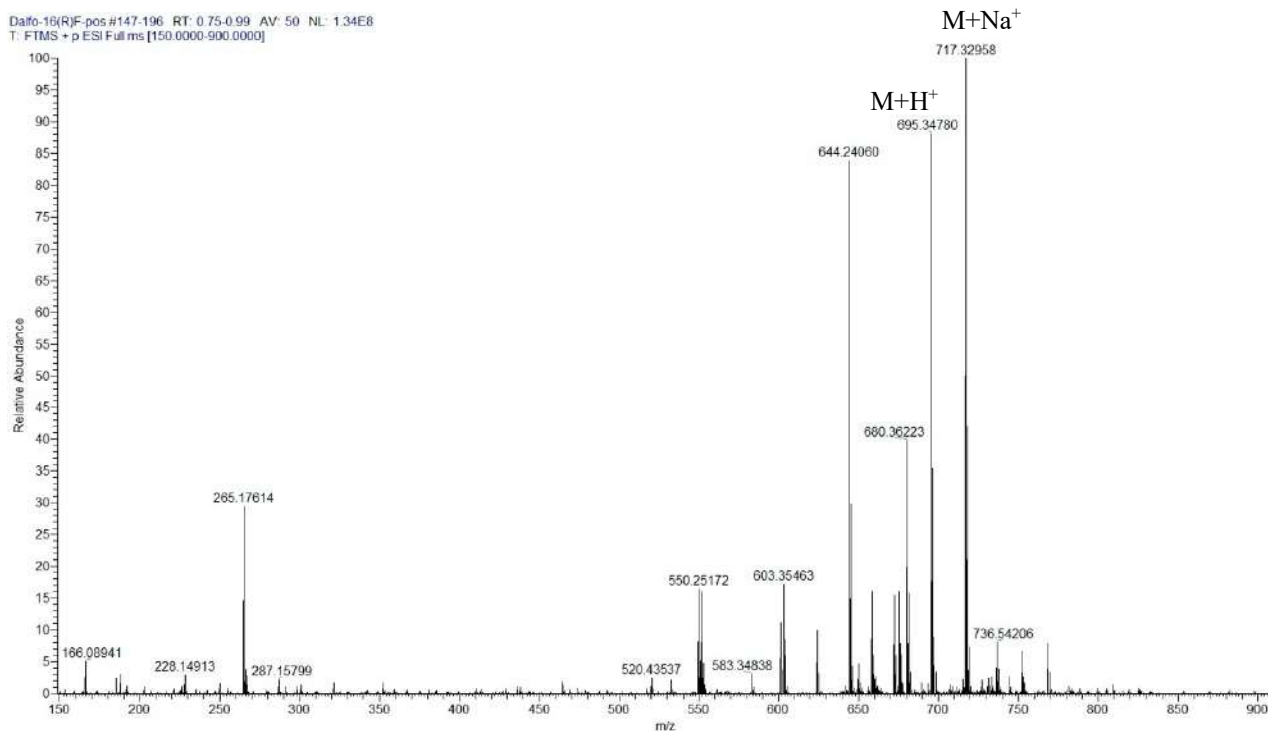


Fig. S52. High resolution ESI(+) MS spectrum of compound **(16R)-1e**.

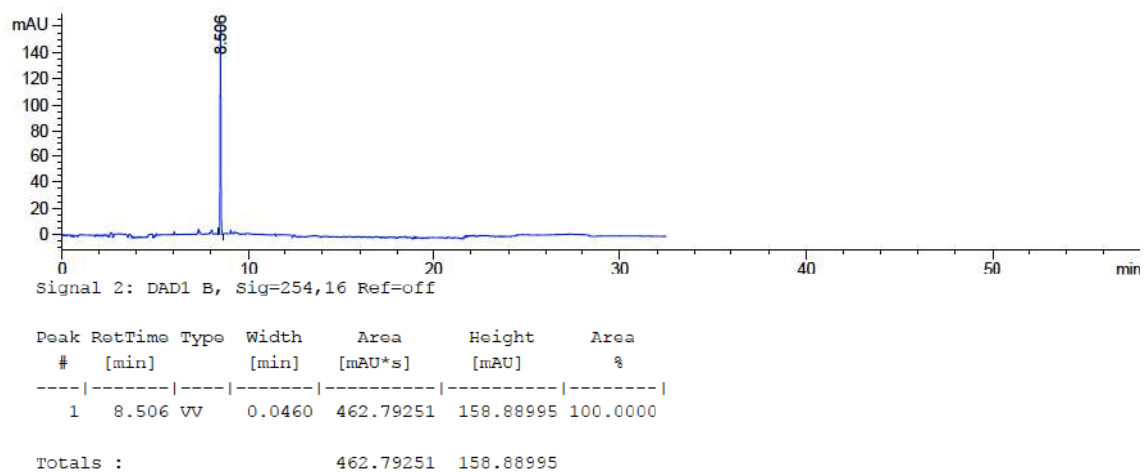


Fig. S53. HPLC spectrum of compound **(16R)-1e** (RP18, isocratic water/acetonitrile 30:70 + 1% trifluoroacetic acid).

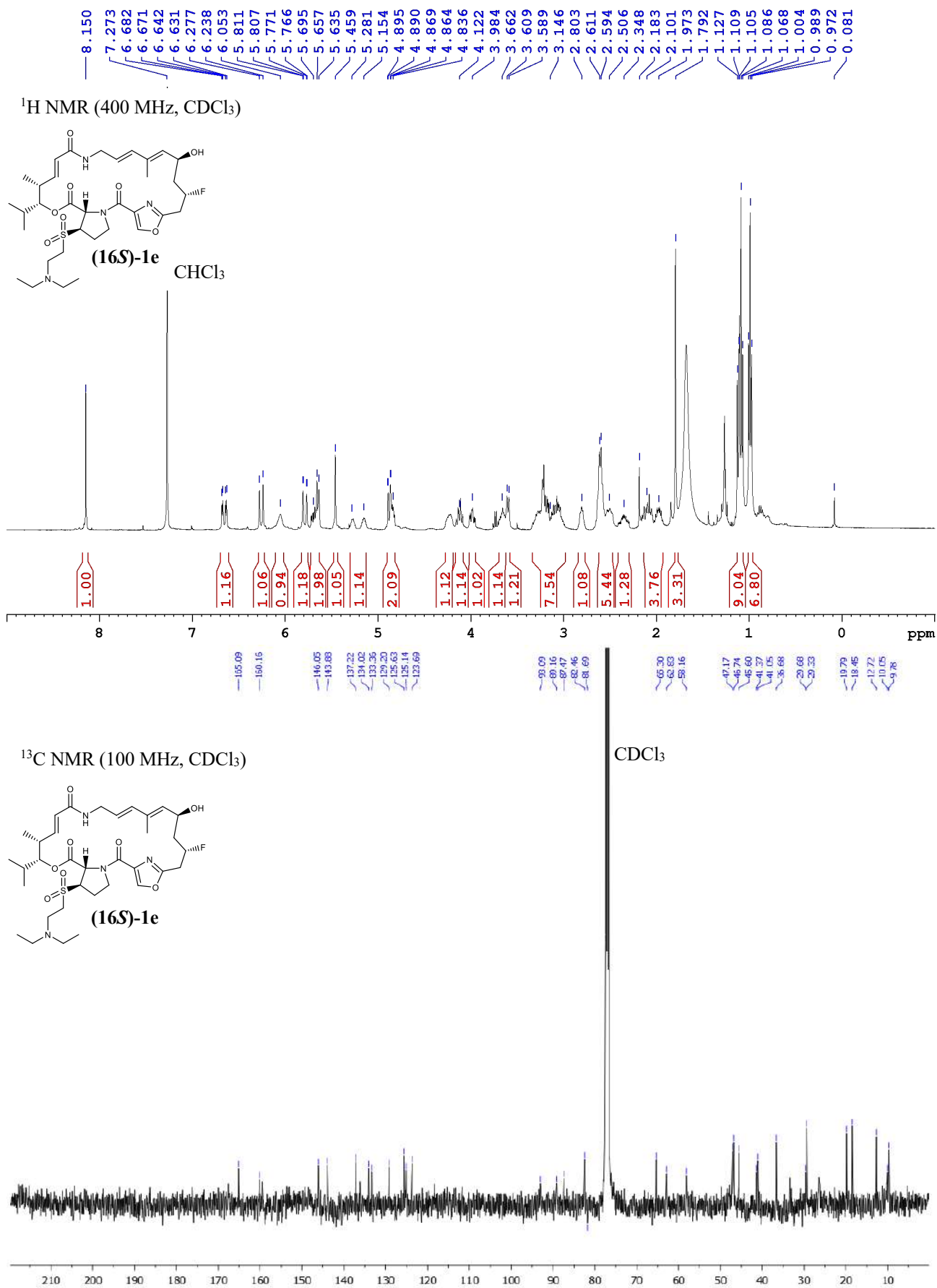


Fig. S54. ¹H NMR and ¹³C NMR spectra of compound **(16S)-1e**.

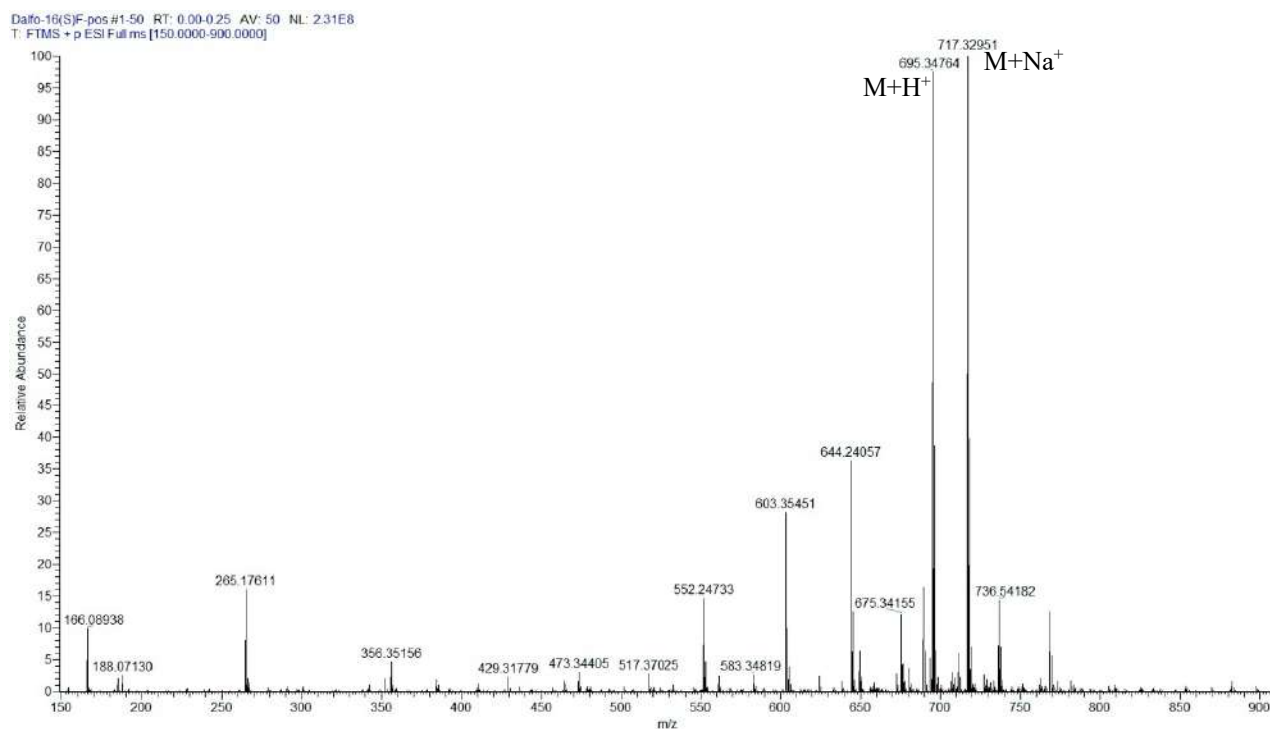


Fig. S55. High resolution ESI(+)-MS spectrum of compound (16S)-1e.

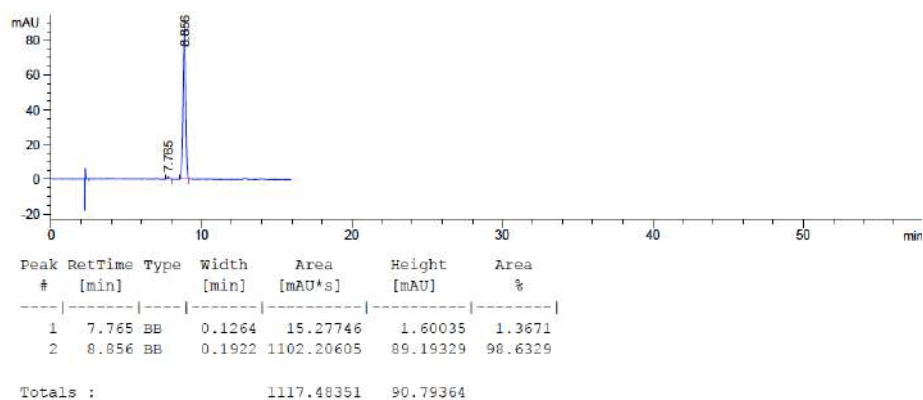


Fig. S56. HPLC chromatogram of compound (16S)-1e (RP18, isocratic water/acetonitrile 30:70 + 1% trifluoroacetic acid).

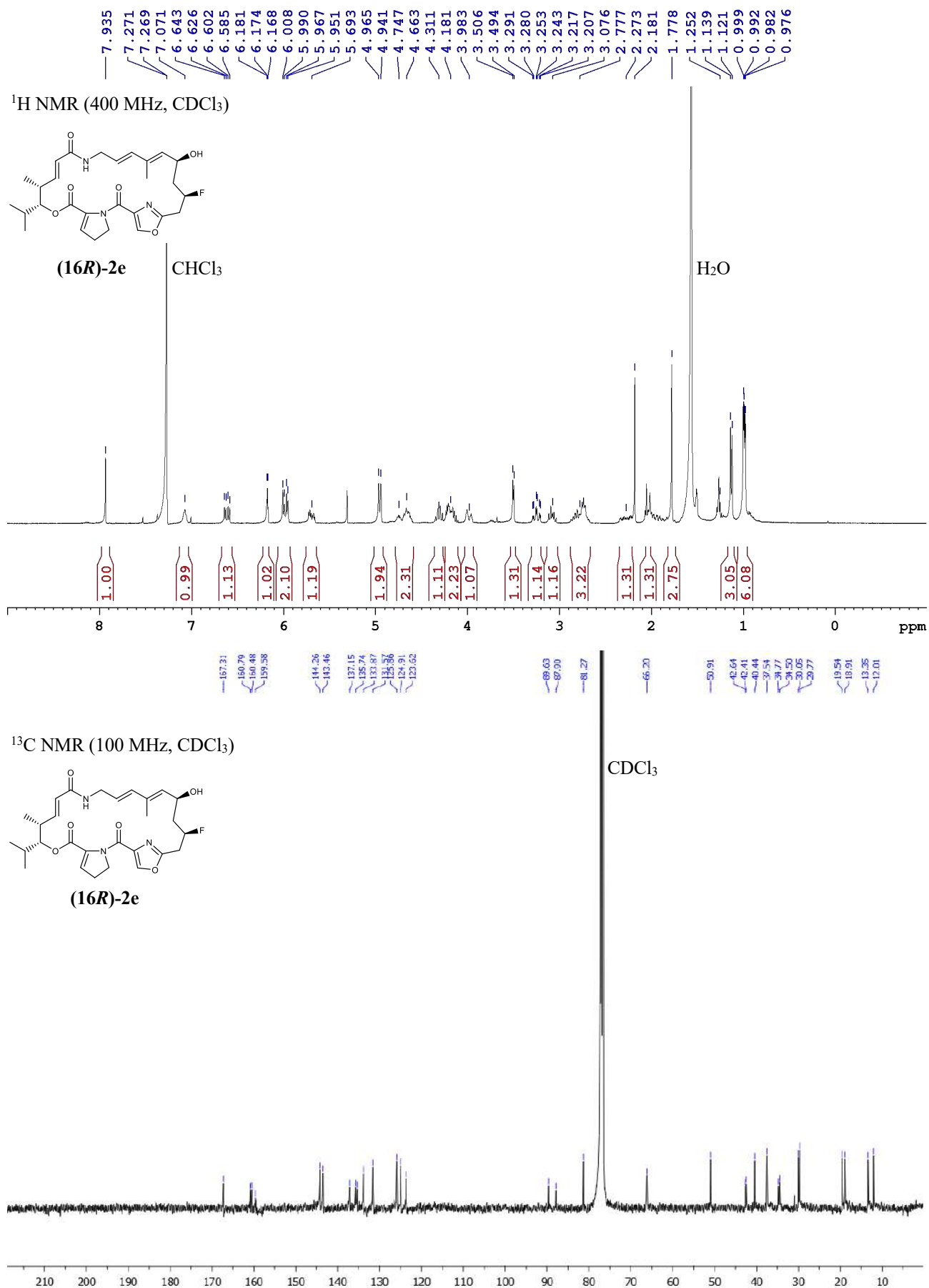


Fig. S57. ¹H NMR and ¹³C NMR spectra of compound (16R)-2e.

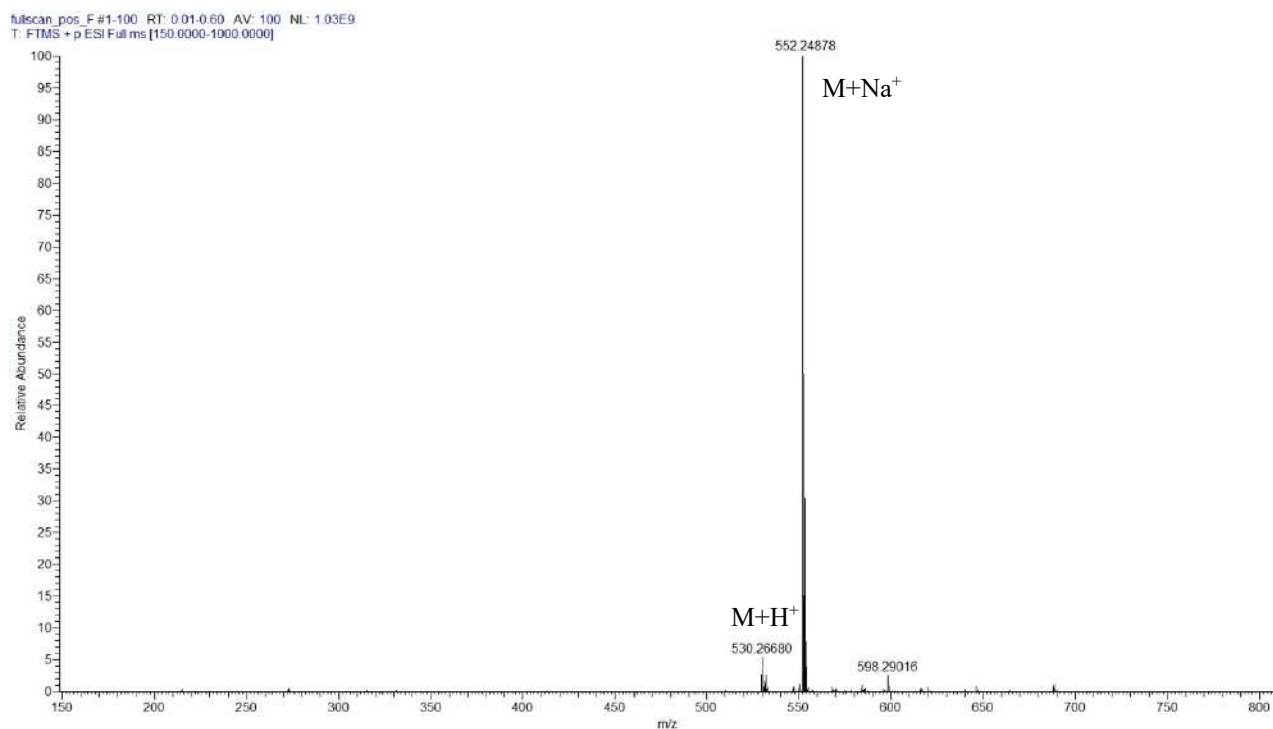


Fig. S58. High resolution ESI(+)-MS spectrum of compound (16R)-2e.

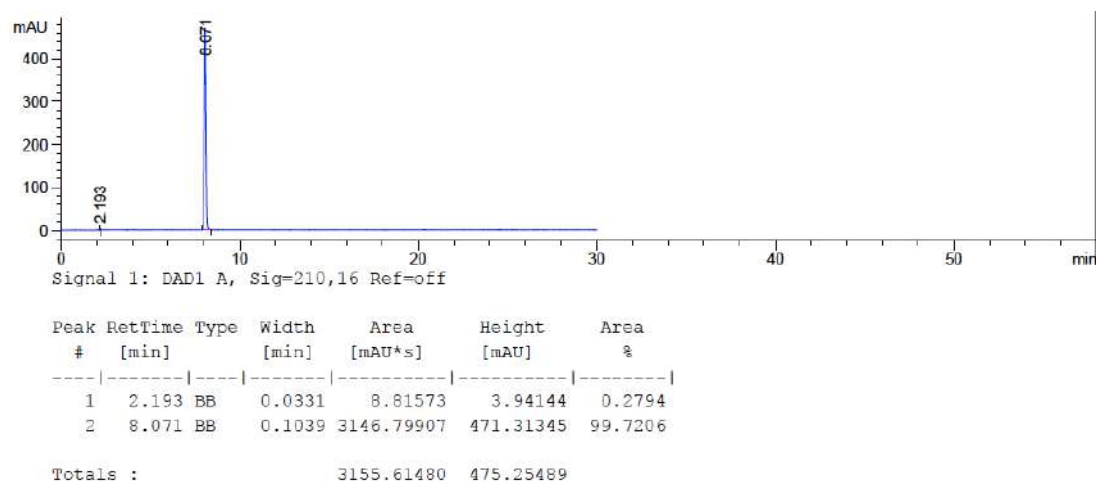


Fig. S59. HPLC chromatogram of compound (16R)-2e (RP18, gradient water/acetonitrile 30:70 to 80:20).

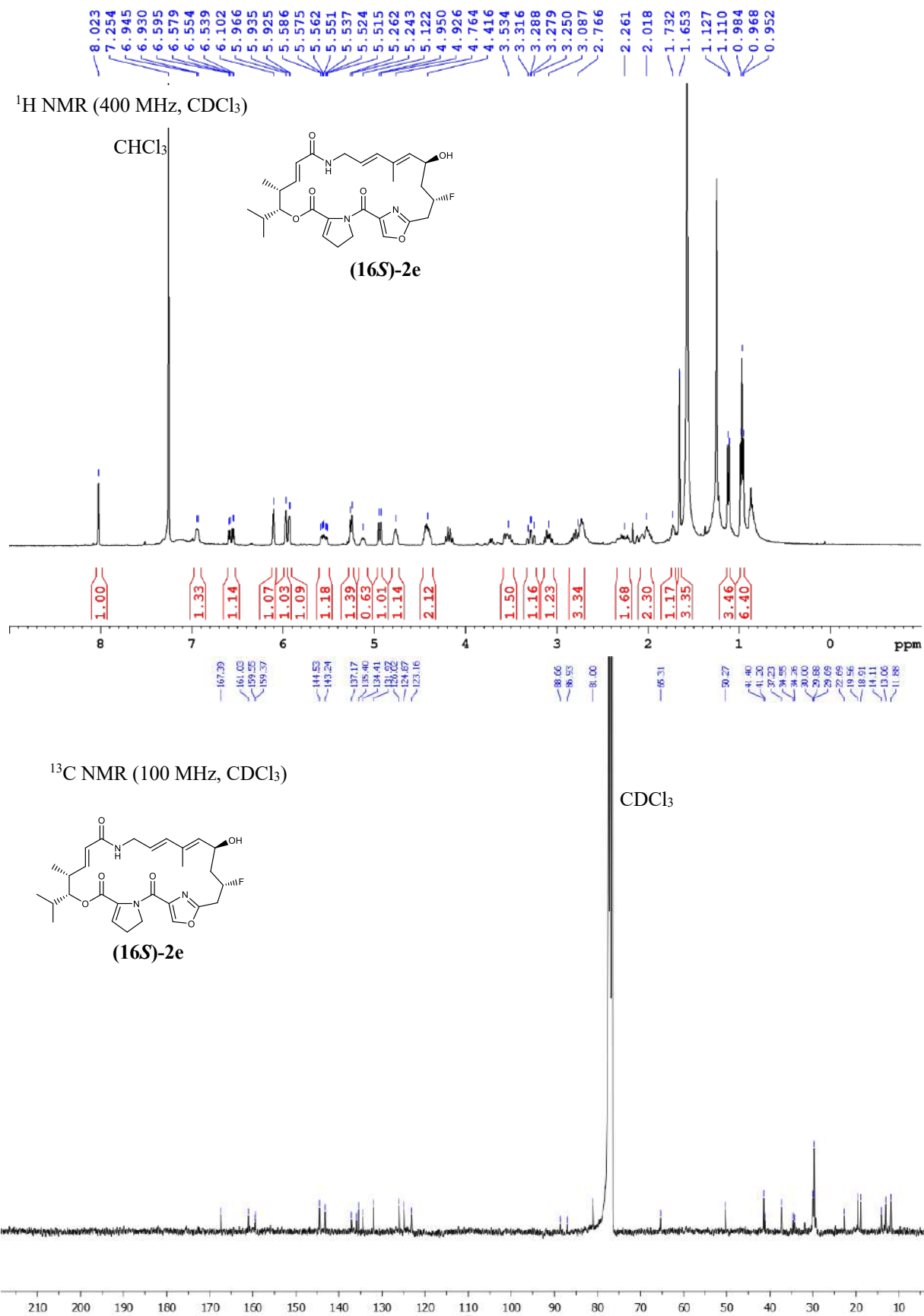


Fig. S60. ¹H NMR and ¹³C NMR spectra of compound (16S)-2e.

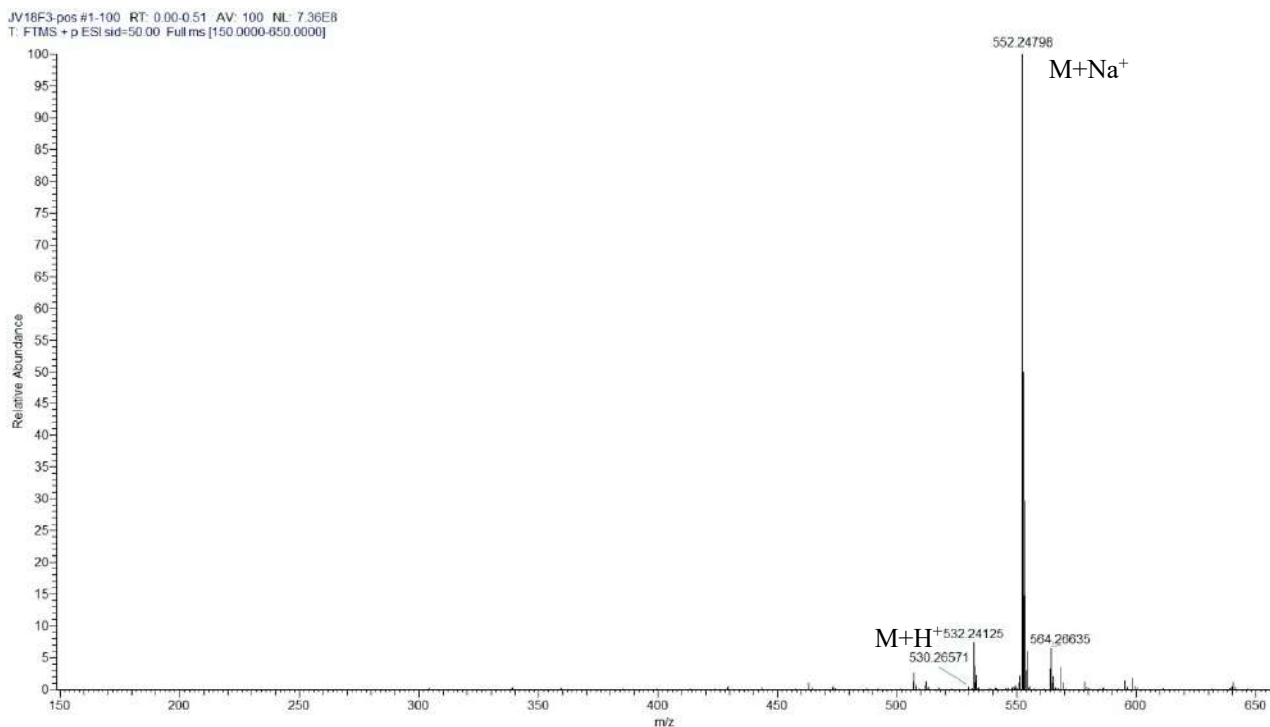


Fig. S61. High resolution ESI(+)-MS spectrum of compound **(16S)-2e**.

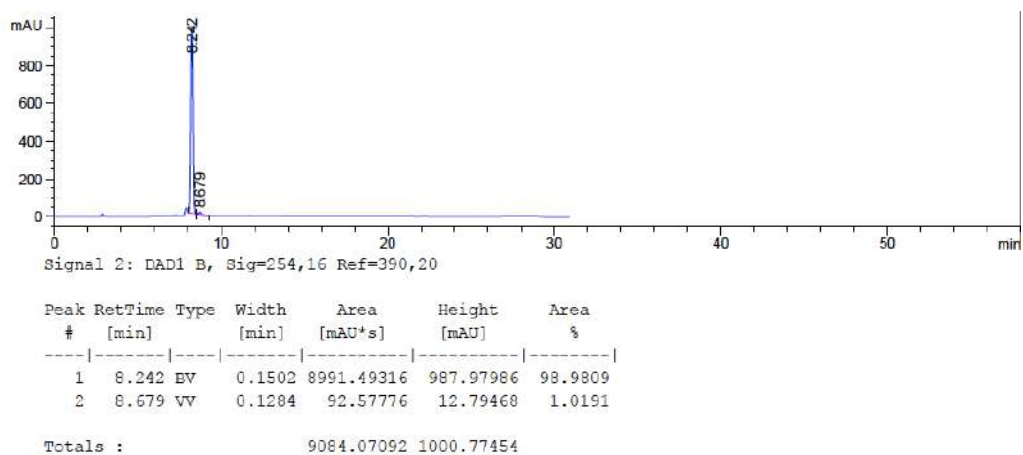


Fig. S62. HPLC chromatogram of compound **(16S)-2e** (RP18, gradient water/acetonitrile 30:70 to 80:20).

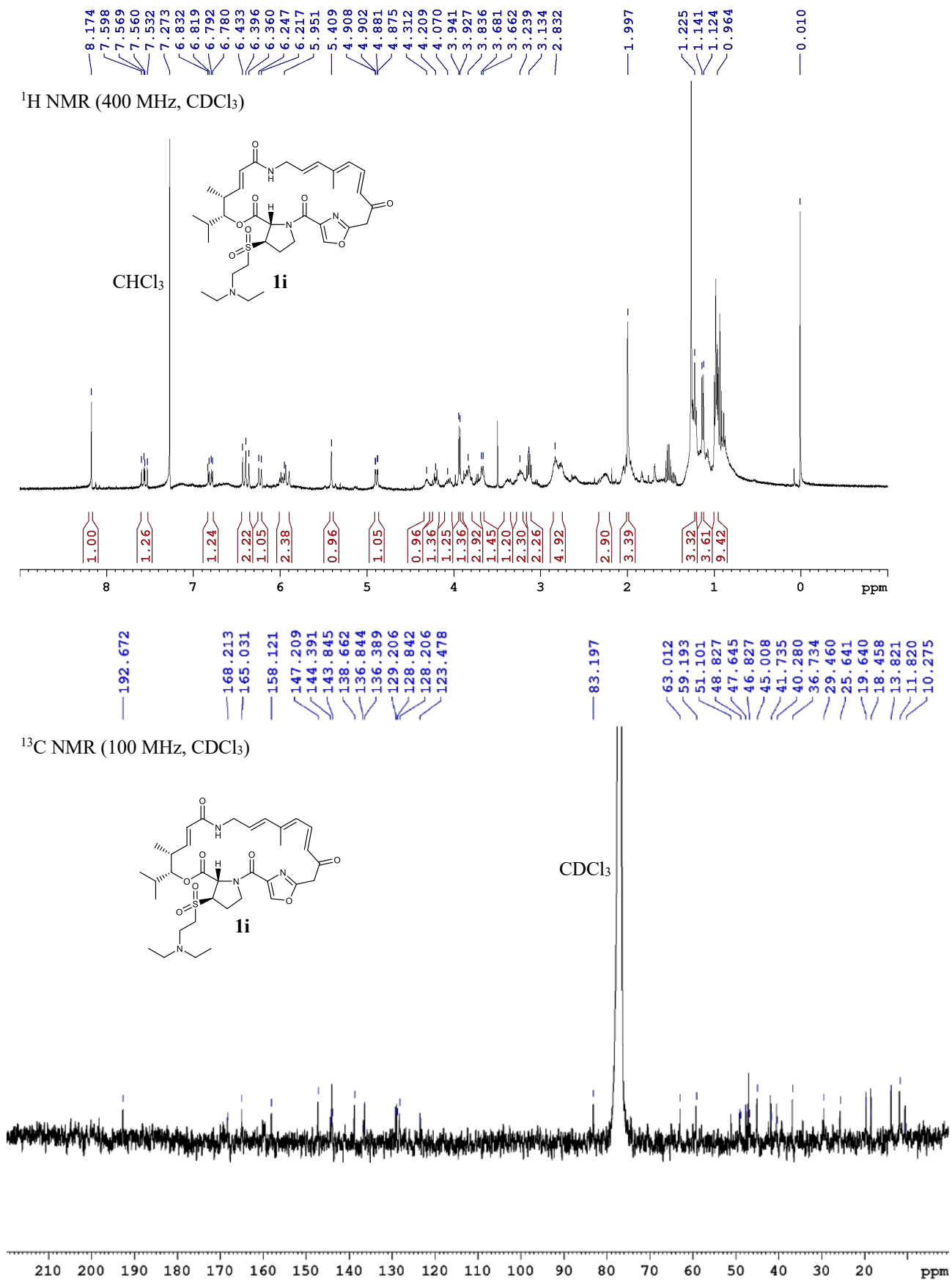


Fig. S63. ¹H NMR and ¹³C NMR spectra of compound **1i**.

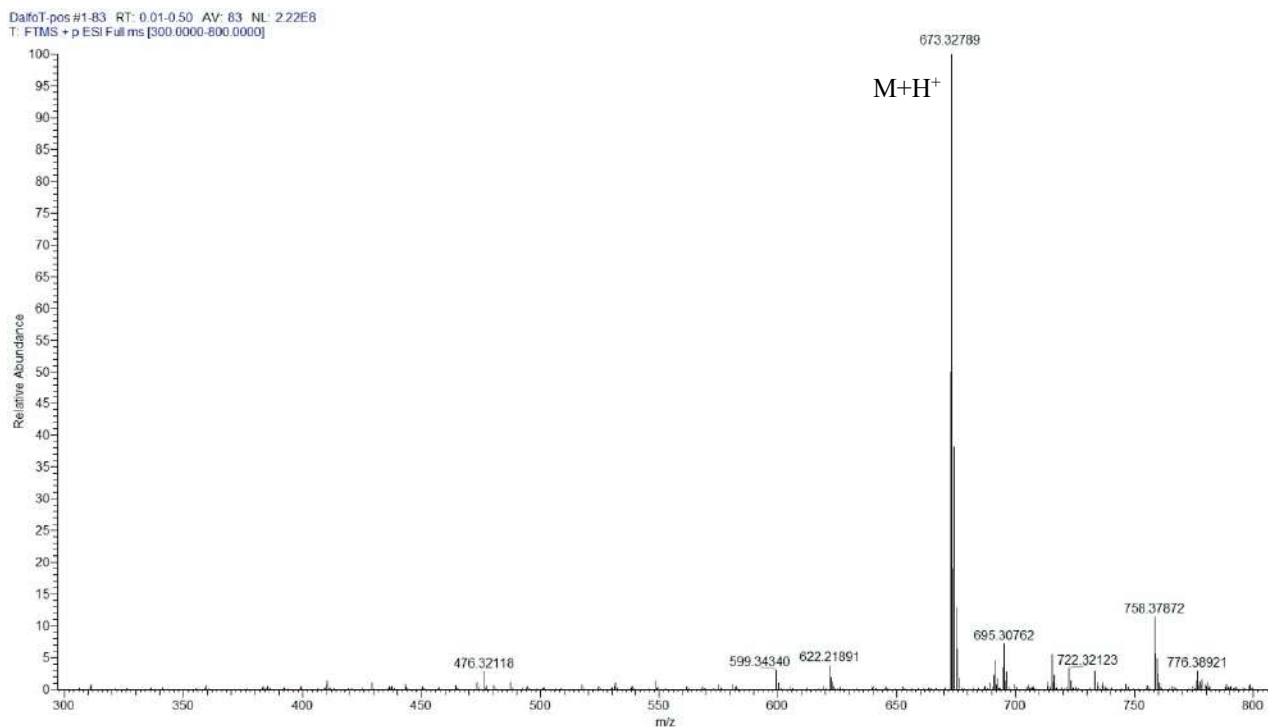
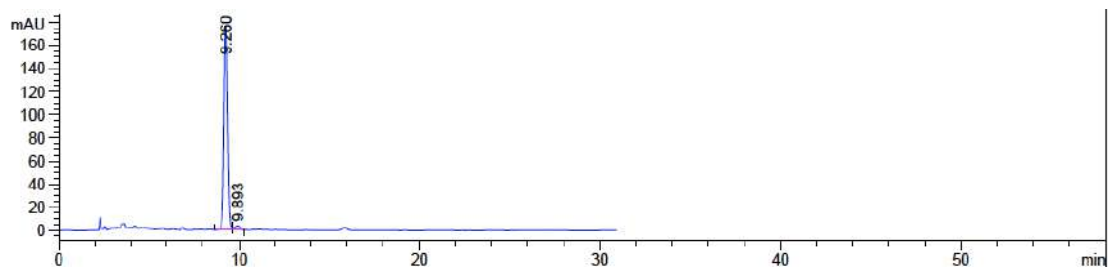


Fig. S64. High resolution ESI(+) MS spectrum of compound **1i**.



Signal 2: DAD1 B, Sig=254,16 Ref=390,20

Peak #	RetTime [min]	Type	Width [min]	Area [mAU*s]	Height [mAU]	Area %
1	9.260	VV	0.2124	2431.16602	176.79109	97.2352
2	9.893	VV	0.2779	69.12883	3.77092	2.7648

Totals : 2500.29485 180.56201

Fig. S65. HPLC chromatogram of compound **1i** (RP18, isocratic water/acetonitrile 30:70 + 1% trifluoroacetic acid).

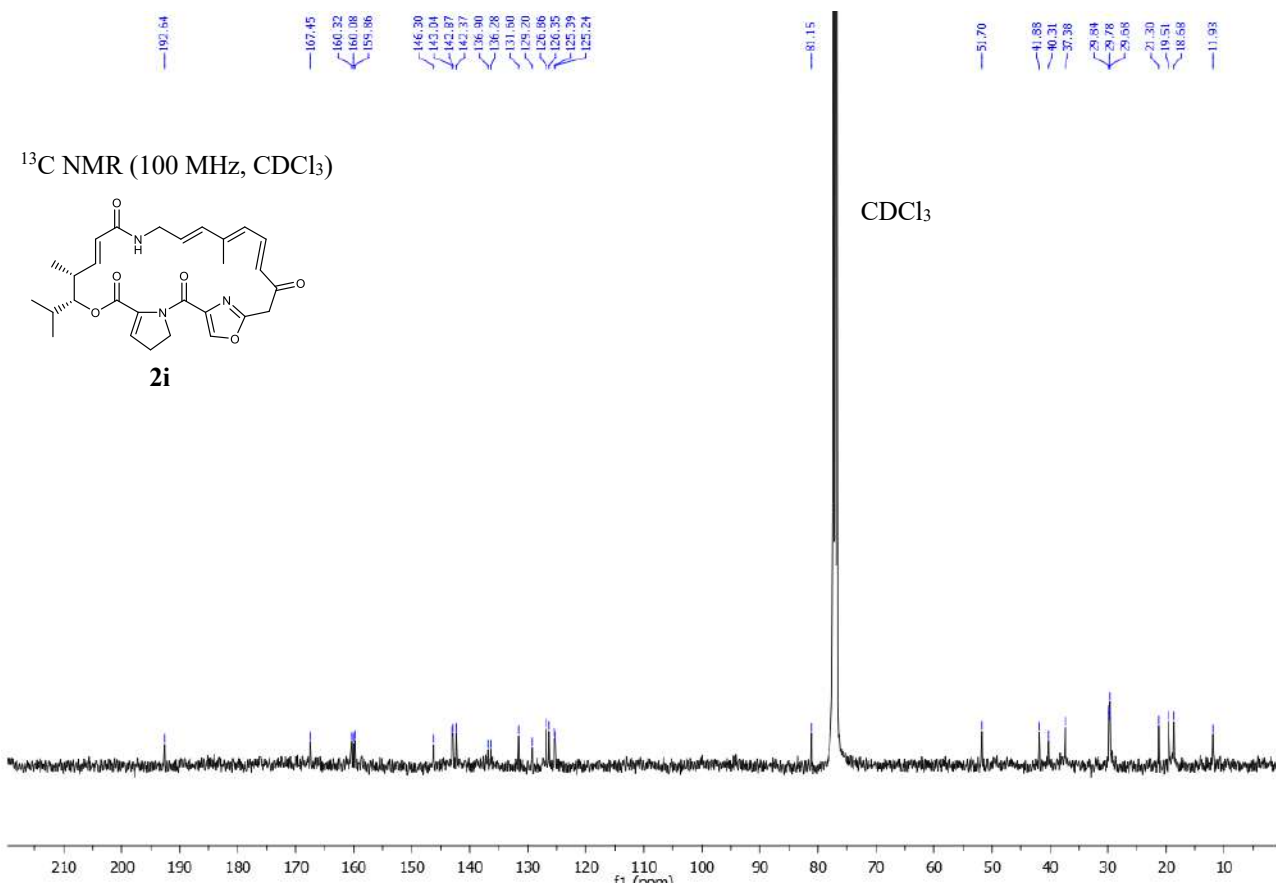
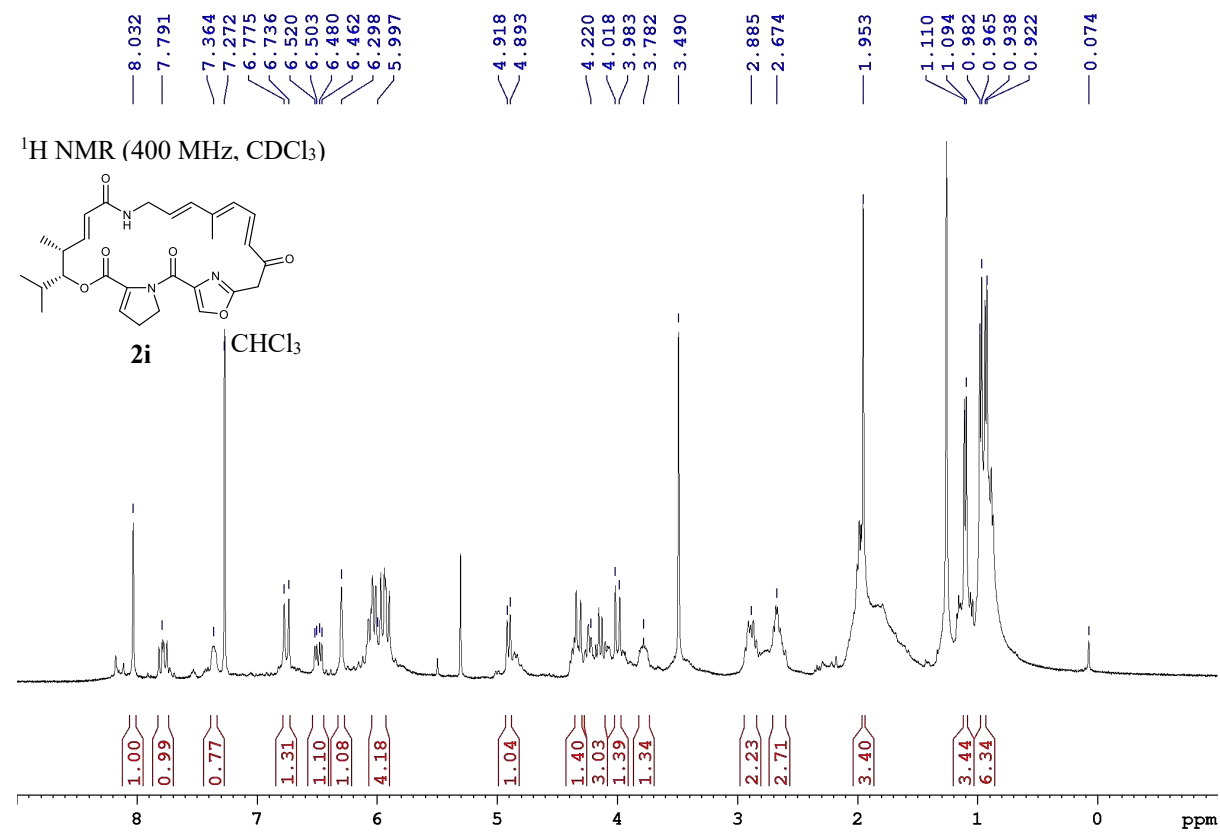


Fig. S66. ¹H NMR and ¹³C NMR spectra of compound **2i**.

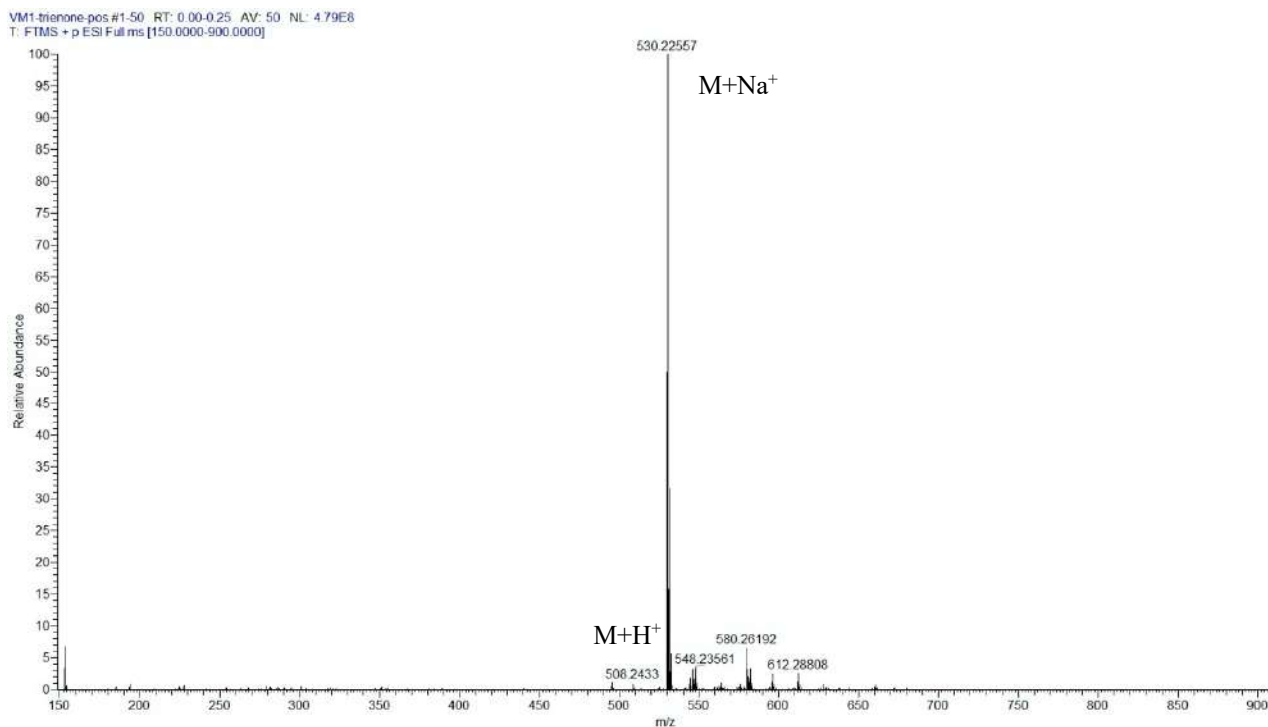


Fig. S67. High resolution ESI(+)-MS spectra of compound **2i**.

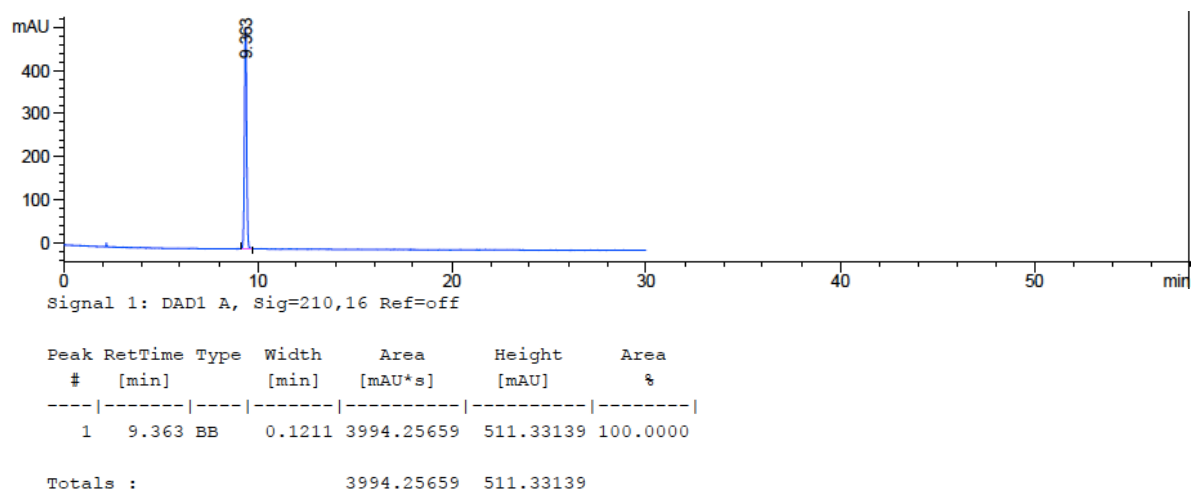


Fig. S68. HPLC chromatogram of compound **2i** (RP18, gradient water/acetonitrile 30:70 to 80:20).

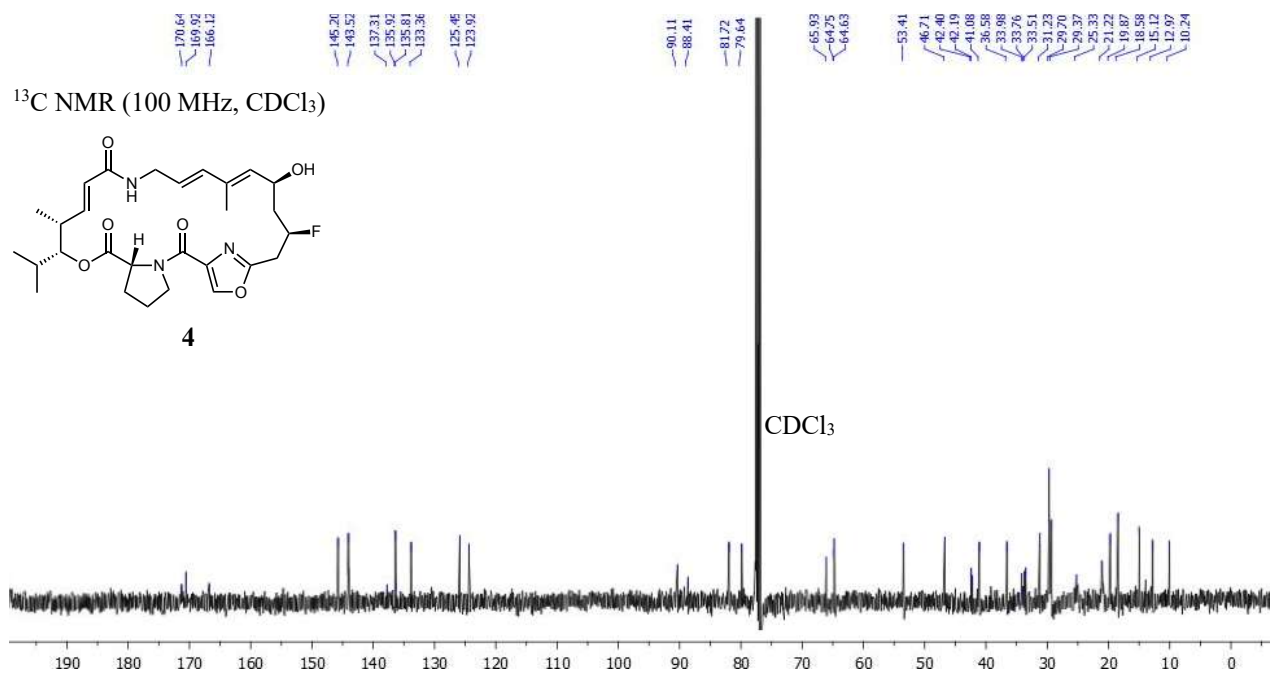
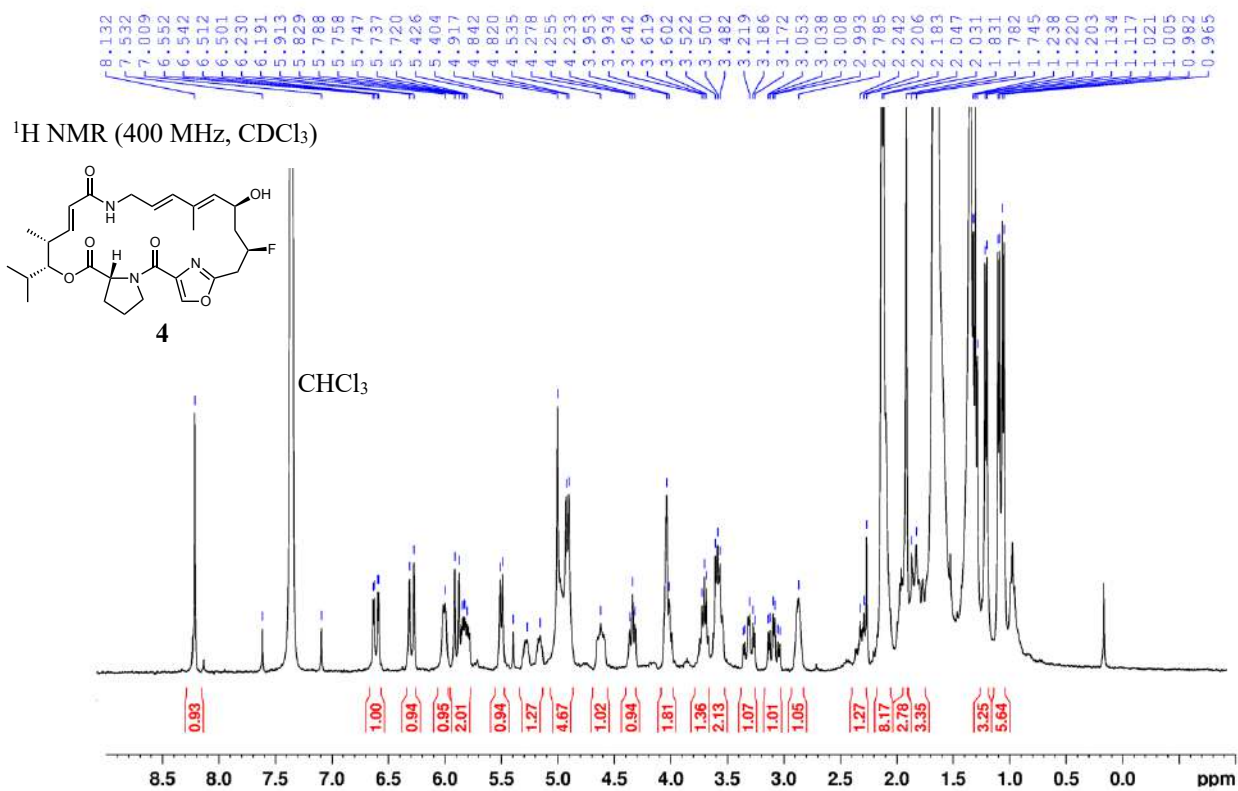


Fig. S69. ¹H NMR and ¹³C NMR spectra of compound 4.

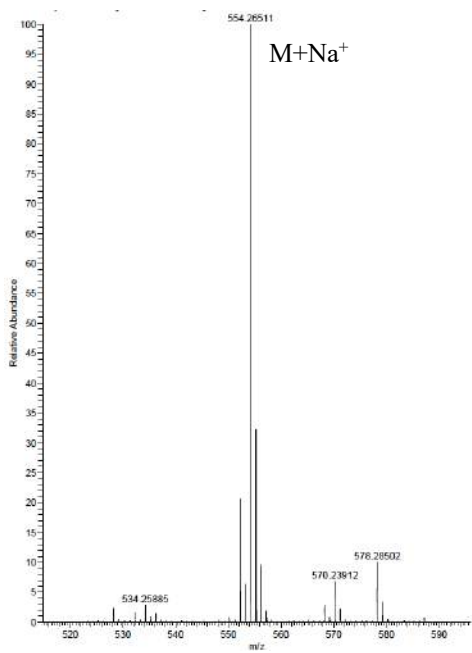


Fig. S70. High resolution ESI(+)-MS spectrum of compound 4.

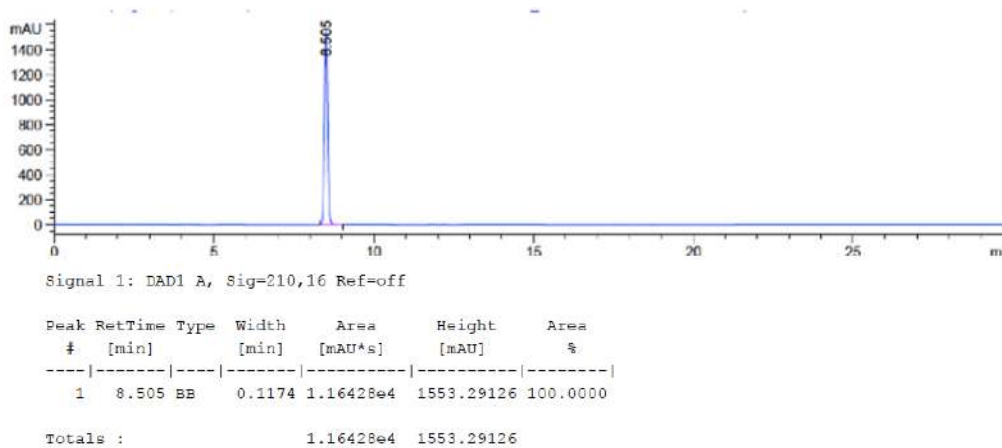


Fig. S71. HPLC chromatogram of compound 4 (RP18, gradient water/acetonitrile 30:70 to 80:20).

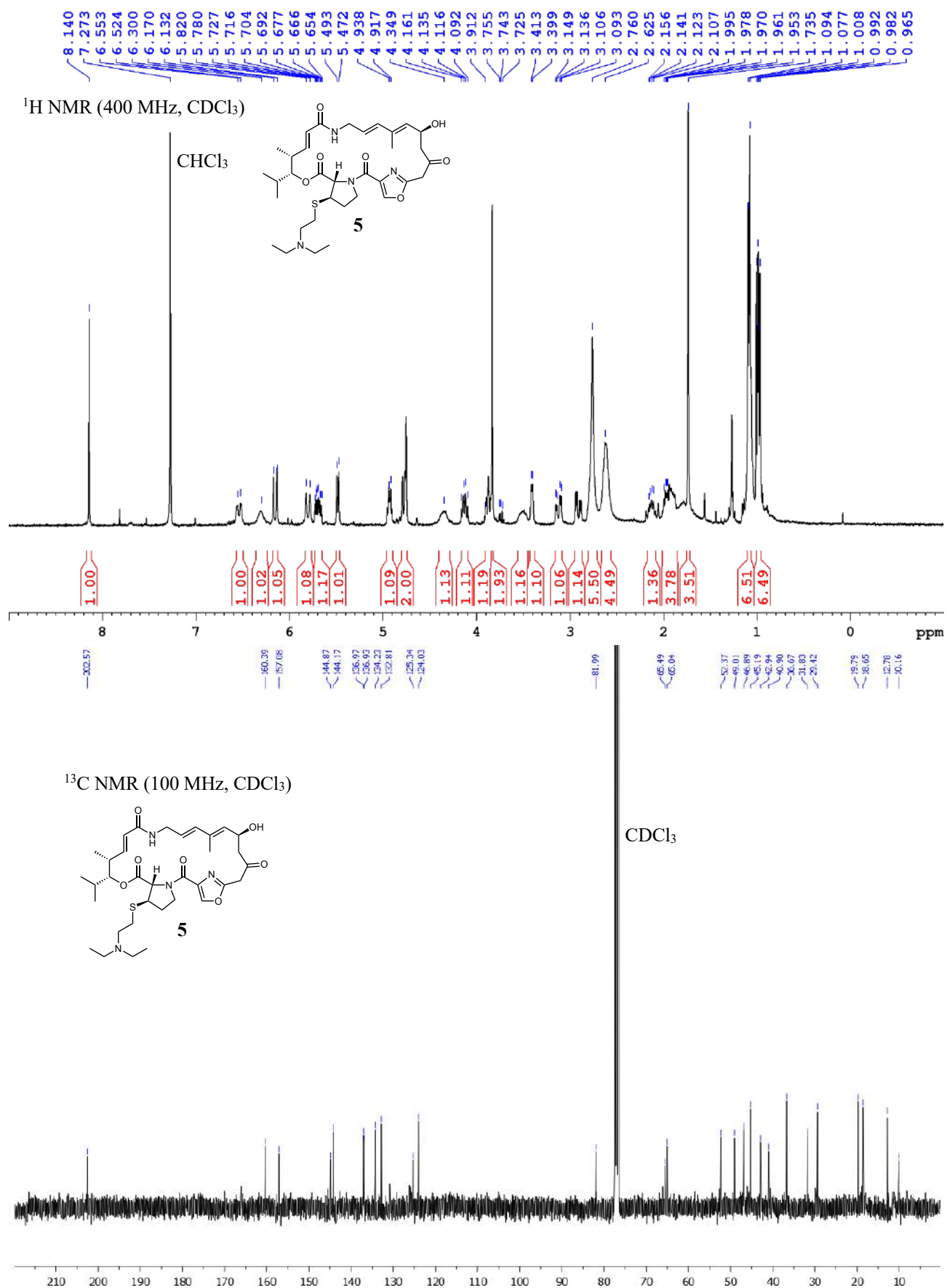


Fig. S72. ¹H NMR and ¹³C NMR spectra of compound **5**.

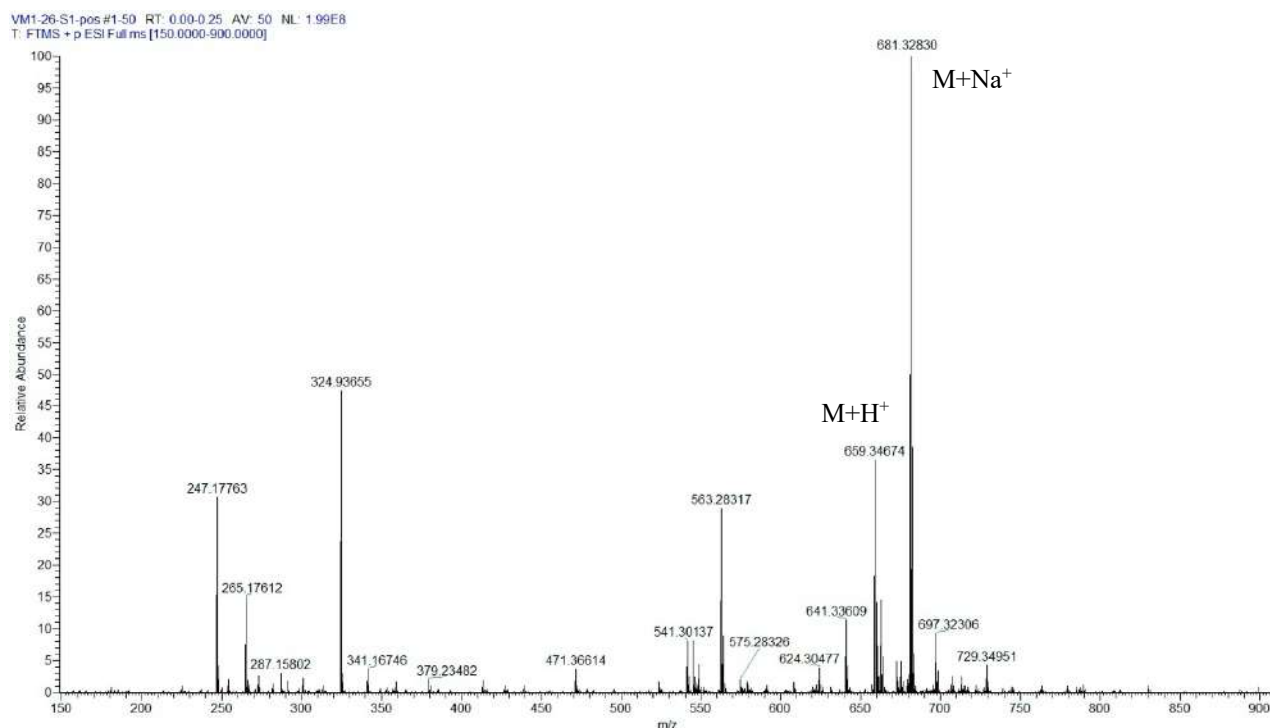


Fig. S73. High resolution ESI(+) MS spectrum of compound 5.

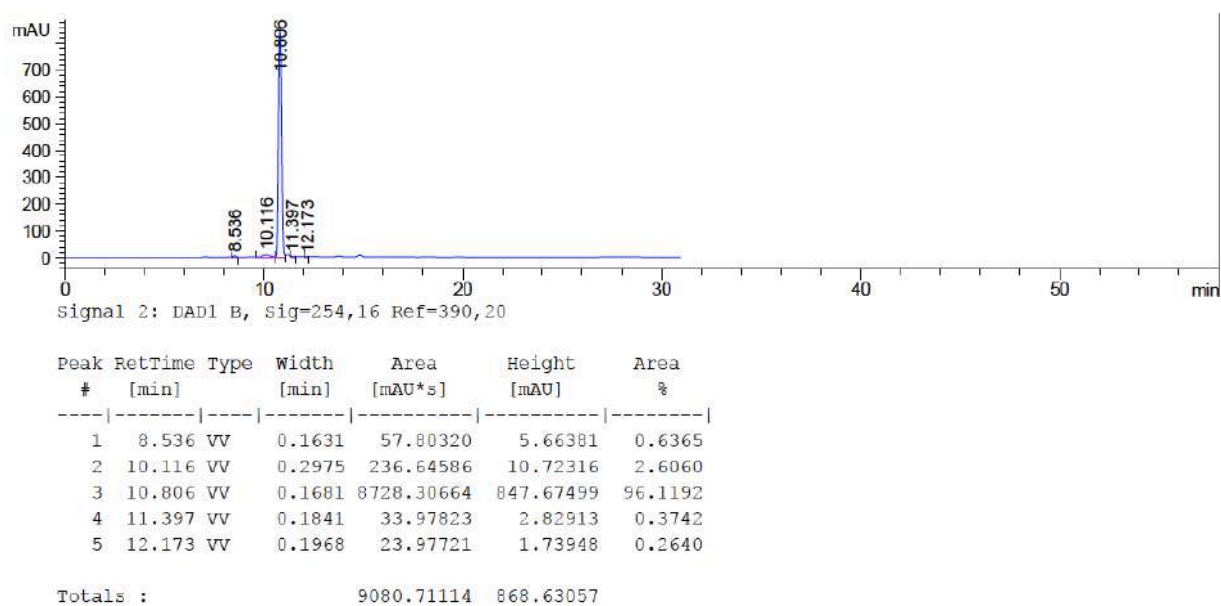


Fig. S74. HPLC chromatogram of compound 5 (RP18, isocratic water/acetonitrile 30:70 + 1% trifluoroacetic acid).

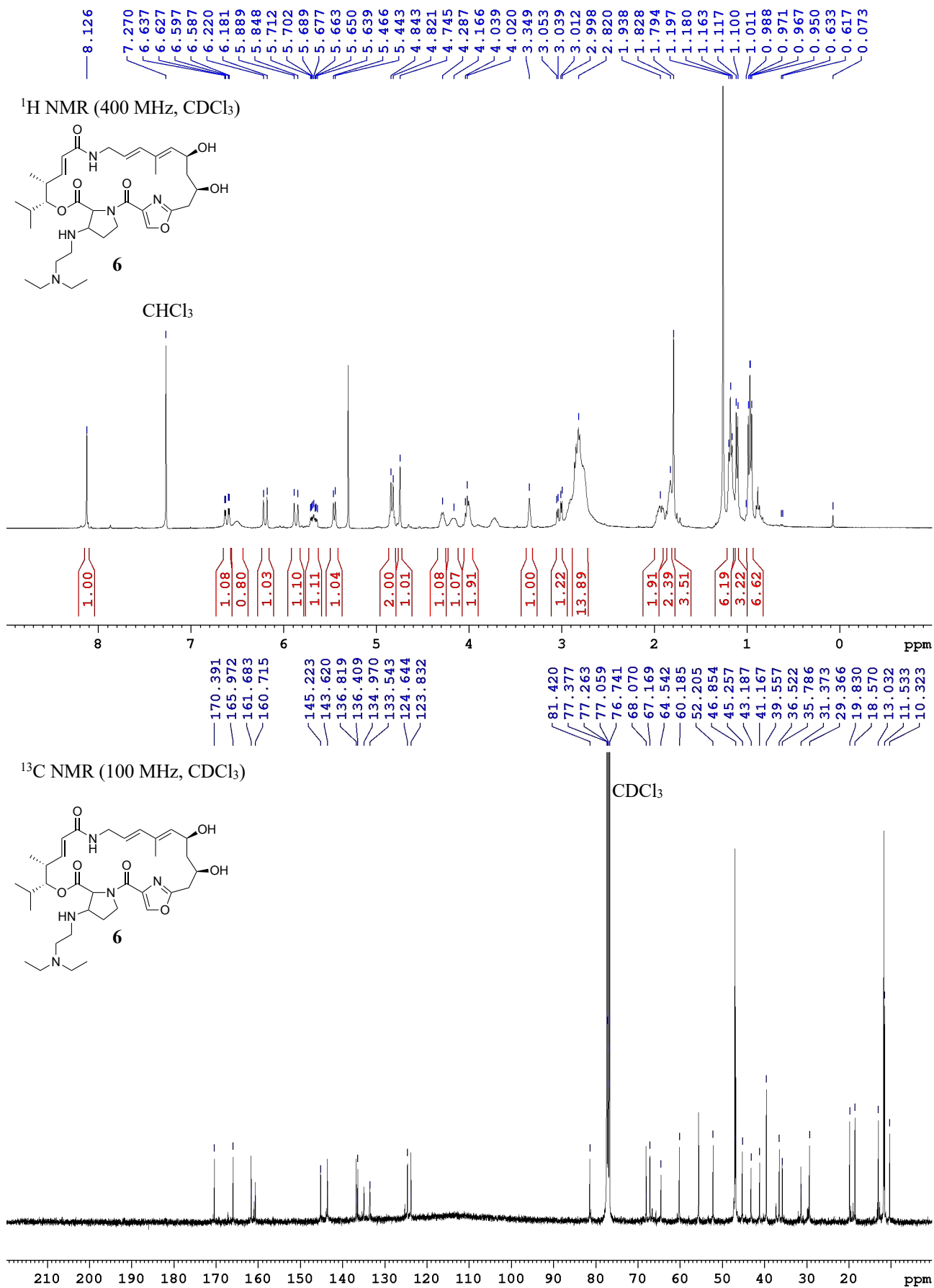


Fig. S75. ¹H NMR and ¹³C NMR spectra of compound **6**.

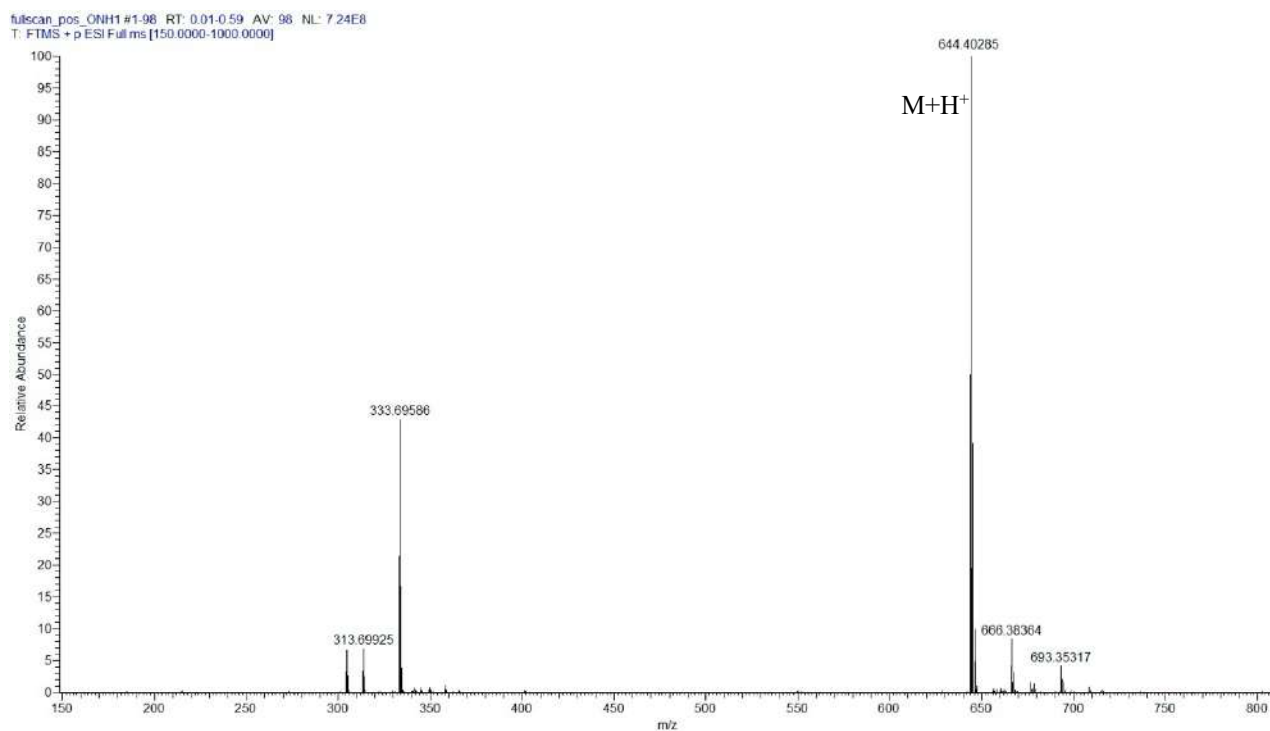


Fig. S76. High resolution ESI(+)-MS spectrum of compound **6**.

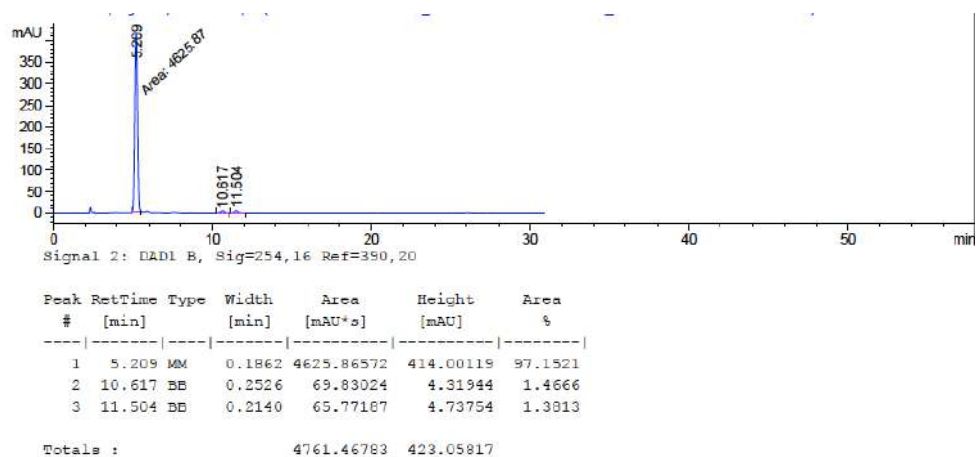


Fig. S77. HPLC chromatogram of compound **6** (RP18, isocratic water/acetonitrile 30:70 + 1% trifluoroacetic acid).

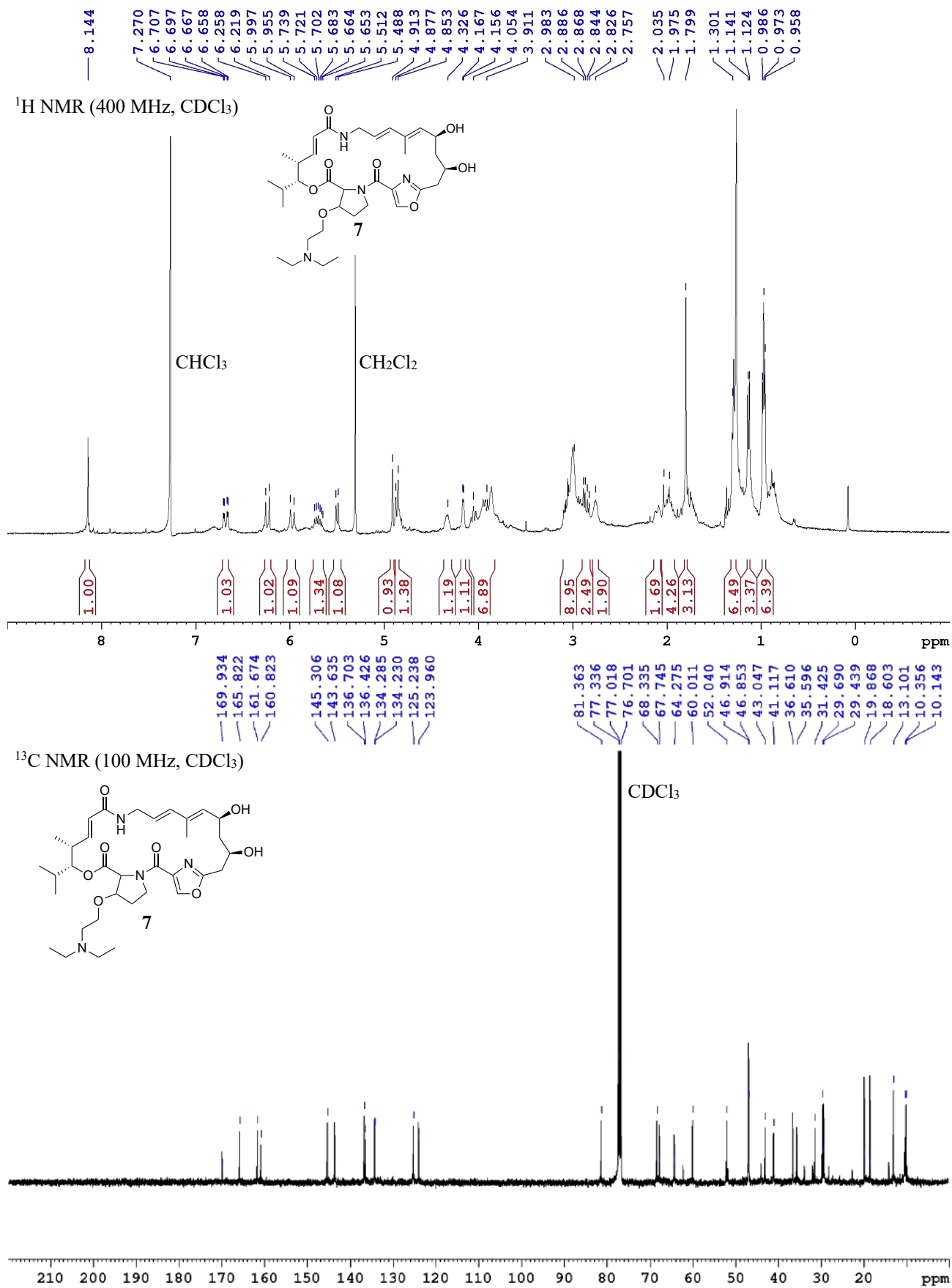


Fig. S78. ¹H NMR and ¹³C NMR spectra of compound 7.

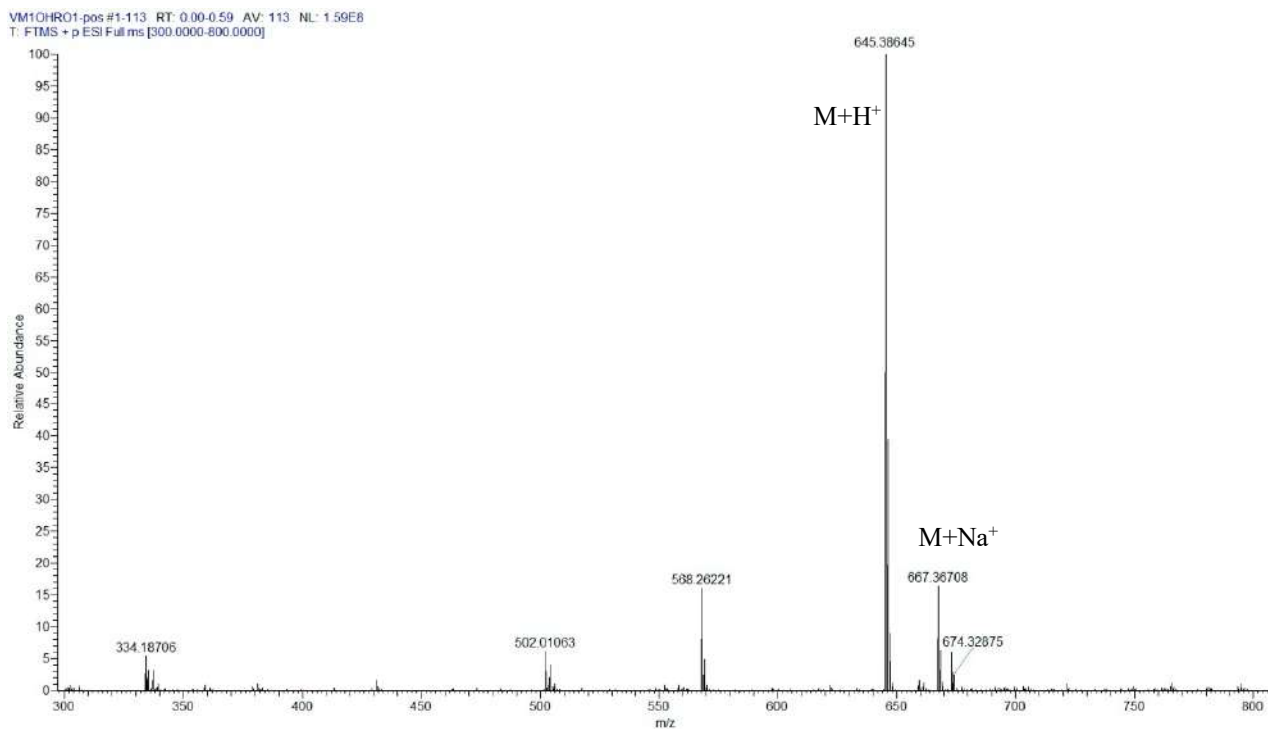


Fig. S79. High resolution ESI(+)-MS spectrum of compound 7.

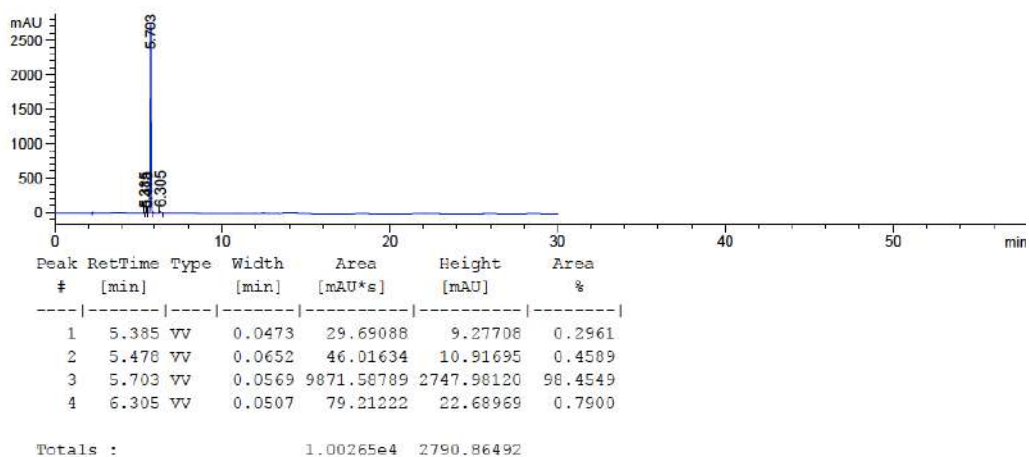


Fig. S80. HPLC chromatogram of compound 7 (RP18, isocratic water/acetonitrile 30:70 + 1% trifluoroacetic acid).